MASTER THESIS

Fluid flow and heat transfer simulation of an electro hydraulic actuator

Executed at the Institute of Fluid Mechanics and Heat Transfer (E322) of Vienna University of Technology

Supervised by

Ao. Prof. Dr. Herbert Steinrück

Of

Daniel Oehler Couso

Matriculation number 1428354

Vienna, January 2016

TABLE OF CONTENTS

Acknowledgments

I want thank Ao. Prof. Dr. Herbert Steinrück, professor at the fluid mechanics and heat transfer department at the Vienna University of Technology, for all the guidance and support through this complicated thesis and all the people of the Institute for Powertrains and Automotive Technology that work with STAR-CCM+ and could help me in my first steps with the program and to advance in this project.

List of figures

List of tables

Nomenclature

Symbols

Re	*Reynolds Number*	$\dot{q}$	*Energy generated per unit volume (W/m³)*
$\bar{u}$	*Mean velocity (m/s)*	h	*Convective heat transfer coefficient (W/(m²*K))*
d	*Characteristic length (m)*	V	*Volume (m³)*
υ	*Kinematic viscosity (m²/s)*	S	*Surface (m²)*
$\dot{m}$	*Mass flow rate (kg/s)*	T	*Stress tensor (N/m²)*
v	*Velocity (m/s)*	Γ	*Diffusivity coefficient (m²/s)*
r	*Radius (m)*	Ra	*Rayleigh Number*
p	*Pressure (Pa)*	Pr	*Prandtl Number*
ρ	*Density (kg/m³)*	Fr	*Froude Number*
Gr	*Grashof Number*	β	*Thermal expansion coefficient (1/K)*
Ra	*Rayleigh Number*	g	*Gravity acceleration (m²/s)*
z	*Coordinate of the axial direction (m)*	H	*Characteristic length (m)*
μ	*Dynamic viscosity (Pa*s)*	α	*Thermal diffusivity (m²/s)*
L	*Gap length (m)*		
Q	*Volumetric flow rate (m³/s)*	λ	*Thermal conductivity (W/(m*K))*
k	*Thermal conductivity (W/(m*K))*		
w	*Angular velocity (rad/s)*	*Abbreviations*	
q''	*Heat flux density (W/m²)*	*CFD*	*Computational Fluid Dynamics*
Ta	*Taylor Number*	*CV*	*Control Volume*
T	*Temperature (K)*	*CAD*	*Computer aided design*
C_p	*Specific heat (J/(kg*K))*	*VOF*	*Volume of Fluids*
		PDE	*Partial differential equation*

1 Introduction

Every technological system has to be improved and developed with time to stay competitive in the market. These means anticipate and solvent every possible problem that can appear in a mechanical system and propose new features and characteristics.

Since the appearance of mechanised rail transport systems appeared in England in the 1820s, train transport system has been continuously developing. The introduction of high-speed rail passenger service between metropolitan areas has stimulated considerable interest in the effects of vibration on passenger comfort. Vibrations are caused by track irregularities, and reduction of these vibrations at high speeds is a particularly difficult task. The high and increasing demand of requisite for this transport have encouraged research in many different areas that affect rail transport. One of these areas is the dampening system, especially in passenger trains.

Due to internal heat generation and the influence of external temperatures, inside the actuator can be established temperatures that can affect the efficiency of the different elements from the actuator. So an imperative is to have a total control of the development of temperatures inside.

The knowledge of the thermal behaviour of the actuator is performed through a Computational Fluid Dynamics (CFD) simulation, in this case with STAR-CCM+ software. Through this a detailed thermal analysis of the entire system is possible. The main objectives with this simulation are the study of heat transfer in different load simulations and varying model conditions to study how this effect the general solution. After implementing this changes, analysis from heat distribution, maximum temperatures and detection of hot spots

1.1 Objective

The objective of this project is to study and understand heat transfer and fluid flow inside this actuator in order to comprehend possible problems and suggest solutions to improve overall performance. This implies the simulation of our known study case with the gives conditions. This study case includes fluid flow and thermal simulation, with special attention in the thermal behaviour. The main objective is to decrease overall temperatures from all the actuators components, but mainly from the critical areas as can be the motor region.

The objectives of this project can be specified as:

- Simplify actuators design in a problem where further work can be undertaken
- Optimize actuators design and components
- Study of thermal behaviour and critical spots
- Accurate CFD simulation of actuator

In order to achieve these goals CFD was implemented in a progressive way where simulation was improved in each studies case, arriving at the most truthful simulation.

1.2 Actuator

Rail technology has to confront are continuously rising requirements concerning comfort, running safety, and speed from the side of the railway operators. These requirements contrast with the fact that with time tracks condition is worse. In view of this situation, conventional suspension concepts are quickly at their limits. At this point, active measures become more relevant for the industry. Active suspensions control the position and can exert an independent force on the suspension with an onboard system, rather than in passive suspensions where the movement is being determined entirely by the road surface.

This increase in railway demand contrasts with the fact that also one of the imperative objectives in the railway industry is to reduce costs and maintenance effort. A logical solution to this question is the implementation of a mechatronic system. Mechatronics is the integrated design and development of a system formed by mechanical, electrical, and control components taking in account their interdependencies and interfaces.

The main propose of this actuator is a motion damper for lateral adjustment. The extremely compact design integrates a complete hydraulic system and has the electronics fully integrated inside the actuator. This new development is a combination of damper and operating cylinder, which actively drives the car into the middle position in curves and improves the lateral comfort.

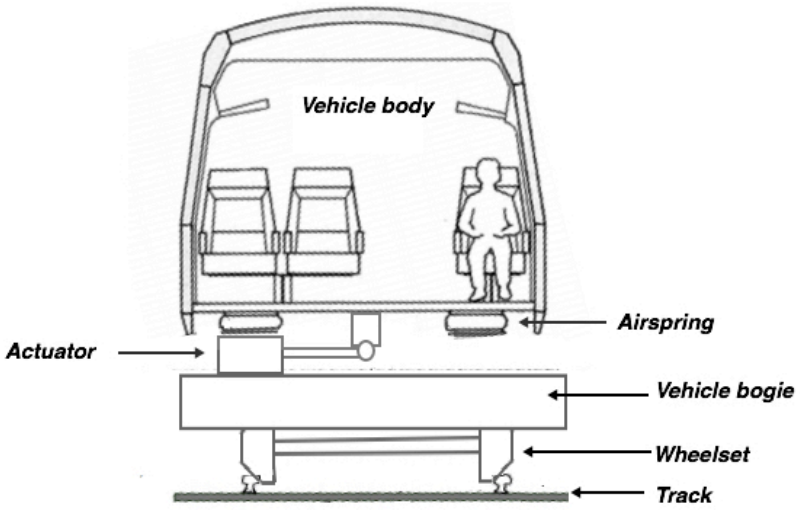

Figure 1: Actuator situation in train structure

The damper further provides a continuous active damping system of the lateral forces. It is situated under the car body and drags the whole structure restoring it to a centre position. This happens in situation where due to inertial forces, for example taking a curve, the car body is driven into a more external position than initially. See references [6] and [9].

This kind of lateral suspension offers following advantages.

- The increase of passenger comfort. One of the main critics from passengers are the abrupt movements that sometimes happens in a passenger train due to the combination of speed and rail trajectory that causes undesired inertial forces. To palliate these effects, one of the solutions is a lateral dampening system.
- The decrease of wear on car, wheels and rails. One of the main objectives in every technological market is to decrease maintenance's expenses. Vibrations in trains inevitably lead to a lower expectancy life from multiple parts in the train industry. In special attention are the parts that induce to the motion of the trains, as can be wheels and rails. The maintenance of these elements (especially rails) is very high and has to be avoided at any cost.

- Increase average speed. As technology advances new opportunities open and situations that 20 years ago were impossible to achieve are in nowadays possible. Speed has been always one of these barriers that is continuous been broken. But this increase in speed thanks to an improved propulsion system has to be combined with a proper dampening system that provides stability and safety to the whole system.
- Reduce noise. Noise has always been a problem not only for the passengers in the train but also for the surrounding areas near a railway. To make a feasible coexistence, it is necessary to dampen possible problems, as it is noise.

1.2.2 Components

As a compact system that integrates multiple functions, we can appreciate different parts, each one with their own function.

The first differentiation to take in account is the electronics and the actuator. The electronics are integrated with the actuator. Its placed on a lateral region of the tank and isolated by an aluminium wall.

The actuator is composed by different mechanical elements that in combination fulfil the requisites imposed. We can find four basic components for the actuator:

- Cylinder
- Hydraulic pump
- Filter
- Induction motor

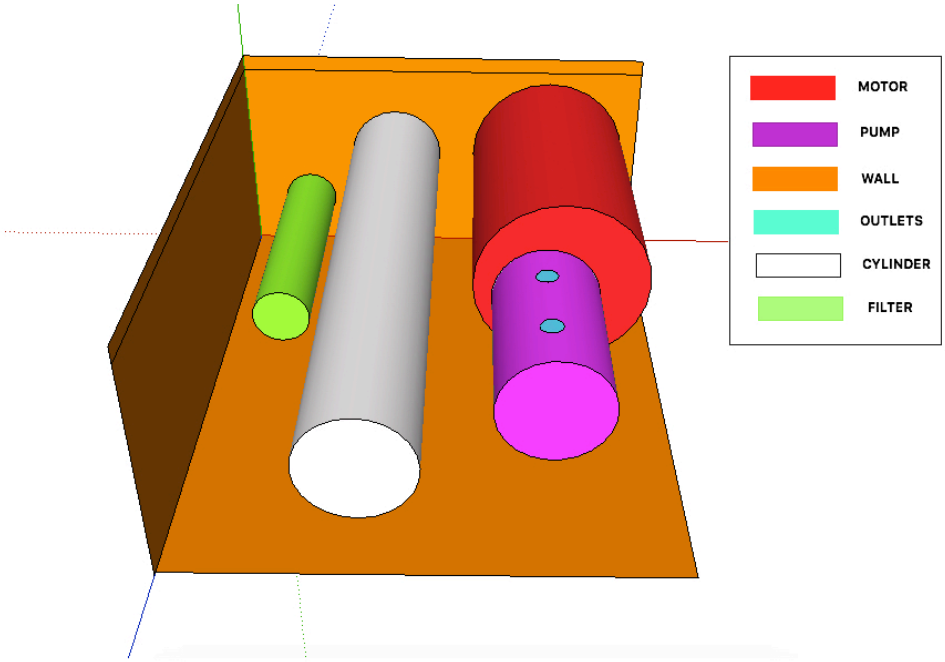

Figure 2: 3D actuator model

To achieve the lateral dampening desired, these elements have to work in conjunction. A general overview of these components can be seen in the Figure 2 and 3:

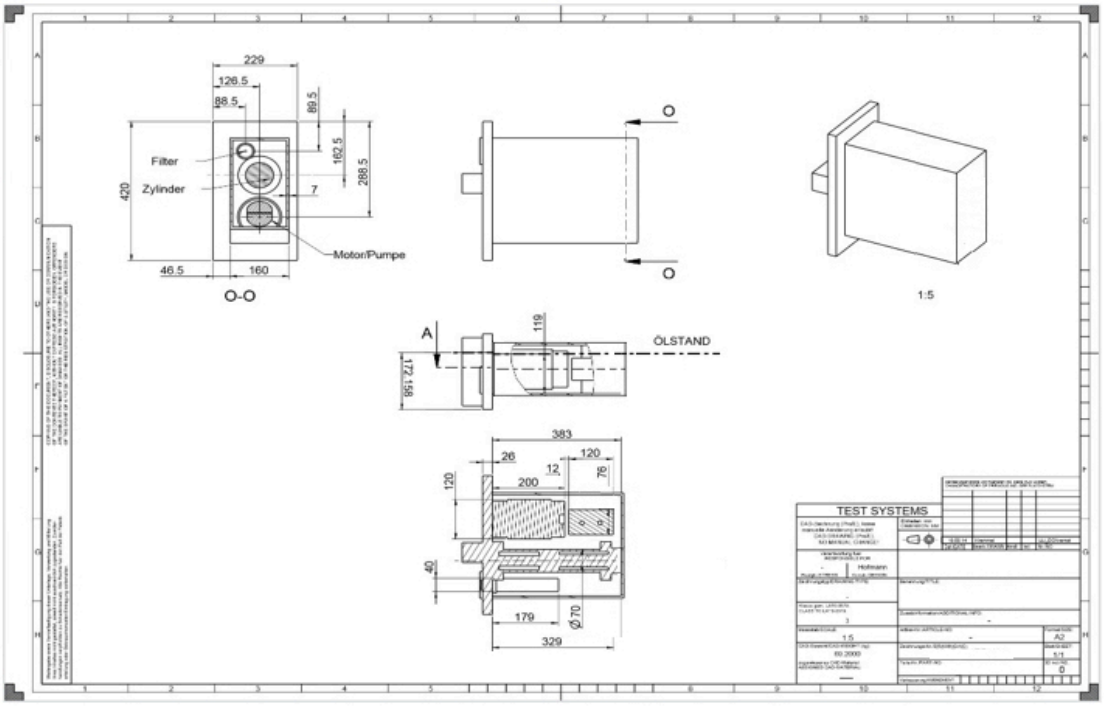

Figure 3: Actuator plans

On the one side, there is the active system of dampening composed by the cylinder. The main purpose of the hydraulic cylinder is to give a unidirectional force through a unidirectional stroke. It gets its power from the pressurized hydraulic fluid. It also consists of a cylinder barrel, in which a piston moves back and forth (see Figure 7). The barrel is closed on one end by the cylinder bottom and the other end by the cylinder head where the piston rod comes out the cylinder. The generation of this movement comes from the hydraulic pump, which brings in a regulated flow of oil to the cylinder, to move the piston. The piston moves the oil in the other chamber back to the reservoir.

The hydraulic pump drives the fluid back outside, through the cylinder, providing the necessary pressure in it and finally to the filter. The filter works as an inlet for the hydraulic fluid in the tank and as an outlet for the hydraulic pump system. It is vital to ensure that particle contaminants are filtered out from the hydraulic fluid before components are jammed or damaged through abrasive wear.

On the other side, there is the cooling system for the actuator and heat source. A filter, hydraulic pump and an induction motor compose this system. The whole cavity of the tank is full with hydraulic fluid, with a high thermal conductivity, and a thin air region. The air region function is to insolate the upper side of the tank so that a lower heat transfer through this wall is achieved in comparison with a full tank with hydraulic fluid. The actuator is cooled due to the thermal dissipative effect that the hydraulic fluid has.

The hydraulic pump is a mechanical source of power that converts mechanical power into hydraulic energy. It generates flow with enough power to overcome pressure induced by the load at the pump outlet. It creates a vacuum at the pump inlet that forces liquid from the inside region of the tank to the pump and by mechanical action delivers this liquid into the hydraulic system. In this case, the hydraulic pump is driven by gear pump with external teeth. These pumps create pressure through the meshing of the gear teeth, which forces fluid around the gears to pressurize the outlet side.

An induction motor transmits the necessary torque to the pump that powers the mechanical system of the hydraulic pump. This motor consists in an alternating current motor in which torque is produced by the reaction between a varying magnetic field generated in the stator and the current induced in the coils of the rotor.

2 Actuator problematic

An important point in this study case is to understand how the actuator works and which are the problematic that we can find in this thesis due to fluid flow or heat transfer.

As we have a complex geometry, implementation in CFD represents a higher complexity as it can be thought in the first moment. Also we have to take in account that there is a heat transfer from the motor region to the hydraulic fluid. After that, heat is driven into the walls where it exchanges with the environment. So in order to implement the right physical models, development in fluid flow and heat transfer has to be observed in a first stage to extract afterwards conclusions for the simulation, as this two phenomenon are crucial to understand the problem and the solutions implemented.

2.1 Fluid flow description

As said in Chapter 1, we have a fluid flow through two actuator components: the filter acts as an inlet for the hydraulic fluid that enters inside the actuators box, filling almost all the region (leaving only a thin air region), and the hydraulic pump that acts as the outlet through two outlet lines, pumping the fluid into the components.

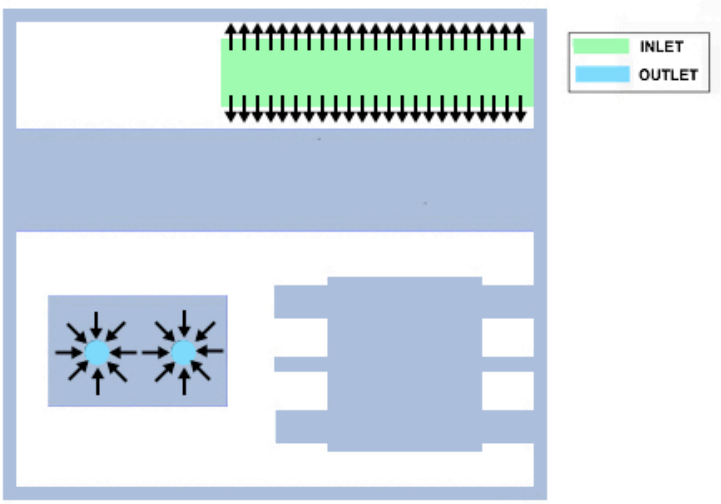

Figure 4: Fluid flow scheme inside actuator region

The actuator box delimits our actuator domain. Inside we have all the components (cylinder, motor, filter and motor) that are submerged in the hydraulic fluid. Hydraulic fluid comes inside the actuator region flowing in a perpendicular direction to the filter lateral surface. Velocities of the inlet fluid flow are very low as we have little fluid mass flowing inside per second, distributed in a large surface. Therefore, as the actuators box is even larger, we have an approximately equal slow fluid flow inside the actuator until it reaches the hydraulic pump. This component creates a pressure different that drags the hydraulic fluid outside our actuator system. As we have very little flow velocities we get a little Reynolds number value in our case. This means that we deal with a laminar flow and do not expect big instabilities.

Once it is outside our actuator region, this fluid is driven back to our system through a specific way until it reaches again the filter region. As this way is very complex, fluid flow inside the components was not considered in the model. In a first moment leaves the hydraulic pump region thanks to two pipes (1) and reaches the hydraulic cylinder, entering its chambers. After that, leaves the hydraulic cylinder and flows to the throttle region (2). Fluid flows then back to the base plate (3) and following some channels carved inside, returns to the filter region (4), where all the process begins again.

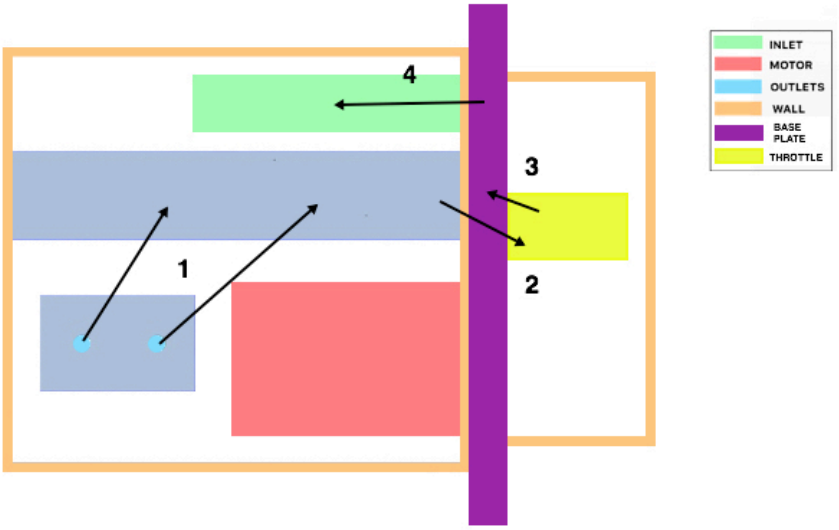

Figure 5: Fluid flow scheme after leaving actuator region

2.2 Energy losses

As we have an actuator with multiple components we can also think that we can have more than one heat source. Heat is produced in more than one component

due to mechanical losses, friction losses or just because of the resistance effect of a component.

Knowing all the components that we have in our actuator, we can expect heat losses in: electrical motor, hydraulic pump, throttle and hydraulic cylinder.

2.2.1 Heat losses in Electrical Machines

This is the most crucial heat loss in this thesis research due to the importance of temperatures reached in the motor region. Electric devices produce heat as a by-product of normal operation. When electrical current flows through a semiconductor or a passive device, a portion of the power is dissipated in the form of heat, this is called dissipated power. Objects containing high temperatures, transfer energy to low temperature status surroundings without extra force or work. Energy is hence released from this object to either other objects or the ambient environment through thermal conduction, convection or radiation. This is called heat transfer and results in a temperature decrease if this heat dissipated object. When cooling an object, this can be achieved in two different ways, either by decreasing heat losses that are generated in the system or by increasing the total heat transfer.

This thesis will focus in both techniques and study how the combination of both factors can lead to a general and specific decrease in some parts of their temperatures. The direct cooling system studied consists in hydraulic oil fluid that improves heat transfer performances since the convective heat transfer capabilities increase.

Motor winding resistance is the main cause of heat generation within the motor. In order for any electric motor to generate torque, current needs to be forced through the motor windings. Copper is an excellent conductor, however, it's not perfect; material physics and impurities will cause the atoms to vibrate at a faster rate as more current flows. The result is a steady temperature increase in the motor windings. All metal conductors have a positive temperature coefficient of resistance. This means as temperature increase, the resistance of the material also increases as a function of the type of conductor used. Electric motors typically use copper conductor material, except in special cases. Many induction motor squirrel cages use cast aluminium for ease of manufacturing, but the vast majority of motors use copper magnet wire.

Excessive heat in motors can cause a number of performance problems. Overheating causes the motor winding insulation to deteriorate quickly. For every ten centigrade rise in temperature, the insulation life is cut in half. It has been

concluded that more than 55% of the insulating failures are caused by over heating.

Magnet losses (W) in high-speed permanent magnet machines can also decrease the motor efficiency. The motor torque constant (KT) and voltage constant (KE) are directly related to the magnetic flux density (Br) of the permanent magnets. Depending on the physics of the magnet material used, overall flux density will change at a given percentage with an increase in magnet temperature. As the material temperature increases, atomic vibrations cause once-aligned magnetic moments to "randomize" resulting in a decrease in magnetic flux density. Assuming the motor is operating within its intended design window, the decrease in flux density is temporary and will begin to recover as the magnet cools. If the maximum temperature rating of the magnets is exceeded, however, partial demagnetization will occur and permanently alter the performance of the motor. The cost is affected by the thermal class; to be precise, a higher thermal class increases the prize. Magnets also need to be larger when in a system with higher temperatures. Therefore an effective cooling method of the rotor, and hence the magnets, is also essentially for decreasing the size and costs of the magnets. Further information can be found in [2] and [12].

2.2.1.1 Cooling techniques of Electrical Machines

The main objective of cooling electric motor is to reduce the temperature in this critical spots. Air cooling with fans is mostly investigated in the gap between the rotor and the stator. Investigations of fan cooling are the most common, i.e. removing heat by using cool air with a high velocity. For enclosed motors with no ventilation, the dissipation of losses is by radiation and natural convection. This is usually satisfactory for small motors and for motor with light thermal loads. See reference [5].

In enclosed regions is typical the use of different liquid cooling types. In the actuator case, we can find hydraulic oil fluid as the dissipation environmental element. The main factors that for the use of hydraulic fluid in this system is that it provides a higher heat transfer coefficient in comparison with air, leading to a higher thermal dissipation in equal conditions and that this hydraulic oil fluid is also used to the motion and maintain mechanical properties in the hydraulic cylinder.

2.2.2 Heat losses in Hydraulic Pump

A hydraulic pump, as a mechanical machine has an efficiency that depends on the energy that can transform from mechanical to hydraulic energy. In our actuator, we have two gear pump with external teeth working as one component.

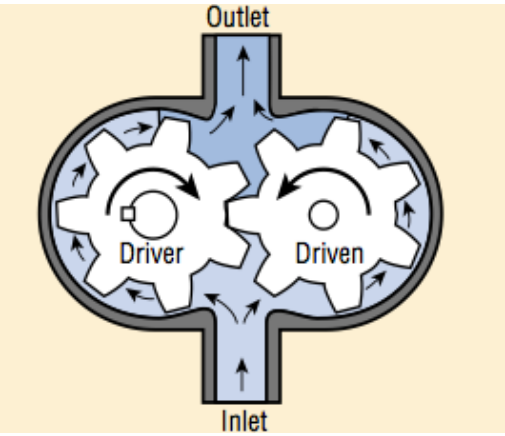

Figure 6: Gearpump with external teeth

Mechanical components, like transmission gear and bearings, create mechanical losses that reduce the power transferred from the motor shaft to the pump.

$$\eta_{Pump} = \frac{P - P_t}{P} \tag{1}$$

η_{Pump} represents mechanical efficiency of the hydraulic pump. P (W) indicates power transferred from the motor to the shaft, and P_t (W) is the power lost in the transmission. This power lost in transmission transforms in thermal energy, and for that hydraulic pump components tend to raise temperature.

2.2.3 Heat losses in Hydraulic Cylinder

We have a hydraulic fluid flow from the hydraulic pump to the throttle and finally to the filter. For that, we have hydraulic losses due to friction between the viscous fluid and the walls. This effect can be seen also inside the pipes and channels that guide the fluid through the system.

As we have a large complex geometry inside the hydraulic cylinder, there is a vast contact inside the cylinder between the fluid and the walls. The bigger this contact surface area is, the bigger will be this hydraulic loss due to friction.

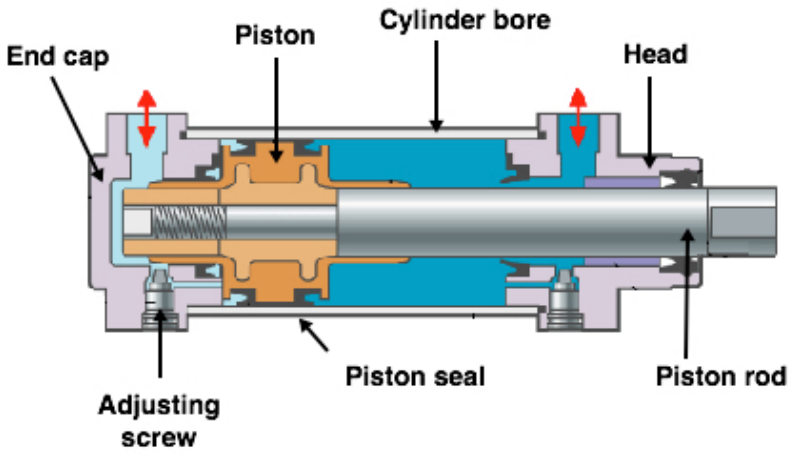

Figure 7: Hydraulic cylinder view

The actuator has a double acting hydraulic cylinder. This means depending on the situation of the piston, we will have more fluid inside one chamber or the other, implying more losses in one of the side than in the other. A possible model for this actuator is the assumption of some heat losses due to this effect reduced to the hydraulic cylinder.

2.2.4 Losses in Throttle

A throttle is a mechanism designed to regulate the supply of a fluid. The largest piece inside the throttle body is the throttle plate, which is the mechanical component that regulates the flow.

Even for an "incompressible fluid" such as hydraulic fluid, there is some compressibility. The first law of thermodynamics applies to a liquid every bit as much as it applies to a gas. The PdV energy in the liquid must be exchanged with the internal energy. This pressure drop is referred as "unrecoverable" pressure drop. The unrecoverable pressure drop is a change of internal energy into PdV energy. All this implies a differential in entropy in the system that explain the losses that we can find in a throttling valve.

We have a fluid escaping from the hydraulic cylinder region escaping at a concrete pressure. As we have a valve element, we are controlling this pass of fluid to the next region. Depending if we let the fluid flow or not, we will be increasing or decreasing fluid pressure and therefore the velocity. Combining this factor with fluid viscosity we get hydraulic losses that can generate heat losses. Also the mechanical component is in movement, so there can be some losses due to mechanical friction of this component.

3 Basic Fluid Mechanics and heat transfer theory

A quick summary of the most important concepts will be stated along this thesis report to have an overall look of the physics phenomena that have a crucial effect in this simulation. Main references of interest for further information are [3], [4], [8], [10], [11], [13] and [15].

3.1 Governing equations

To solve this problem, we should know the physical properties of fluid by using Fluid Mechanics. Then we can use mathematical equations to describe these physical properties using the CFD program. Because the equations governing fluid flows of practical importance are very complicated, computers have to be used to solve the partial differential equations describing the problem at hand. Also, analytical solution for these types of problems do not exist, only solutions for very few and simple physical cases. In computational techniques, the governing PDE's are replaced with systems of algebraic equations solvable by a computer. In most general cases, the following quantities are needed in order to describe fluid flow phenomena:

- Velocity field: $u = [u(x, y, z, t), v(x, y, z, t), w(x, y, z, t)]T$
- Pressure field: $p(x, y, z, t)$
- Density distribution: $\rho(x, y, z, t)$
- Temperature distribution: $T(x, y, z, t)$

The CFD software STAR CCM+ is based as said before on a finite-volume method and starts from conservation equations in integral form. In the computations, an algebraic equation system solvable on a computer is obtained by means of discrete approximations with appropriate initial and boundary conditions. As a first step, the spatial solution domain is subdivided into a finite number of contiguous control volumes. These volumes can be of arbitrary polyhedral shape. The governing equations used contain surface and volume integrals, as well as time and space derivatives.

For a viscous three-dimensional flow, the flow is assumed to be governed by the Reynolds-averaged Navier-Stokes equations (see reference [8]), in which the turbulence effects are included via and eddy-viscosity model. In this case, the continuity equation, three momentum components equations, and two equations

for turbulence properties are solved. In addition, the space-conservation law must be satisfied as the CVs move as the solid moves. The equations are:

Mass conservation:

$$\frac{d}{dt}\int_V \rho \, dV + \int_S \rho(v - v_b) * n \, dS = 0. \quad (2)$$

Momentum conservation:

$$\frac{d}{dt}\int_V \rho v \, dV + \int_S \rho v(v - v_b) * n \, dS = \int_S (\mathrm{T} - pI) * n \, dS + \int_V \rho b \, dV. \quad (3)$$

General transport equation:

$$\frac{d}{dt}\int_V \rho\phi \, dV + \int_S \rho\phi(v - v_b) * n \, dS = \int_S \Gamma\nabla\phi * n \, dS + \int_V \rho b_\phi \, dV. \quad (4)$$

In these equations, ρ stands for fluid velocity, v is the fluid velocity vector and v_b is the velocity of the CV surface; n is the unit vector normal to the CV surface with area S and volume V. T stands for the stress tensor (expressed in terms of velocity gradients and eddy viscosity), p is the pressure, I is the unit tensor, φ stands for the scalar variable (k, ε or ω), Γ is the diffusivity coefficient, b is the vector of body forces per unit mass and b_φ represents sources and sinks of φ.

3.2 Viscous flow

In a first moment, different facts had to be taken in account to select the proper fluid region. This fluid is going to be the responsible of the heat transfer inside the actuator and that will lower the components temperatures. The determinant facts that led to the selection of hydraulic fluid as the dissipation element were that this fluid held a low Re value (indicating that we are in a laminar situation) and a high Pr number. Due to the fluid flux, heat transfer is increased due to the fact that convection is the diffusivity that dominates.

The two different types of viscous flows occurring in nature are laminar and turbulent flows. A laminar flow is smooth, well ordered and moves in parallel layers, it occurs when the ratio of viscous to inertial forces is lower than the value of transition to a turbulent flow. This is described as the Reynolds number ($Re = \frac{\bar{u}*d}{v}$). If the Reynolds number is small, inertia forces are insignificant relative

to viscous forces. The disturbances are then dissipated, and the flow remains laminar.

$$Re = \frac{\bar{u} * d}{v} \tag{5}$$

In this thesis, we are working with a complex geometry that needs to be discretized in smaller parts that can be studied. Mainly in our case study, we have the situation of two parallel infinite plates, where we have one with a constant directional velocity. The flow is laminar when $Re \leq 2000$, which is the case for the oil flow in all the actuators regions. The mean velocity is defined as $\bar{u} = \frac{\dot{m}}{\rho * A}$ where $\dot{m}$ is the mass flow rate (Kg/s), v is the kinematic viscosity (m^2/s) and d the characteristic length (m). An estimated Reynolds number, if we take 0.005 m/s as the average fluid flow velocity, we get a Reynolds number of 0.32, a very low value.

Another valuable constants to observe are the Prandtl number ($Pr = \frac{C_p * \mu}{k}$), Grashof number ($Gr = \frac{g * \beta * (T_S - T_\infty) * L^3}{v^2}$) and the Rayleigh number ($Ra = Gr * Pr = \frac{C_p * g * \beta * \rho^2}{\mu * k} * (T_S - T_\infty) * L^3$). The Prandtl number is defined as the ratio of the kinemtic viscosity, also referred to as the momentum diffusivity, v, to the thermal diffudivity α. Provides a measure of the relative effectiveness of momentum and energy transport by diffusion in the velocity and thermal boundary layers, respectively. Small values of the Prandtl number, Pr << 1, means the thermal diffusivity dominates. Whereas with large values, Pr >> 1, the momentum diffusivity dominates the behaviour.

$$Pr = \frac{C_p * \mu}{k} = 66{,}6. \tag{6}$$

Cp stands for the specific heat of the fluid (J/kg*K), k (W/m*K) is the thermal conductivity and μ is the dynamic viscosity (Pa*s). All the fluid values are specified in APPENDIX A. As we can see in our case we have a big Prandtl number. This means that convection is very effective in transferring energy from an area in comparison to pure conduction, so momentum diffusivity is dominant. So an important fact in our actuator is the heat dissipated through convection. The Prandtl number also controls the relative thickness of the momentum and thermal boundary layers. When Pr is small, it means that the heat diffuses quickly compared to the velocity (momentum). This means that for liquid metals the thickness of the thermal boundary layer is much bigger than the velocity boundary layer. At this point we can also briefly talk about the Peclet number ($Pe = Re * Pr$). The Peclet number is a dimensionless number used in calculations involving convective heat transfer. It is the ratio of the thermal energy transferred to the

fluid to the thermal energy conducted within the fluid. If Pe is big, as it is in our case, convection is important.

The Grashof number and Rayleigh number are indicators for our thin air region. This numbers indicate which kind of heat transfer dominates in this region. Grashof number ($Gr = \frac{g*\beta*(T_S-T_\infty)*L^3}{\upsilon^2}$) is a nondimensional parameter used in correlation of heat and mass transfer due to thermally induced natural convection at a solid surface immersed in a fluid. The significance of the Grashof number is that it represents the ratio between the buoyancy forces due to spatial variation in fluid density (caused by temperature differences) to the restraining force due to the viscosity of the fluid.

$$Gr = \frac{g * \beta * (T_S - T_\infty) * L^3}{\upsilon^2} \tag{7}$$

β represents the coefficient of thermal expansion (equal to 1/T for ideal gases). T_S (K) stands for the temperature at the surface and T_∞ (K) for the temperature of the fluid. L (m) is the characteristic length and υ (Pa*s) the dynamic viscosity of the fluid.

Rayleigh number ($Ra = Gr * Pr = \frac{C_p*g*\beta*\rho^2}{\mu*k} * (T_S - T_\infty) * L^3$) is also a dimensionless number associated with buoyancy-driven flow or natural convection. When the Rayleigh number is below a critical value for that fluid, heat transfer is primarily in the form of conduction. When it exceeds the critical value, heat transfer is primarily in the form of convection. Rayleigh number can be expressed as:

$$Ra = Gr * Pr = \frac{C_p * g * \beta * \rho^2}{\mu * k} * (T_S - T_\infty) * L^3. \tag{8}$$

We have to know that C_p is the specific heat of the fluid (J/kg*K). k (W/m*K) is the thermal conductivity.

Finally, we can also study the fluid flow stability inside the actuator box through the Froude number ($Fr = \frac{u}{\sqrt{g*h}}$). As we have two different regions in contact it is important to know how the flow is in these regions. The Froude number is a dimensionless value that describes different flow regimes of open channel flow. In our case would be a rectangular surface where the fluid flows in a direction. The Froude number is a ratio of inertial and gravitational forces. The Froude number is a measurement of bulk flow characteristics such as waves, sand bedforms, flow/depth interactions at a cross section or between boulders.

Flow conditions within a sewer are directly related to the Froude number. If Fr < 1, flow conditions are classified as subcritical and are often described as tranquil or streaming. If Fr > 1, flow conditions are classified as supercritical and are often described as rapid or shooting. If Fr = 1, flow conditions are classified as critical and are often described as unstable.

$$Fr = \frac{u}{\sqrt{g * h}} \tag{9}$$

See references [4], [10], [13] and [15] for more detailed information.

3.2.1 Internal gap flow

In this case study, we have a complex velocity field and for that a complex heat transfer inside the electrical motor. On the one side we have an axial flow inside the motor gap driven by a differential pressure and on the other hand, we have a radial velocity field caused by the rotation of the rotor part.

Depending the direction we are studying we can find different flow situations:

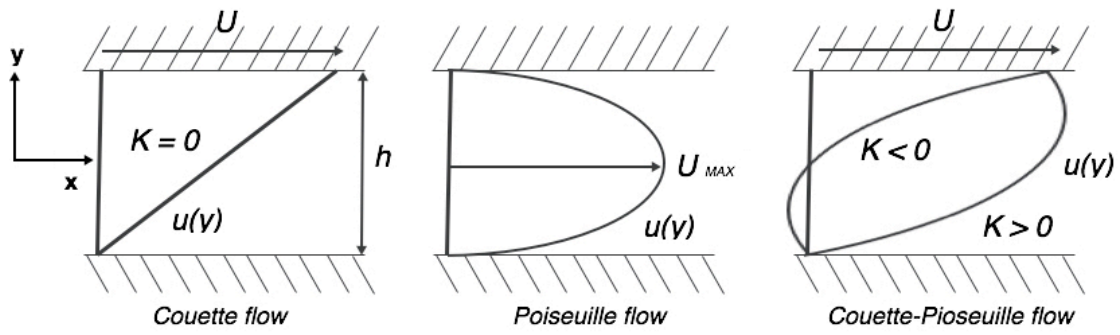

Figure 8: Plane unidirectional flow

K stands for $\frac{\partial P}{\partial x}$. U(x) indicates the velocity fluid function in the streaming.

3.2.1.1 Axial gap flow

Steady viscous fluid flow driven by an effective pressure gradient established between the two ends of a long straight pipe of a uniform circular cross-section is generally known as Poiseuille flow (see Figure 9).

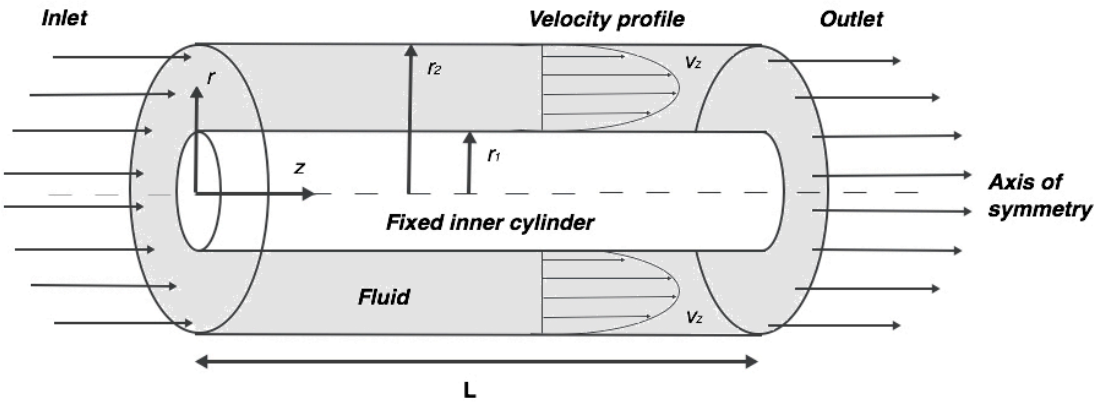

Figure 9: Geometry for flow through an annular gap

In the die of length L, a pressure difference $p_2 - p_3$ causes a liquid of viscosity μ to flow steadily from left to right in the annular area between two fixed concentric cylinders. The inner and the outer cylinder are solid, and their radii are r_1 and r_2, respectively.

To analyse the situation, again start from the continuity equation:

$$\frac{\partial \rho}{\partial t} + \frac{1}{r}\frac{\partial(\rho r v_r)}{\partial r} + \frac{1}{r}\frac{\partial(\rho v_\theta)}{\partial \theta} + \frac{\partial(\rho v_z)}{\partial z} = 0; \tag{10}$$

which, for constant density and $v_r = v_\theta = 0$, reduces to:

$$\frac{\partial v_z}{\partial z} = 0; \tag{11}$$

verifying that v_z is independent of distance from the inlet, and that the velocity profile $v_z = v_{z(r)}$ appears the same for all values of z.

There are again three momentum balances, one for each of the r, θ, and z directions. If explored, the first two of these would ultimately lead to the pressure variation with r and θ at any cross section. We extract the z-momentum balance:

$$\rho\left(\frac{\partial v_z}{\partial t} + v_r\frac{\partial v_z}{\partial r} + \frac{v_\theta}{r}\frac{\partial v_z}{\partial \theta} + v_z\frac{\partial v_z}{\partial z}\right) = -\frac{\partial p}{\partial z} + \mu\left[\frac{1}{r}\frac{\partial}{\partial r}\left(r\frac{\partial v_z}{\partial r}\right) + \frac{1}{r^2}\frac{\partial^2 v_z}{\partial \theta^2} + \frac{\partial^2 v_z}{\partial z^2}\right] + \rho g_z. \tag{12}$$

With $v_r = v_\theta = 0$ (assuming we do not have a velocity component in the radial direction), $\partial vz/\partial z = 0$, $\partial vz/\partial \theta = 0$, and $gz = 0$, this momentum balance simplifies to:

$$\mu\left[\frac{1}{r}\frac{d}{dr}\left(r\frac{dv_z}{dr}\right)\right]=\frac{\partial p}{\partial z}. \tag{13}$$

Problems in which total derivatives are used because of v_z depends only on r. We shall prove that the pressure gradient is uniform between the die inlet and exit, being given by:

$$-\frac{\partial p}{\partial z}=\frac{p_2-p_3}{D}, \tag{14}$$

in which both sides of the equation are positive quantities. Two successive integrations of the equation may then be performed, yielding:

$$v_z=-\frac{1}{4\mu}\left(-\frac{\partial p}{\partial z}\right)r^2+c_1\ln r+c_2. \tag{15}$$

The two constants may be evaluated by applying the boundary conditions of zero velocity at the inner and outer walls,

r = r1: $v_z = 0$, r = r2: $v_z = 0$,

giving:

$$c_1=\frac{1}{4\mu}\left(-\frac{\partial p}{\partial z}\right)\frac{r_2^2-r_1^2}{\ln(\frac{r_2}{r_1})}, \tag{16}$$

$$c_2=\frac{1}{4\mu}\left(-\frac{\partial p}{\partial z}\right)r_2^2-c_1\ln r_2. \tag{17}$$

Substitution of these values for the constants of integration into previous equation yields the final expression for the velocity profile:

$$v_z=\frac{1}{4\mu}\left(-\frac{\partial p}{\partial z}\right)\left[\frac{\ln\left(\frac{r}{r_1}\right)}{\ln\left(\frac{r_2}{r_1}\right)}(r_2^2-r_1^2)-(r^2-r_1^2)\right]. \tag{18}$$

Note that the maximum velocity occurs somewhat before the halfway point in progressing from the inner cylinder to the outer cylinder.

The final quantity of interest is the volumetric flow rate Q. Observing first that the flow rate through an annulus of internal radius r and external radius r + dr is $dQ = v_Z * 2 * \pi * r\,dr$, integration yields:

$$Q = \int_0^Q dQ = \int_{r_1}^{r_2} v_z 2\pi r \; dr. \tag{19}$$

Since r ln(r) is involved in the expression for v_z, the following indefinite integral is needed:

$$\int r \; \ln r \; dr = \frac{r^2}{2} \ln r - \frac{r^2}{4}, \tag{20}$$

giving the final result:

$$Q = \frac{\pi(r_2^2 - r_1^1)}{8\mu} \left(-\frac{\partial p}{\partial z}\right) \left[r_2^2 + r_1^2 - \frac{r_2^2 + r_1^2}{\ln\left(\frac{r_2}{r_1}\right)}\right]. \tag{21}$$

Since Q, μ, r1, and r2 are constant throughout the die, $\partial p/\partial z$ is also constant, thus verifying the hypothesis previously made.

3.2.1.2 Radial gap flow

Couette Flow is drag-induced flow either between parallel flat plates or between concentric rotating cylinders as in our study case.

It is assumed that there is Laminar Flow of an incompressible Newtonian Fluid of density ρ and viscosity η between two parallel flat plates a constant distance H apart. The lower plate is of length L >> H and infinite width; it is stationary. The upper plate can be considered of infinite length and infinite width; it moves at constant speed u in its own plane in the direction of the length of the lower plate. There is no variation in pressure p anywhere in the flow.

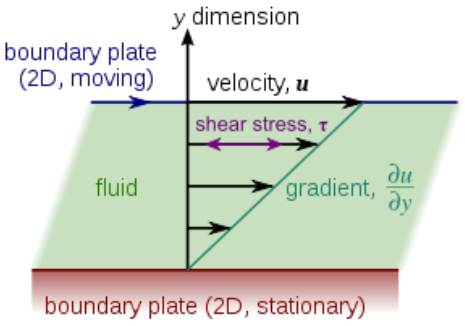

Figure 10: Simple Couette configuration using two infinite planes

Because of the geometry, Couette flow is analysed using rectangular or Cartesian coordinates (x, y). The x-direction is aligned with the direction of motion of the upper plate and the y-direction is aligned vertically upwards (see Figure 10). Because L >> H, Couette flow is fully developed, that is the velocity u is

independent of axial position x everywhere except near the ends of the stationary plate (at x = 0 and x = L). Solution of the mass and linear momentum Conservation Equations, specifically the *Navier-Stokes equations*, with boundary conditions of no-slip at both plates (y = 0 and y = H) yields:

$$u_x = \frac{u_y}{H}. \tag{22}$$

Thus, the axial velocity profile is linear (see 10) and depends only on flow geometry and speed of the moving plate: it is independent of fluid properties. The mean axial velocity u_x is given by:

$$u_x = \frac{1}{2}U. \tag{23}$$

Practical realization of Couette flow between parallel flat plates is difficult. A good approximation can, however, be obtained in the annular gap between two rotating concentric cylinders of a slightly differing radius. Thus, if the inner cylinder has an outer radius R1 and the outer cylinder has an inner radius R2, the flow between them is very similar to that given by Eq. (1) provided that $r_2 \cong r_1$.

But flow between rotating concentric cylinders is susceptible to a centrifugal instability called the Taylor Instability, which occurs when the inner cylinder is rotated and the outer cylinder is kept stationary and the Taylor Number Ta defined by:

$$Ta = \frac{4w^2 r_1^2 \rho^2 (r_2 - r_1)^4}{\mu^2 (r_2^2 - r_1^2)} \tag{24}$$

If it exceeds a critical value $Ta_c \cong 1700$, where ω denotes the angular velocity of the inner cylinder. In order to avoid the Taylor instability, it is usual to rotate the outer cylinder and keep the inner cylinder stationary.

3.3 Fundamental Heat Transfer

Heat transfer mechanisms can be grouped into 3 broad categories:

3.3.1 Conductive Heat Transfer

Heat conduction is the transfer of energy from more energetic particles to particles with lower energy level, through interaction between particles such as atoms or electrons where there is no bulk, or macroscopic, motion. Briefly, it can be explained as the flow of internal energy, the energy transfer, from a region of higher temperature to a low temperature region when a temperature gradient exists in a body. Conduction can exist in all forms of matter. In solids vibrations of molecules and diffusion of free electrons cause it. Heat conduction in liquids and gases is due to collisions between the particles, the more conductive a matter is, therefore conduction is a greater in solids.

Heat conduction depends on the material properties, the geometry and on the surfaces in the body. The heat transfer rate is specified by the conduction rate equation known as Fourier's law.

$$q'' = -k * \nabla T. \tag{25}$$

Where q'' (W/m^2) is the local heat flux vector, which represents the heat transfer rate per unit area. Hence the heat transfer rate, q (W), is the product of the heat flux and the area that transmits this heat, A (m^2). Furthermore, k (W/(m*K)) is the thermal conductivity of the material, it is a transport property of the material and describes how fast the heat transports in the material, The scalar temperature field in three dimensions, T (K), and, ∇, the three dimensional operator describe the temperature gradient in the different directions due to the temperature difference in the volume. As a conclusion, one could say that conduction occurs in motionless fluids and through solid bodies, where the energy is transported from hot to cold regions.

In cases where heat sources are present within a body, the previous equation needs to be substituted for a one based on the principles of energy balance and valid for three-dimensional cases as:

$$\rho c_p \frac{\partial T}{\partial t} = \nabla * (k \nabla T) + \dot{q}. \tag{26}$$

This equation adds the term energy generated per unit volume, $\dot{q}$ (W/m^3), and the change in internal energy, knowing densityρ (Kg/m^3) and specific heat of the material c_p (J/(Kg*K))

3.3.2 Convective Heat Transfer

Convection heat transfer is the transfer of inner energy by the movement of a fluid. Convective heat transfer essentially includes two different types of energy transfer, the energy transfer due to the diffusion and the one due to advection. Advection is the energy transferred caused by a larger scale bulk motion of the fluid, whereas diffusion is the random molecular motion which dominates when the bulk velocity is zero.

Convection is usually divided into two categories, natural or forced convection. Natural convection occurs when the density, and consequently the relative buoyancy, changes because of heating of the fluid. The denser components descend while less dense components rise. This results in a movement of the bulk fluid. Forced convection, however, is fluid motion due to for example a pump or a fan, i.e. when the fluid is forced to move by external sources. Forced convection provides an increase of the heat transfer rate at a surface, and is often used when natural convection is not sufficient for cooling or heating applications.

At the surface of a wall where the fluid velocity is zero, there is no advection and the heat from a solid is transported by diffusion and conduction. The velocity of the fluid is important because the temperature gradient is dependent on the rate of which the heat is carried away by the fluid. Therefore, a high velocity is proportional to a high-temperature gradient and results in a greater convection rate.

Newton's law expresses the overall effect of convective heat transfer at a surface.

$$q'' = h * (T_S - T_{ref}). \tag{27}$$

The local surface heat flux q'' (W/m^2), is the energy transported per square meter, h (W/(K*m^2)), is the local convection heat transfer coefficient, T_S is the surface temperature of the wall and T_{ref} is a characteristic temperature of the fluid moving over the surface.

3.3.3 Radiation Heat Transfer

The third heat transfer model is the radiation. Electromagnetic radiation does not need matter to spread, unlike convection and conduction heat transfer. Nevertheless, all kinds of matter emit radiation. The heat flux emitted by a surface is given by:

$$E = \varepsilon * \sigma * T_s^4. \tag{28}$$

Where E (W/m^2) is the rate at which radiation is emitted from a surface per unit area. T_s is the surface temperature and σ ($W/(m^2*K^4)$) is the Stefan-Boltzmann constant. The surface emissivity ε ranges between the values zero and one.

If the amounts of radiation energy absorbed, reflected, and transmitted when radiation strikes a surface are measured in percentage of the total energy in the incident electromagnetic waves. The total energy would be divided into three groups; they are called absorptivity (α), reflectivity (ρ) and transmissivity (t).

$$\alpha + \rho + t = 1 \tag{29}$$

- Absorption is the fraction of irradiation absorbed by a surface.
- Reflectivity is the fraction reflected by the surface.
- Transmissivity is the fraction transmitted by the surface.

4 Computational Fluid Dynamics (CFD)

Computational Fluid Dynamics (CFD) can be described as the investigation of fluid motion, heat transfer and other related phenomena, through the use of numerical methods to solve systems of differential equations with the use of computers. The vast majority of real world problems do not have an easy solution and can not be solved as a single and discretized problem. For these cases, a mathematical model solution is required.

CFD (in this case study with STAR-CCM+) is a powerful engineering tool when trying to understand the thermal processes in complex systems as an actuator. Some physicals phenomena are difficult to predict and measure. For that reason, CFD is a useful tool to understand the complexity of the studied system. It also provides the possibility to do multiple study cases without having to perform them in a test bench. This procedure implies a save of money and time to the investigation. This kind of programs is usually used in an early step in the development of an engineering product to anticipate possible problems and suggest improvements in the design.

Develop of the project through CD-adapco software STAR-CCM+, is explained in the following chapters. The fundamental equations used by the program, along with other important variables, as can be physical and meshing models, are also exposed. Further information can be found in [3] and [11].

4.1 Basics of STAR-CCM+

Computational fluid dynamic programs are based in Navier-Stokes equations. These results in every simulation are controlled through the residual plot that indicates the accuracy of the studied simulation. The accuracy of these values follows the criteria of a balanced system where three fundamental law physics happen:

- Conservation of mass,
- Conservation of momentum
- Conservation of energy.

STAR-CCM+ software is based on the finite volume method. This method takes the solution domain and discretizes it in a finite number of control volumes, which corresponds to the cells of the computational grid generated by the mesh. The discretized transport equations are solved for each control volume.

The system is composed by the $n * n$ matrix A, which contains the known coefficients, the vector K that characterizes the unknowns in each computational cell and the vector b representing the residuals.

$$A(k) * k = b. \tag{30}$$

Generally, two kinds of solution methods exist, for the equation, specifically direct solvers and iterative solvers. A direct solver solves the linear system of equations directly by finding an approximation of the solution by matrix factorization, where the operations depend on the number of unknowns. Direct methods, such as Gauss elimination, are costly from a computational resource and time point of view. Consequently, more memory and CPU time will be required to find a solution. These types of methods are therefore not suitable for practical problems including large grids. As the physical phenomena of the transport equations are complex and non-linear, an iterative solution approach is needed. Iterative methods begin with an approximated initial guess and then proceed to improve it by successions of iterations. Iterative methods have much lower memory consumption than the direct method.

Two numerical methods are utilized to solve the numerical form of the transport equations: the segregated solver and the coupled solver. The coupled solver approach solves the flow equations simultaneously and is suitable for compressible flows. The segregated approach solves the equations sequentially. The segregated solver then links every solved equation using a correction equation. It is both quicker and uses less memory than the coupled solver. The model is suitable for constant density and middle compressible flows.

The segregated flow solver can be combined with a steady state or implicit unsteady model. Transient flows generally govern the physical time-step; it is, therefore, necessary to set the physical time-step when running an unsteady simulation. The segregated flow solver carries out a selected amount of inner iterations within each time step, the greater amount of inner iterations the better solution converges. A smaller physical time-step mean that the solution changing less from one time-step to the next, the outcome is that less inner iterations are required.

4.2 STAR-CCM+ simulation

STAR-CCM+ (STAR) is a CFD-software developed by CD-Adapco with the purpose to introduce an easy-to-use engineering tool not only reserved for experts within the CFD discipline. Besides being a CFD solver, STAR is an entire engineering process for solving problems involving flow, heat transfer and stress. This is made possible by developing a suite of integrated components, together producing a powerful package that can address a wide variety of modelling needs. These components include:

- 3D-CAD modeller
- CAD embedding
- Surface preparation tools
- Automatic meshing technology
- Physics modelling
- Laminar/Turbulence modelling
- Post-processing

As for all CFD software, STAR follows a strict workflow when numerically solving a given CFD problem. Figure 11 below gives an overview of the workflow implemented in the STAR software.

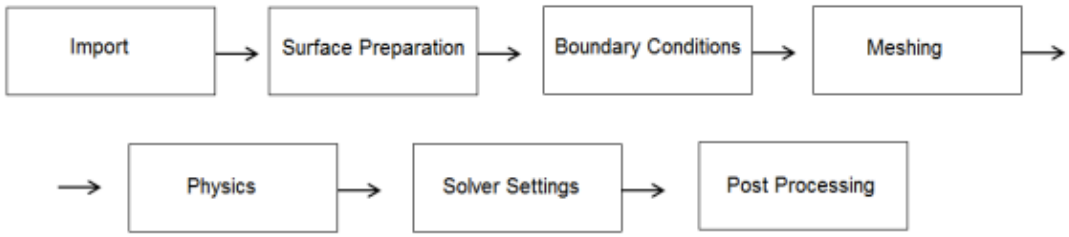

Figure 11: Workflow overview in STAR-CCM+

4.2.1 Modeling

Always in a STAR-CCM+ simulation, the first step to take into account is the preparation of the geometry that we are going to use for our study. This geometry can be implemented in the program through two ways: imported from an external CAD program (Solidworks, Catia,...) or created directly with STAR-CCM+ using a 3D-CAD tool that the program provides. This last method was implemented in this thesis due to the fact that this tool offers an easy way for further improvements and modifications in the initial geometry settings. This avoids the need of having to modify the initial geometry with an external CAD program and has to reimport it

to the CFD program. The 3D-CAD tool allows the possibility to change size on one or more components and re-run the analyses quickly.

The simulation was done in an initial stage with a simplified model of the actuator in order to avoid a cumbersome grid. Further improvements (more complex geometry including material properties adjustment for each part) in the electric motor area had to be done to get more realistic thermal results in the simulation. 3D-CAD tool allowed a more easy and quick environment for the development of the simulation. The evolution of the model at the end had the structure:

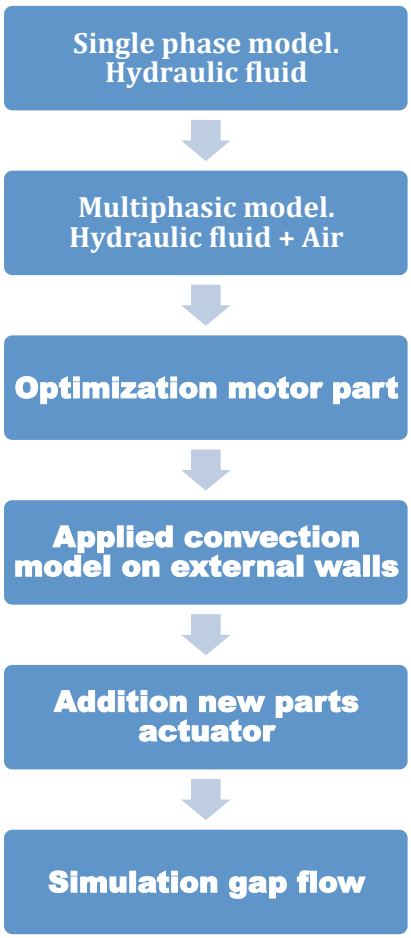

Figure 12: Model structure evolution

4.2.2 Mesh

An appropriated mesh allows good results through the analysis and avoids possible incongruences. Two steps are needed in order to get the best meshing possible: surface remesher and volume meshing.

- Surface remesher. This is one of the tools that STAR-CCM+ contains that is usually used to prepare the starting surface geometry to achieve a high-quality volume mesh. The surface remesher is used to re-triangulate an existing surface in order to improve the overall quality of the surface and optimize it for the volume mesh models. To provide a closed, manifold, non-intersecting surface (eliminating future volume mesh problems), the surface repair tool is also used in collaboration with the surface remesher to achieve the desired mesh.

- Volume mesh. Three types of core meshing models can be used to generate a volume mesh. The core meshing models are the tetrahedral, polyhedral and trimmed meshing models. The tetrahedral volume model has a tetrahedral cell shape based core mesh, such as a pyramid, and the polyhedral model produces a random core mesh with polyhedral cells. The trimmed volume model is based on a hexahedral cell shape core mesh. The polyhedral and the tetrahedral volume quality rely on the quality of the surface mesh, it is therefore really important to ensure a high quality starting surface. Polyhedral mesh is usually used for general purpose because is reliable, robust and suitable for conjugate heat transfer simulations. Trimmer mesh is used because it is fast and ensures a high quality. Although it is more suited for simulations with large domains as wind tunnels.

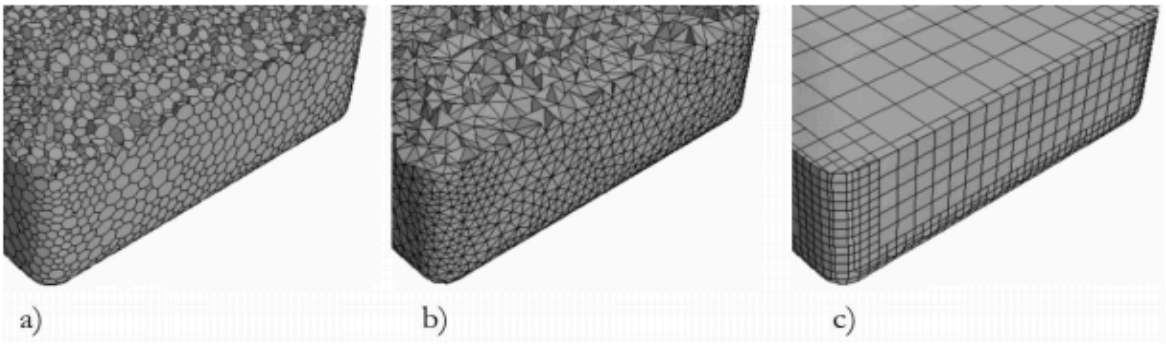

Figure 13: Overview different core mesh models a)Polyhedral b)Tetrahedral c)Hexahedral

Another important fact in our simulation is the use of the prism layer mesh. This adds prismatic cells near the walls (in addition to the core model selected). Prism layers allow the solver to resolve near wall flow accurately, which is critical in determining not only the forces and heat transfer on walls, but also flow features such as separation. See reference [3] for more information.

4.2.3 Boundary conditions

An important fact in every CFD simulation is the establishment of appropriately boundary conditions in order to avoid solution and convergence problems. Even with only one variable bad assigned in the model can deliver to an undesired solution. Therefore, it is always important to try to simplify a CFD model to variables that are under our knowledge.

In our case study, we can find different boundary conditions:

- Mass flow inlet. The filters lateral wall will act as a flow inlet for the hydraulic fluid inside the defined fluid region. The mass flow is known and is 0.1566 Kg/s.
- Flow-Split outlets. The pump is in possession of two holes that will act as the region where the hydraulic fluid streams outside our control region. Each one has a different mass flow. The outlet near the motor has a mass flow 1.35 bigger than in the far one.

These elements will make possible a fluid flux inside our actuator.

- Heat source. Referring to other boundary conditions we can talk at this point about the internal heat source that we have in the motor region. The heat losses calculated in this region are estimated in 450 W. This heat is distributed as equal heat transfer in all the motor wall cells. One of the problems that we will find as we take this forward, is the heat source dissipation in the different elements inside the motor and actuator that can effect the overall temperature levels. In an initial stage, motor will be considered as a unique region (this concept will be developed with every simulation).

- Walls. Regarding to the numerous walls that we can find inside in the actuator, as a rough model was considered that all the walls where adiabatic. The only ones where there is an important heat flow through it are the external walls that conform the box where all the actuator is contained. These walls are in contact with the external environment. These were considered to have a constant temperature of 333.15 K. These values are in concordance with the real case simulation measures tested in a controlled environment.

4.2.3.1 Energy balance

Regarding hydraulic flow, the model takes special account mass flux and energy through inlet and outlet. The reason for the special attention of these two factors is the use by the program of the discretization of an area. For that, the program uses a previously established mesh that has to the in concordance with the sizes of the global and punctual distances that can appear in the model.

The inlet is modelled which the lateral surface of the filter is discretized in smaller cells. Fluid flux is established in a perpendicular direction to this cell surface.

The temperatures in outlets, due their round geometry and because its discretized in smaller cells give a temperature distribution in a Gaussian distribution in this surfaces.

For having an exact knowledge of energy balance or imbalance that is occurring in the system, the exact value of the temperatures at these places is needed. To avoid a false value of temperature, and knowing that we have a Gaussian distribution, the best way to calculate it is with the mixing temperature. Knowing that the mixing temperature is:

$$T_M = \int \frac{(\rho * u) * T}{\dot{m}}\, dA. \tag{31}$$

Thanks to this equation to get an exact value of temperature is possible. Without this consideration and taking the surface average temperature, an approximation problem was done. This would mislead to energy imbalance of the system.

An important condition in this actuator was the energy loss dissipated in the hydraulic system (filter, hydraulic pump) of E_{diss}=150 W due to the flow from the hydraulic fluid through inlet and outlet. This value comes from the difference in the temperatures between inlet and outlets observed in the tests done in the laboratory which value was from 0.51 K. Due to the complex geometry of the pipes that drives the hydraulic fluid out from the hydraulic pump to the filter, these losses were directly implemented in the temperature difference from these two boundaries.

To keep this ΔU, the increment of temperature was added to the inlet with a field function:

$$\Delta T = \frac{E_{diss}}{\dot{m} * C_p}. \tag{32}$$

4.2.4 Physics

Depending on the different variables that we have in our model, different physics models need to be applied. Among a high number of models, the most important for this simulation are:

- Space, time and motion
- Materials
- Flow and energy
- Laminar/Turbulence
- Radiation
- Multiphase flow
- Heat transfer

As this thesis is studying a closed region where there are to find two different regions with two immiscible fluids, a multiphasic model approach was needed. The selected Physics for each material in this Thesis is to find in Appendix C.

4.2.4.1 Modelling multiphase

A CFD model can simulate the interaction of different flow materials with different thermodynamics states or phases, as gas, liquid or solid within the same system. STAR-CCM+ dispose of a large number of models that depending on the nature of the simulation fits better. There are two categories of multiphase. The first category is dispersed flows, such as bubbles, droplets and particle flows. For this type of dispersed flow, the phase occupies disconnected regions of space and is defined as a secondary phase when modelling multiphase flow analysis. The second category is stratified flows, for instance, free surface or annular film flows. There is also the possibility of modelling internal combustion and other reaction but does not concern to this thesis. See references [1] and [3] for more detailed information.

In this thesis case, two stratifies regions are studied. It is basically two immiscible regions (air and hydraulic fluid) that are in contact inside the actuator. An obvious approach would have been the implementation of a VOF model. The problem with this kind of approach is that it needs important background knowledge in VOF physics.

The interface between two immiscible fluids is called a free surface. The VOF multiphase model allows you to resolve the position and shape of the free surface, which is also important in evaluating surface tension effects.

A VOF model simulates not only heat transfer but also deformation in the coupled region. In fact, as there is a slow velocity field in the hydraulic fluid, there are no big deformations expected in the interface between the two fluids. So to achieve an easier model, and avoid the use of a complicated VOF model, a different approach was studied. We can see the Froude number to be sure about this affirmation.

In our case we know that we have a very slow stream with an average speed value (v) of 0.015 m/s. Defined by the actuator geometry we have that the mean depth (h) of the flow is 0.119 m. Substituting these values in the formula we obtain 0.01388. This value is very small and under 1. For that reason we know that we have subcritical stream with great accuracy. In this case we do not expect big waves our layer deformations in the upper part of the fluid region, and therefore, a VOF model can be neglected.

Both fluid regions were simulated finally as independent regions where there was no mass exchange between both, so they have a constant volume. Between both regions, a conducting buffer is established to permit the thermal exchange between both regions.

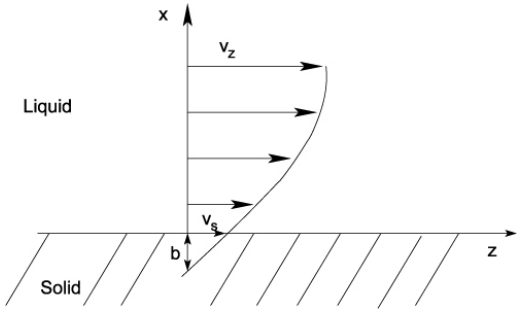

Figure 14: Slip condition model

Only with this method heat transfer would not be perfect between both regions, because we would be avoiding the dissipation effect due to convection. So there is the need to couple also the velocity field in both sides of the interface, so that the hydraulic fluid drag in the interface the air region also, and, therefore, share velocity field. To achieve this, an auto extract table was implemented. On the hydraulic region, a slip condition is implemented so that in the interface we have a velocity field induced by the fluid. This velocity field is extracted each iteration to an internal table. The air region takes this velocity field and implements it in the interface air boundary. As said before, these fluid regions have a constant volume, so there are no visible deformations in their geometries. For that reason, only tangential forces are transmitted (no normal forces). Vertical velocities are omitted.

4.2.4.2 Time

In STAR-CCM+, there are available three ways of modelling time. The function of the time models is to provide solvers that control the iteration and/or unsteady time stepping. The nature of the selected physics model determines what time model to choose, although sometimes the time model to use is not very clear and depends on the experience which one to choose. The three time models are:

- Steady.
- Implicit unsteady.
- Explicit unsteady.

For this simulation, a steady time model simulation was chosen. In steady state calculations, we integrate from some arbitrary state to the asymptotic solution in any manner, which will get us there in the least amount of computational work. This way we arrive at a time converged solution. If there were for example in a time depending model, an implicit unsteady approach were maybe more suitable.
Also, another fact is that with an implicit unsteady approach the definition of a time step is needed. This value depends on primary in two factors: average fluid velocity value and cell size. As in this simulation will be seen, the combination of this both factors is extremely small due a reduced cell size for getting a high accuracy in heat transfer and a small velocity field due to fixes inlet and outlet conditions. This would represent in a very high time simulation although the results would be more accurate.

5 Actuator simulations

5.1 Case 1: Only hydraulic fluid region

5.1.1 Description of the simulation

The first simulation was a simplified model in order to reduce possible complexity to the model due to the fact that the study covers a broad region. The studied region comprehends a multicomponent actuator. Each component with his own thermal and fluid flow characteristics.

As it can be seen in the Figure 15, the most important components where represented as simple geometries in order to avoid work to the grid and prevent possible mesh errors due to a complex geometry setting

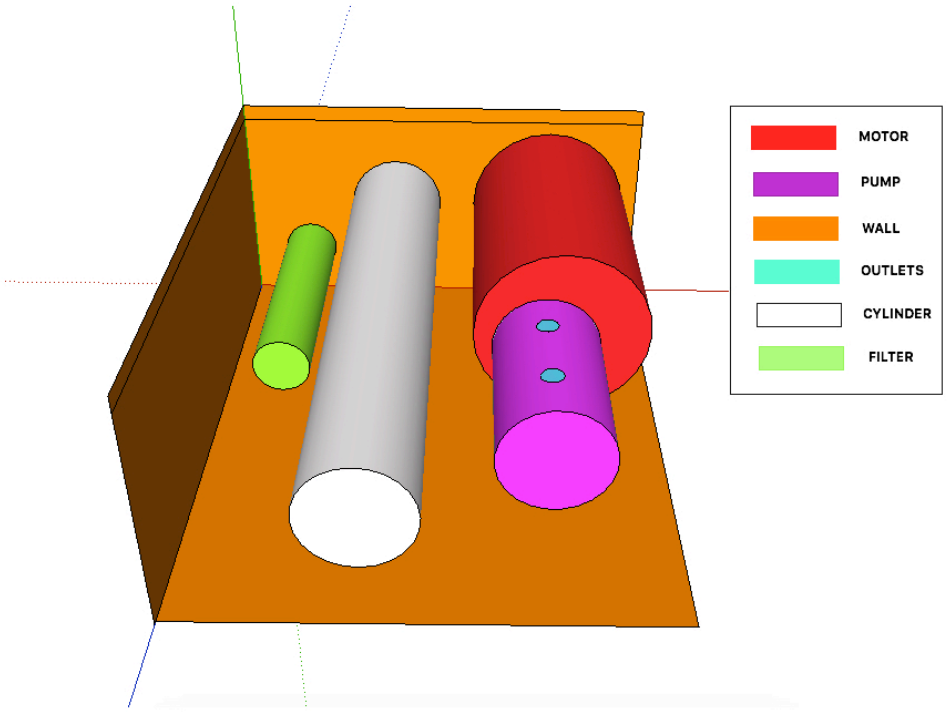

Figure 15: General 3D view (case 1)

5.1.2 Solution in STAR-CCM+

For the first simulation a coarse mesh model was implemented, and starting from that point, we looked if the solution was properly converged and if it needed a mesh improvement.

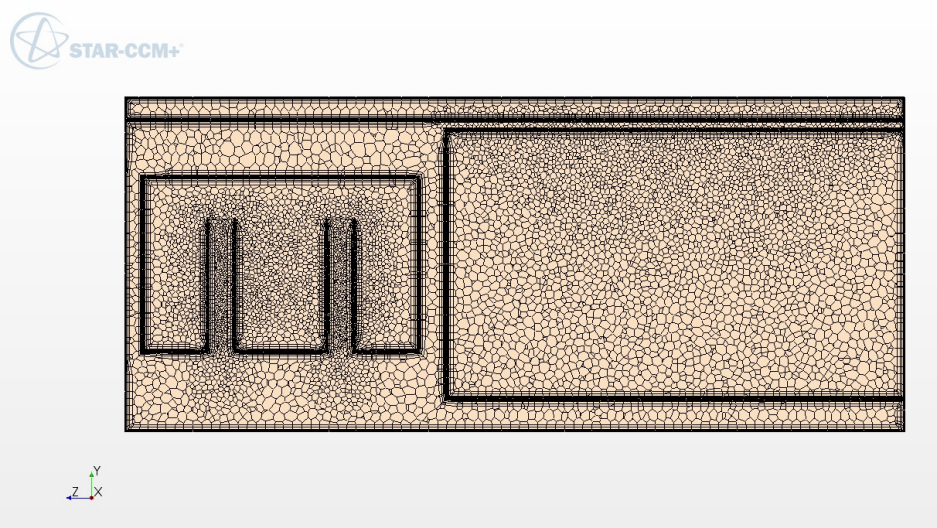

Figure 16: Vertical cut mesh (case 1)

In chapter 3 we can see explained the difference between the different mesh cell types that STAR-CCM+ offers. As we are dealing with a simulation where we are dealing with both fluid flow and heat transfer, the best choice for getting accurate results is the polyhedral mesh, as it is a more flexible mesh and more suited for heat transfer simulations. This kind of mesh cell type will be used for all the next simulations.

In this first simulation, a 4 mm grid was chosen with a growth factor of 1. Minimum cell size was also settled to a 33% value of the cell size. Due to the actuator size, this size cell was already fine enough. Only in the regions where it is smaller due to the geometry (as in the outlets conducts from the pump) we can appreciate a region where maybe an improvement in cell size where possible.

As we are working with heat transfer and fluid flow in this simulation, a prism layer thickness was also needed to define in the simulation. In order to ensure acceptable results, 4 prism layers were simulated.

Material properties are explained in Appendix B and boundary conditions are presented in Appendix C. An important fact to take into account is that from the 430 W that we have in motor losses, not all has been established in the motor region. As we have a multicomponent actuator, there are some mechanical losses in other parts of the system. For that reason, 150 W from this 430 W is established

in unknown areas where we have losses. As we do not know where these losses happen, we can assume that through the fluid flow comes inside the system, so that in a final stage, we still have 430 W that comes out through the actuator walls.

Hydraulic fluid has been considered in a first stage as laminar and with constant density and viscosity. Depending on the simulation results, physics improvements can be implemented.

5.1.3 Result and discussion

From this first simulation, we can see the main hydraulic fluid flow behaviour. This will be important to confirm the physics selected previously.

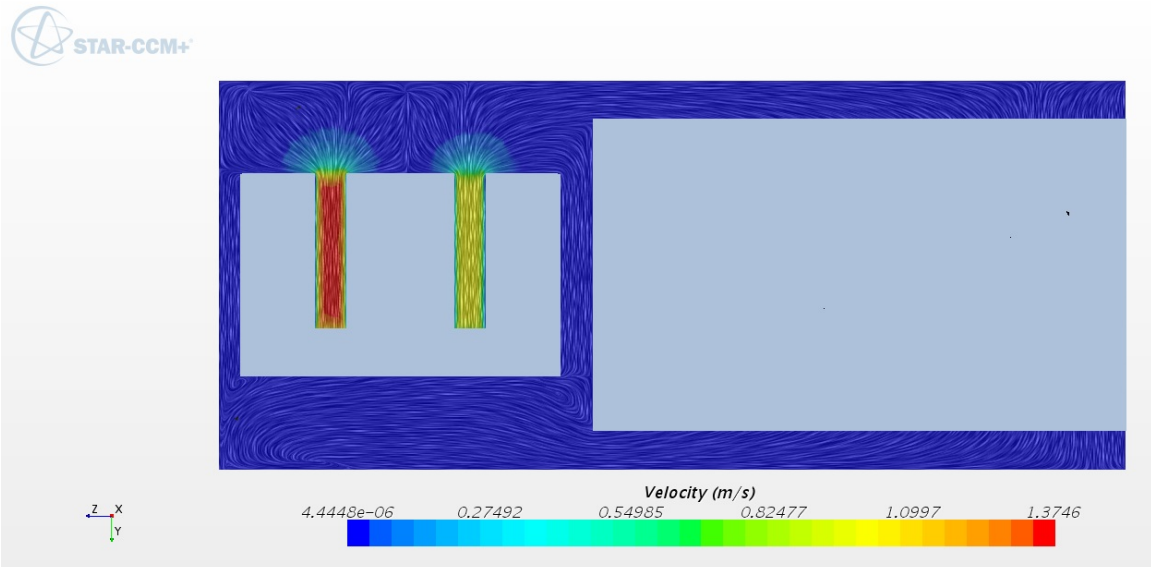

Figure 17: Projection of velocity vector onto the intersection plane - Vertical cut flux outlets-motor (case 1)

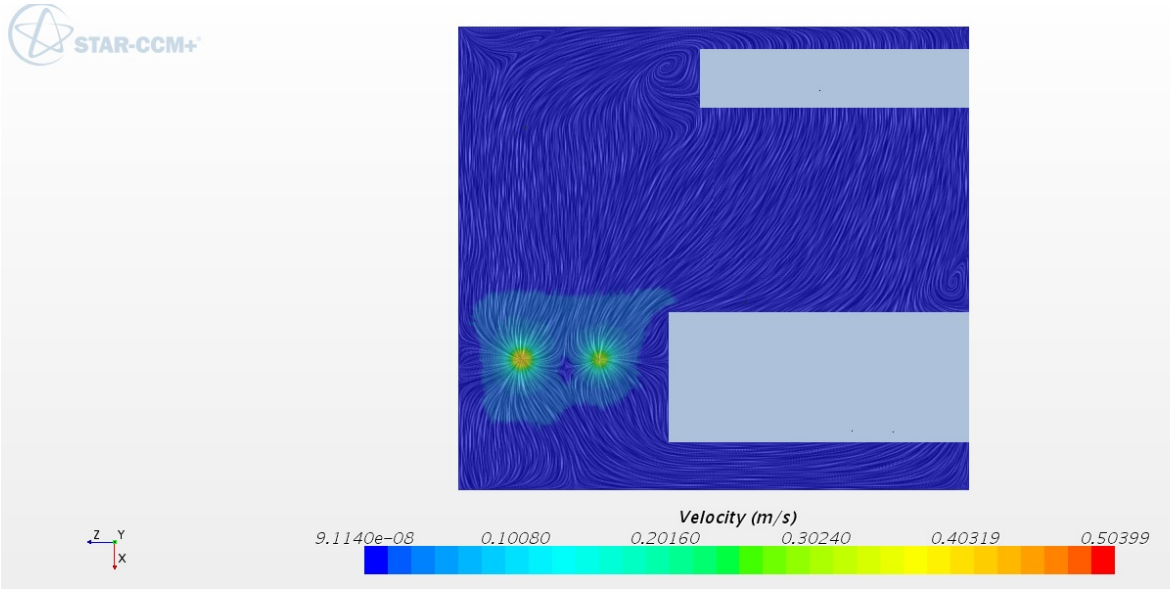

Figure 18: Projection of velocity vector onto the intersection plane - Horizontal cut flow (case 1)

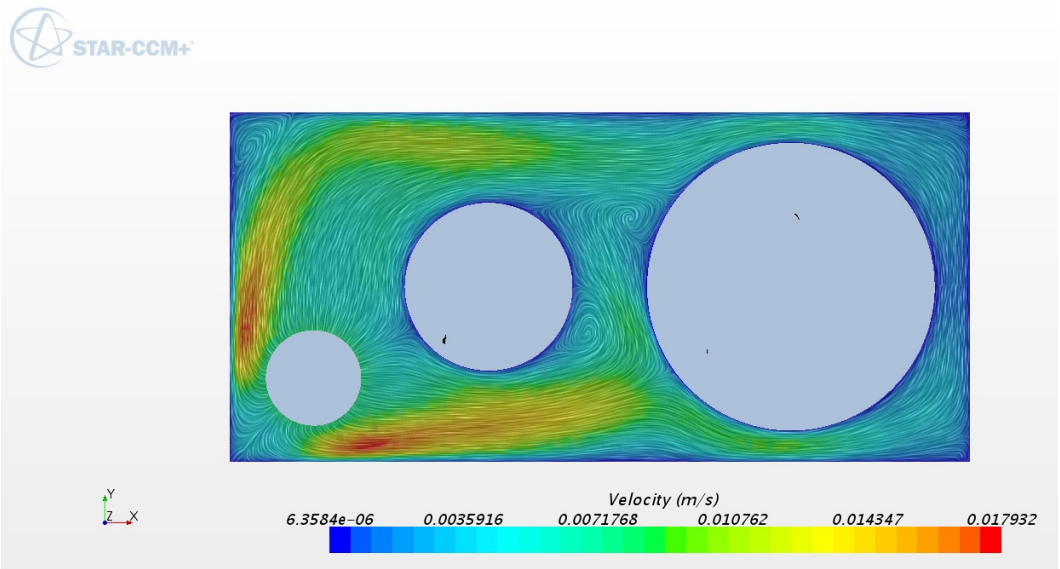

Figure 19: Projection of velocity vector onto the intersection plane - Vertical cut middle section (case 1)

When studying fluid-body interaction, one needs to determine the type of flow around the body. As we can see, we are all the time dealing with very small velocities in the entire fluid field inside the actuator. This means that we will not get very high Reynolds number $Re = \frac{\rho UD}{\mu}$, because of the effect of a low U

(characteristic fluid velocity) even if we have, as in this case, a low kinematic viscosity.
The convergence of the solution can be seen in the following three plots:

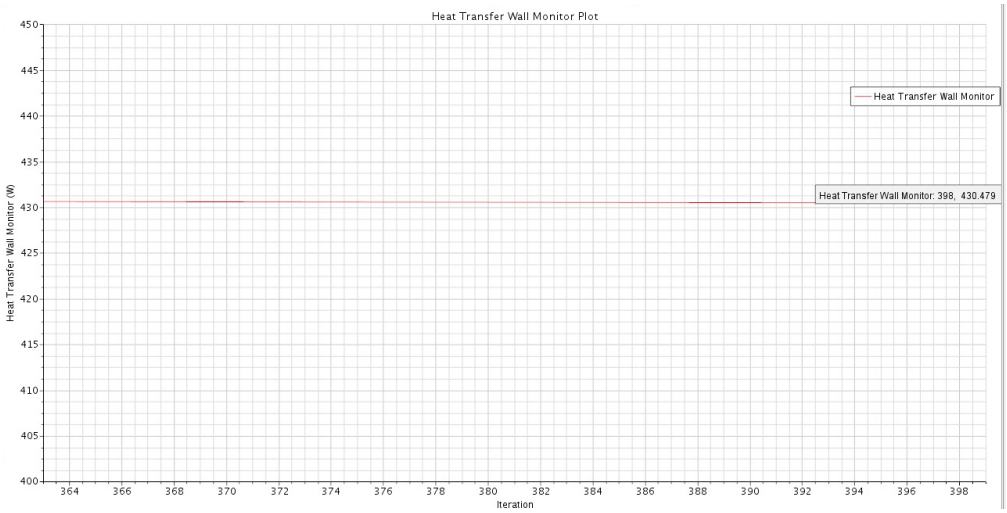

Figure 20: Heat transfer walls plot (case 1)

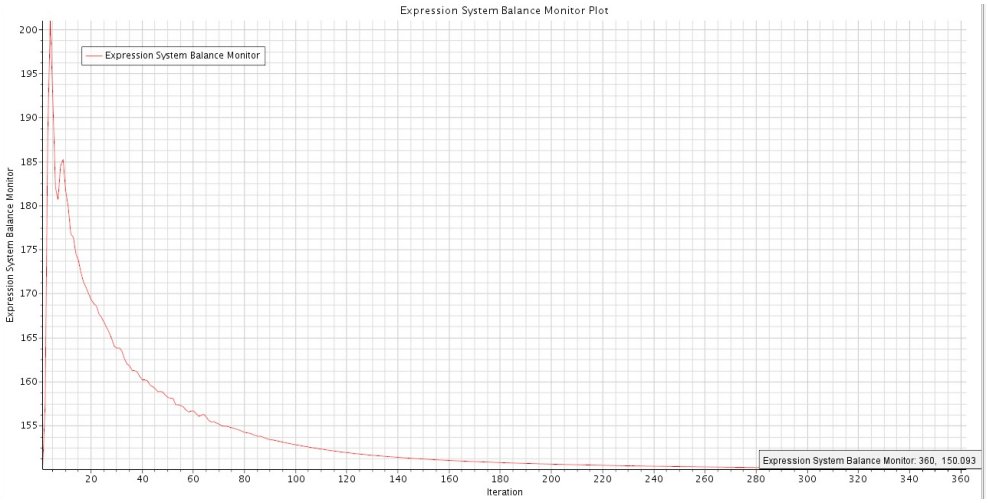

Figure 21: System balance plot (case 1)

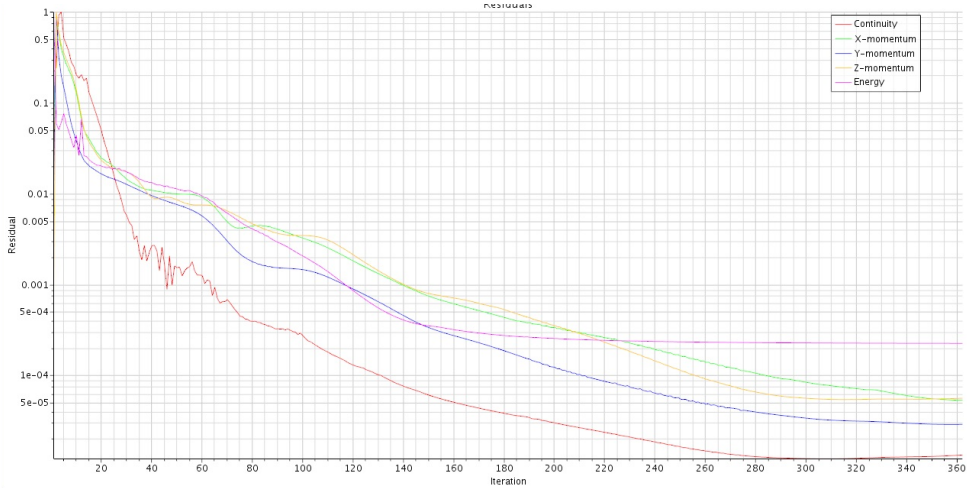

Figure 22: Residuals plot (case 1)

It can be noticed that the system energy balance is stable in the 150 W established with the internal field function so that through inlet and outlet we have this heat losses that come inside the system. We monitor another important variable to be sure that there are no incongruences, heat that does not appear or temperatures that are still not stable. This variable is the total heat transfer through the actuator walls. When this value arrives at the expected one and temperatures does not change with every iteration, we can assume a perfectly converged solution.

Residuals are also another way to be sure that solution is converged. It is recommended to not only use residuals as an indicator for convergence, butt also temperatures and heat transfers. In the graphic we can appreciate that continuity, momentum and energy are already converged and always under 1e-04 value. We can accept this simulation as very accurate and trustful looking at these factors.

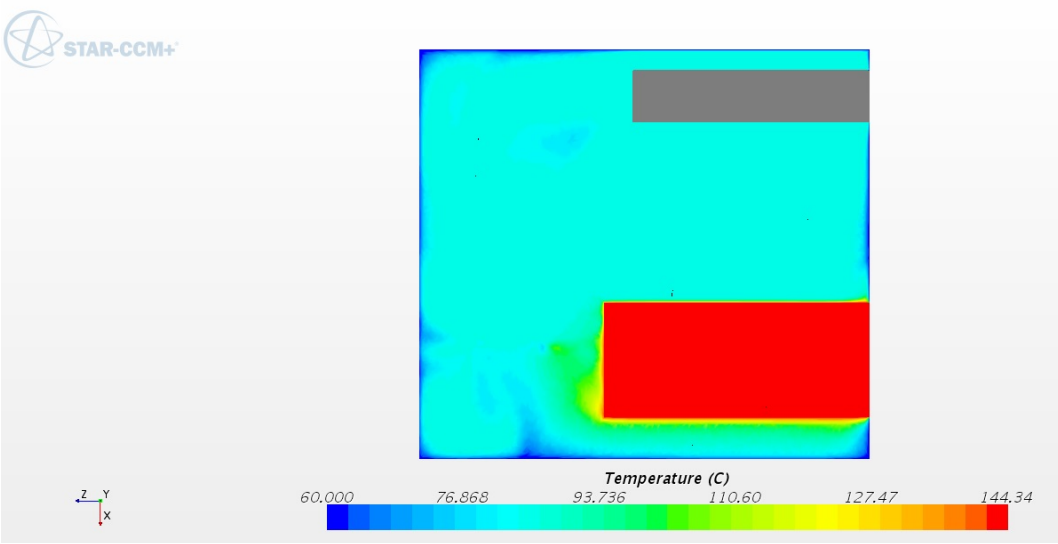

Figure 23: Horizontal cut temperatures (case 1)

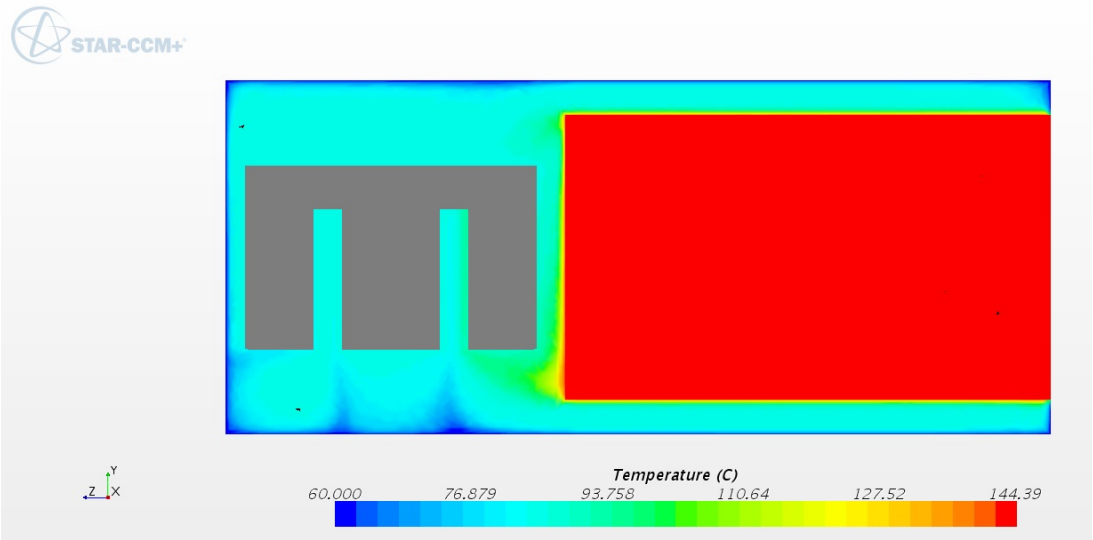

Figure 24: Vertical cut temperatures outlets-motor (case 1)

A curious thing that is to appreciate here is the small temperature gradient that appears in the hydraulic fluid when there is heat dissipation. This means that there is very fast energy absorption from the fluid. Heat distributes very quickly inside the fluid region resulting in a very homogeneous fluid temperature. Near the hydraulic bomb, there is too see how the colder fluid from the tank wall is dragged into the outlets.

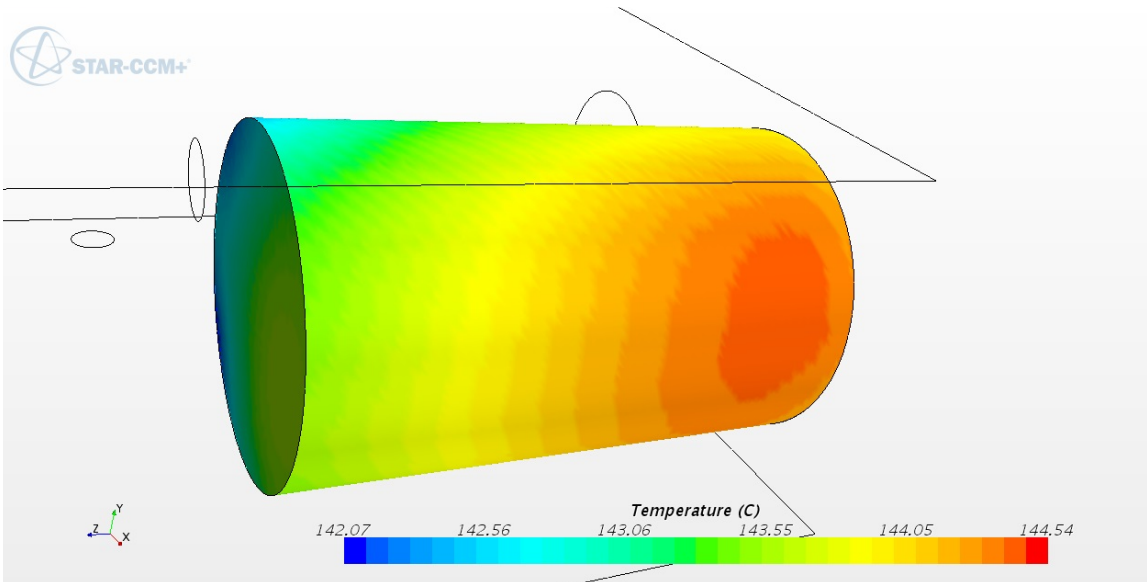

Figure 25: Motor temperatures distribution (case 1)

As we can see, motor region (settled in this first case as a completely aluminium region), obtains a homogeneous surface temperature due to the high temperature transfer that aluminium posses. So the temperature gradient in the motor wall is only of 2º C. We can only appreciate a slightly higher temperature on the side of the motor with a shorter distance to the actuator wall. This phenomenon is

induced because, as we can see in Figure 19, we have fewer streamlines in this side of the fluid region. This means we have lower fluid velocities and therefore the effect of convection is not so high for temperature decrease as in other parts of the motor.

5.1.4 Comparison with theoretical constant motor temperature model

The objective of this new study is the achievement of steady state temperatures in a case where we have constant wall temperatures and a constant motor wall temperature. This last assumption comes from the idea that materials in the electrical motor have high thermal conductivity and for that reason, temperatures inside the motor region will achieve approximately a constant temperature in his entire external surface.

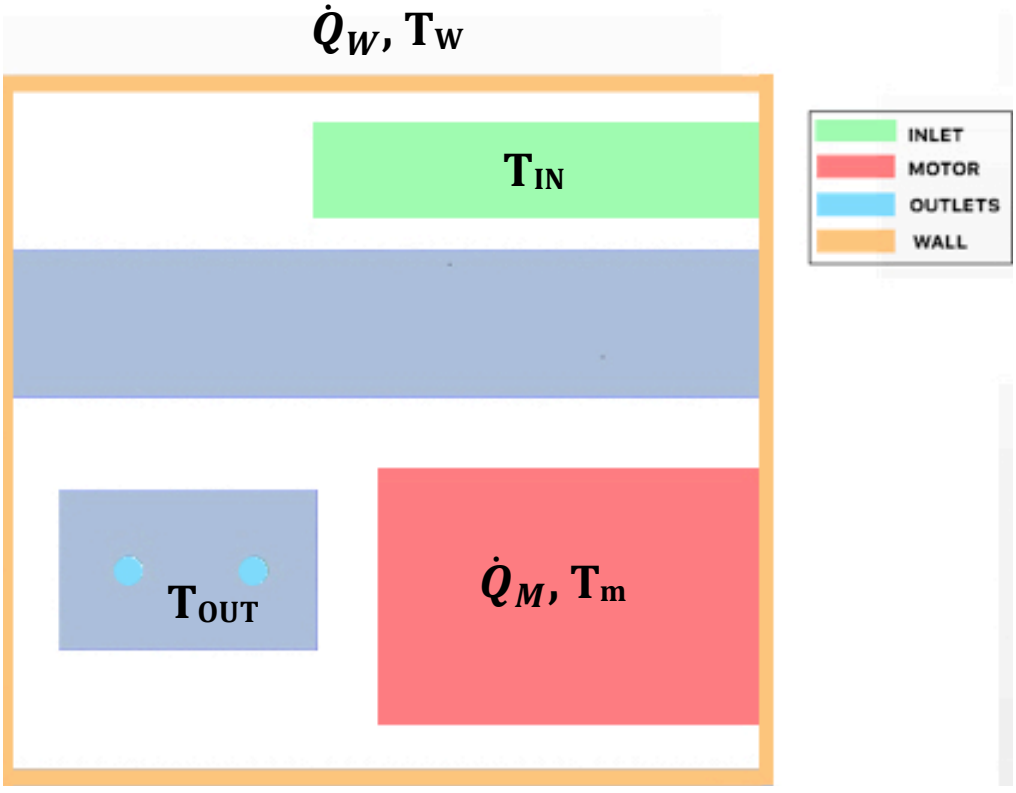

Figure 26: Model sketch heat sources and temperatures

With this assumption, a theoretical model was presented to predict this motor wall temperature. Inside our study region we see three important heat sources and possible transfer directions. As we have a motor that generates a heat we assume that $\dot{Q}_M$ enters our hydraulic fluid domain causing an increase in fluid temperatures. External temperature is assumed to be lower that the temperatures inside the actuator region due to the fact that inside the actuator we have a heat generation caused by the motor. So we can appreciate heat that leaves our study region through the actuator walls. Finally, we have heat flow driven by the effect of a flux between hydraulic fluid inlet and outlets.

Following the first principle of the thermodynamics we have

$$\Delta\dot{H} = Q - W; \tag{33}$$

as we do not have a change in volume we assume W=0 and only a variation in internal energy expressed as:

$$\Delta\dot{H} = \dot{m} * c_p * \Delta T. \tag{34}$$

As we do not know the exact amount of hydraulic fluid mass that transmits energy from one region to another, $\dot{m} * c_p$ is simplified as a constant value for each heat transfer that we consider (assuming that both values are constant).

$$\dot{Q}_M = a * (T_M - T_W) + b * (T_{IN} - T_W). \tag{35}$$

On the one side, we have the heat generated in the motor region that is dissipated through the wall surface and the hydraulic fluid that enters the actuator domain absorbs the rest of it.

$$(T_{OUT} - T_W) = c * (T_M - T_W) + d * (T_{IN} - T_W). \tag{36}$$

On the other side, we saw that part of the heat that absorbs the hydraulic fluid and escapes through the outlet is the consequence of the heat absorbed from the motor and that came inside the actuator region through the inlet, and that does not leave the actuator region through the walls.

$$\dot{Q}_W = e * (T_M - T_W) + f * (T_{IN} - T_W). \tag{37}$$

Finally, we see that the wall heat transfer is the result of the rest of the mass that leaves energy through the walls.

Taking together all this systems we have a three-equation system with six values that we want to know (a, b, c, d, e and f). To solve these two hypothetical situations are presented:

1) $T_M=T_W+100$ K; $T_{IN}=T_W$

2) $T_M=T_W$; $T_{IN}=T_W+100$ K

As we know already from the beginning, motor heat source and ΔU are known. We want that our motor generates 450 W and that we do not lose any heat through inlet and outlets. This means that all the heat flows out of our domain through the actuator walls. Knowing all this facts we get to the following results:

Variable	Value (J/s*K)
a	-0.27
b	-10.997
c	0.0245
d	0.8285
e	2.9396
f	-2.8577

Table 1: Variables table

When we compare these results with the previous simulation we see that $T_{IN}=T_{OUT}=360$ K and $T_M=512.5$ K. Final motor temperature achieves a very high temperature if we propose a constant wall temperature model. This can only mean that considering a perfect conduction of heat in the motor region is an error and that heat is dissipated from the motor to the hydraulic fluid region in a more complex way than predicted in this first supposition. In further simulations improvement in the heat source is proposed to study this phenomenon and discover which factor can influence decisively to achieve lower temperatures.

5.2 Case 2: Multiphase. Hydraulic fluid and air region

5.2.1 Description of the simulation

A next step in the simulation is the implementation of a multiphasic model. This situation represents a challenge due to the fact that as mentioned in chapter 3, we want to avoid the use of a VOF model that adds complexity to the thesis. So in order to achieve this, an alternative method was presented.

With the use of an auto-extract internal table, it was possible the coupling between hydraulic fluid and air region, avoiding this way the use of more complicated methods. For extra information about this point see chapter 3. Both regions were treated as constant volume regions in contact. Between these regions exists the typical heat transfer from solids in contact. The modeling of a thin solid between the two fluids in order to allow this heat transfer between two fluid regions was not necessary for this version of STAR-CCM+. The program automatically detects both regions and establishes a heat transfer condition.

5.2.2 Solution in STAR-CCM+

Same mesh type and size as in the hydraulic fluid region is applied to the air region. This air region comprehends a thin rectangular region above the hydraulic fluid region whose purpose is to work as an insulator for the upper part of the tank.

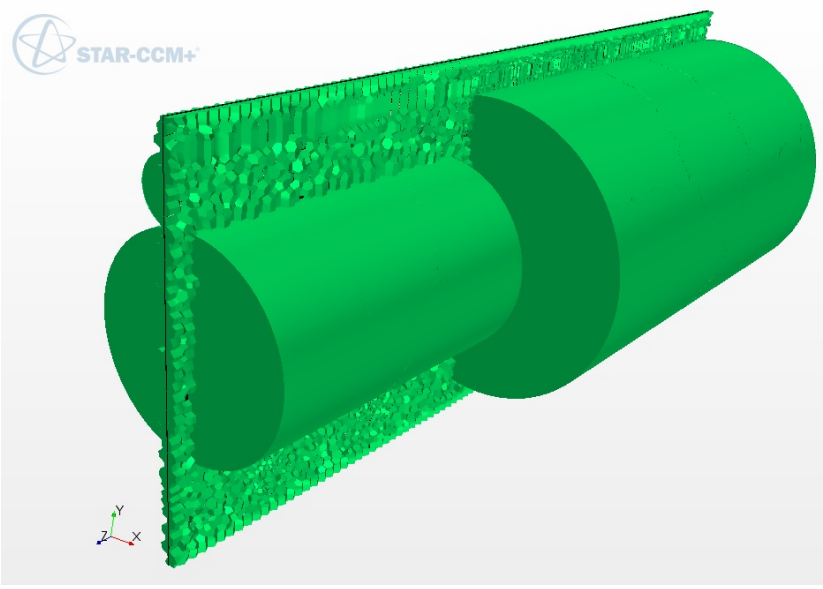

Figure 27: Vertical cut 3D cell representation

5.2.3 Result and discussion

Once applied this new changes we obtain with the program the following simulation results.

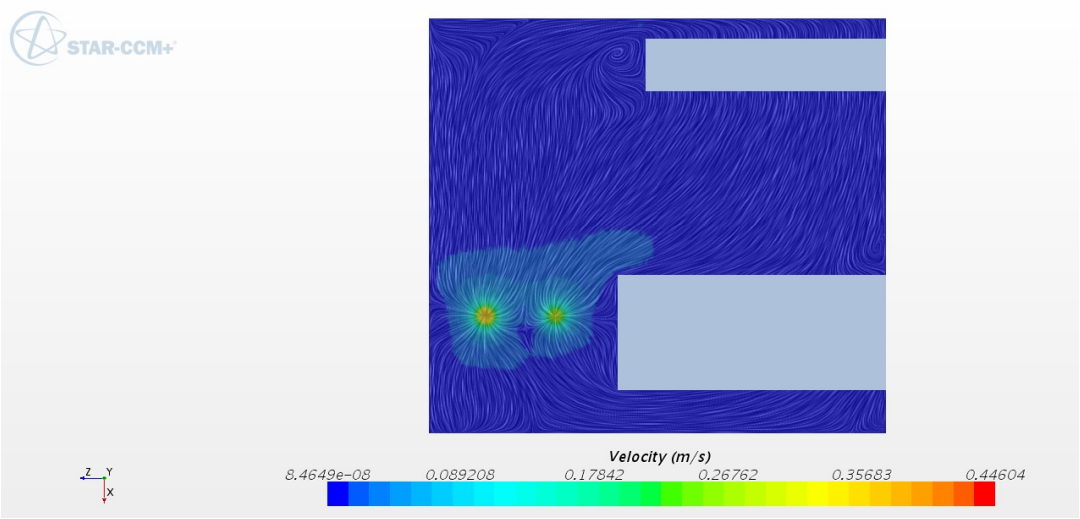

Figure 28: Projection of velocity vector onto the intersection plane - Horizontal cut flow (case 2)

As explained before in 4.4.1, multiphase was modeled following a coupling model between both regions with an auto extract table. Velocities in the hydraulic fluid region were extrapolated to the air region so that the heat transfer effect induced by the moving air is not avoided (for more information see again chapter 4.4.1).

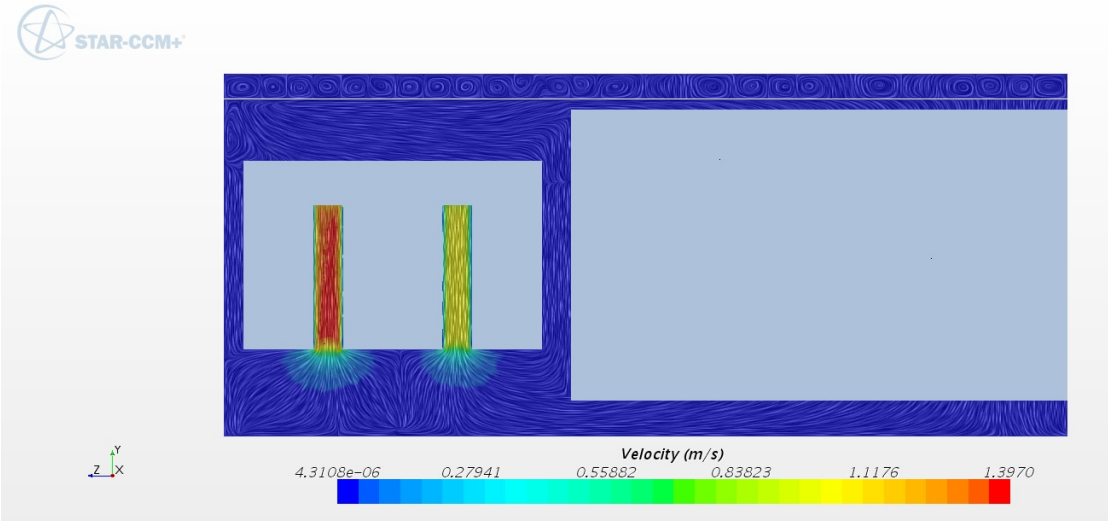

Figure 29: Projection of velocity vector onto the intersection plane - Vertical cut flow outlets-motor (case 2)

As we can still see in the hydraulic fluid region, velocities are very slow. In the air region, we also find low velocities, so a turbulent model can be discarded for the simulation. This theory is maintained for the next simulations, as no big changes in the velocities field are expected. Velocities are coupled in the shared boundary region, but due to the influence of natural convection rapidly change to another velocities values.

A remarkable fact to see in the Figure 29 is the appearance of rotating air rolls in the air region. This phenomenon is driven by the temperature difference between the inferior and superior part of the air region. As we have a Rayleigh number:

$$Ra_H = \frac{g\beta\Delta T H^3}{v\alpha} > 1708, \tag{38}$$

where g is gravity, β is the thermal expansion coefficient (equal to 1/T for the gas region), ΔT is the temperature surface difference (K), H is the characteristic length (m), v is the kinematic viscosity and α is the thermal diffusivity (m^2/s).

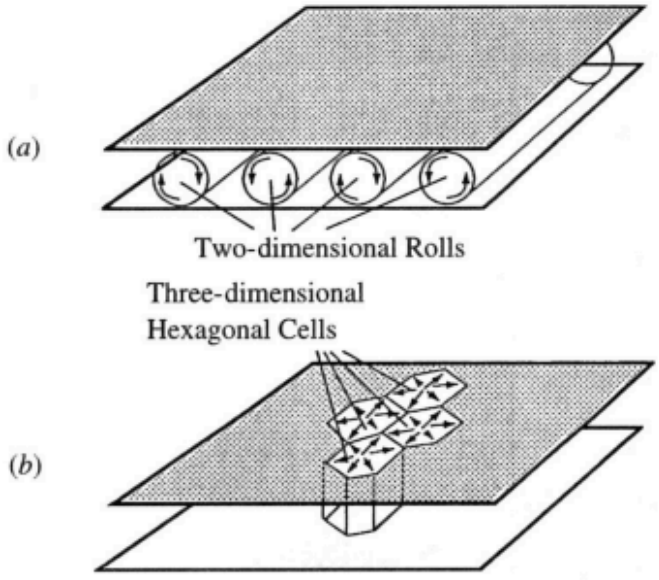

Figure 30: Rolls and hexagonal cells in natural convection in an enclosure heated from below

When the Rayleigh number exceeds the above critical Rayleigh number, the flow pattern is two-dimensional counter rotating rolls, referred as Bénard cells. The function of dimensional rolls is to promote heat transfer from the heated bottom wall to the cooled top wall.

As explained in chapter 2.1, for the calculation of the Rayleigh number we have to know that:

$$Ra = Gr * Pr = \frac{C_p * g * \beta * \rho^2}{\mu * k} * (T_S - T_\infty) * L^3. \quad (39)$$

In a first step we can calculate the Prandtl number from the air. Taking the values from the air from APPENDIX A, we come to the value

$$Pr = \frac{C_p * \mu}{k} = \frac{1003.62 * 1.855E-05}{0.026} = 0.716$$

As expected we get a low Prandtl value as we are dealing in this situation with air as the fluid media.

Knowing how to calculate the Grashof we have to extract the variables from our case study. In this case we have a T_S=94ºC and T_∞=60ºC. The characteristic length in this sitation is defined by the actuators geometry and it is 0.311m. The thermal expansion coefficient is calculated through the assumption of an ideal gas and therefore it is 1/T. Knowing all this we get:

$$Gr = \frac{g * \beta * (T_S - T_\infty) * L^3}{v^2} = \frac{9.81 * 0.00300165 * (94 - 60) * 0.311^3}{(1.855E-5)^2} = 8.7518E+07$$

At this point, it is possible to calculate the Rayleigh number as we already have the Grashof and Prandtl number.

$Ra = Gr * Pr$ =6.266E7

As we can see we have a very high Reynolds number and for that we can confirm a high influence of convection in heat transfer and the apparition of Bénard cells in our case, as we can see in the CFD simulations.

The convergence of the solution can be seen in the following three plots:

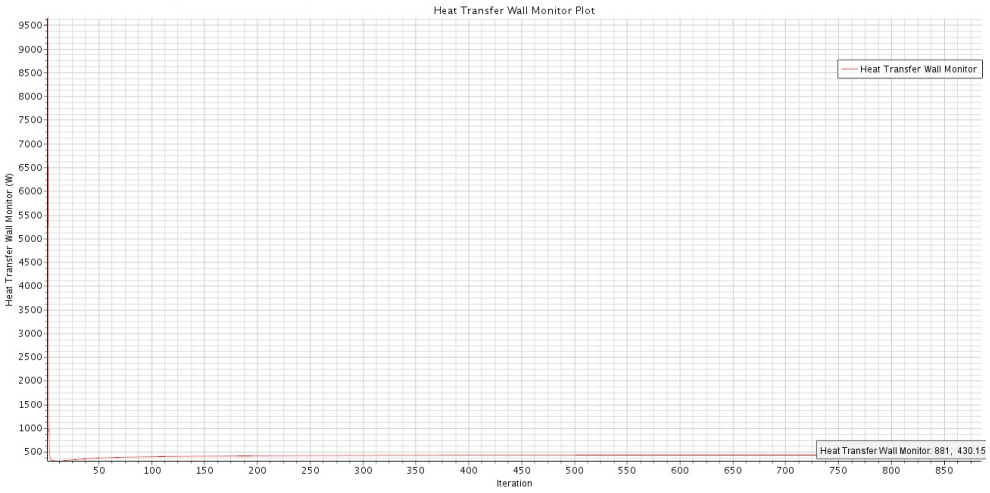

Figure 31: Heat transfer walls plot (case 2)

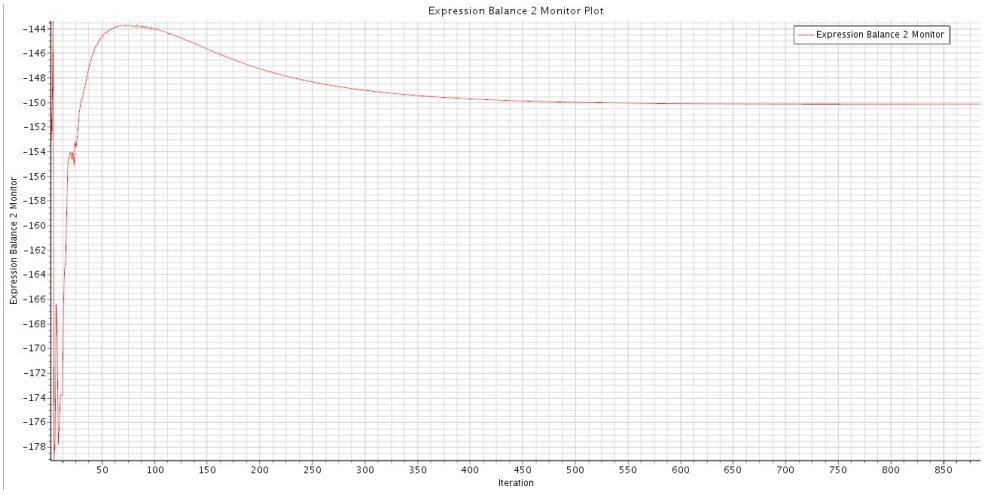

Figure 32: System balance plot (case 2)

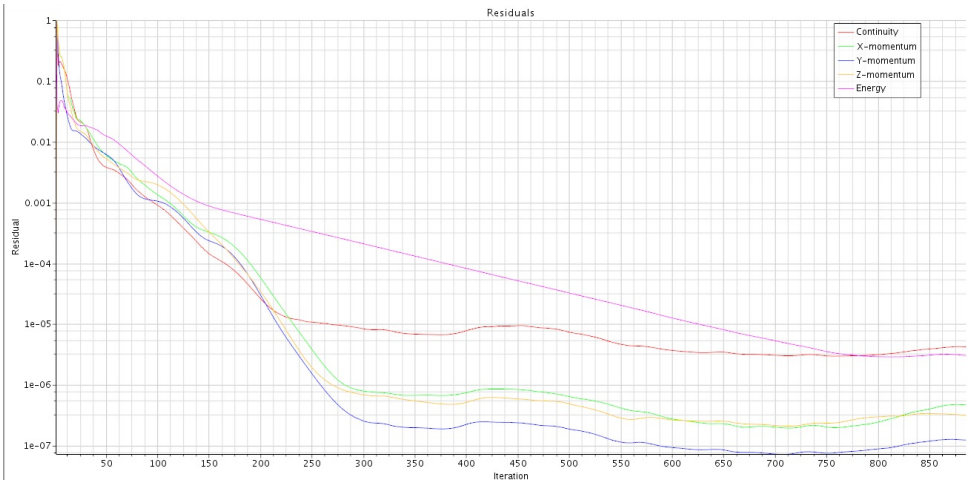

Figure 33: Residuals plot (case 2)

In the first two plots, we can appreciate that our system has accomplishments the requirements of energy balance. Through the walls, we can see 430 W and through the inlet we add to the system this 150W coming from unknown heat losses.

Looking at the residuals, we can see again how all the variables converge to values below a 1e-04 value. With this criterion, a plausible simulation can be estimated, always together with the temperature and heat plots control also.

Regarding temperature inside our actuator we get the following results:

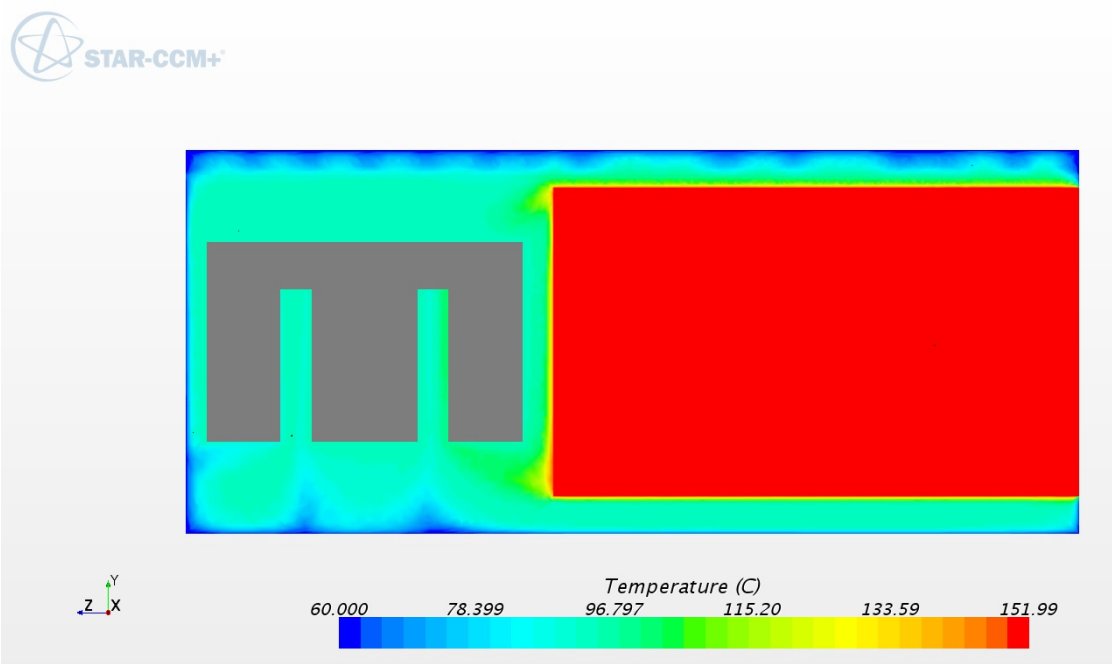

Figure 34: Vertical cut temperatures outlets-motor (case 2)

As explained before, we can see how the Bernard cells works in Figure 34. Heat is promoted from the contact boundary between air and fluid region to the cooled top wall. For that reason we can appreciate how the contact boundary is at ≈ 97ºC and the top at 60 ºC.

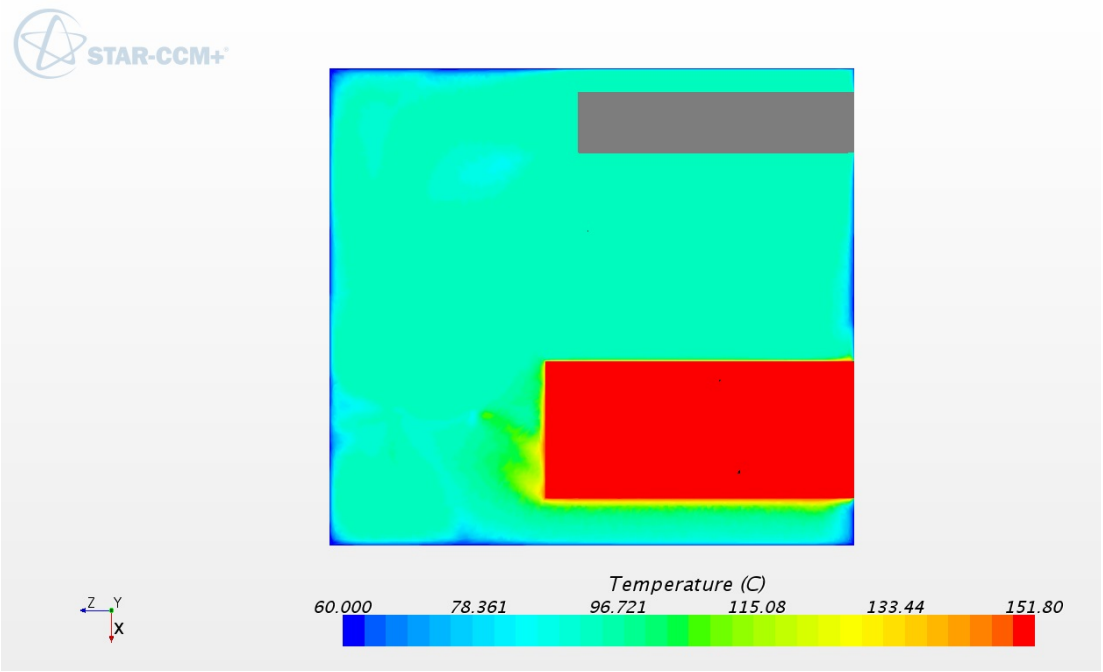

Figure 35: Horizontal cut temperatures (case 2)

In Figures 34 and 35, we can appreciate the same thermal behaviour in the fluid region as in the previous simulation. In Figure 34 we can see how the air region acts as an insulator due his lower heat transfer coefficient and has a bigger temperature degree region compared to the hydraulic fluid region. The overall actuator temperature and his components (motor) have a bigger temperature due to the insulator effect of the air region. Air region impedes heat to be removed from the hydraulic fluid region, causing a rising in temperature. In Figure 34, can be seen how warm air is dragged upwards and then cooled air returns.

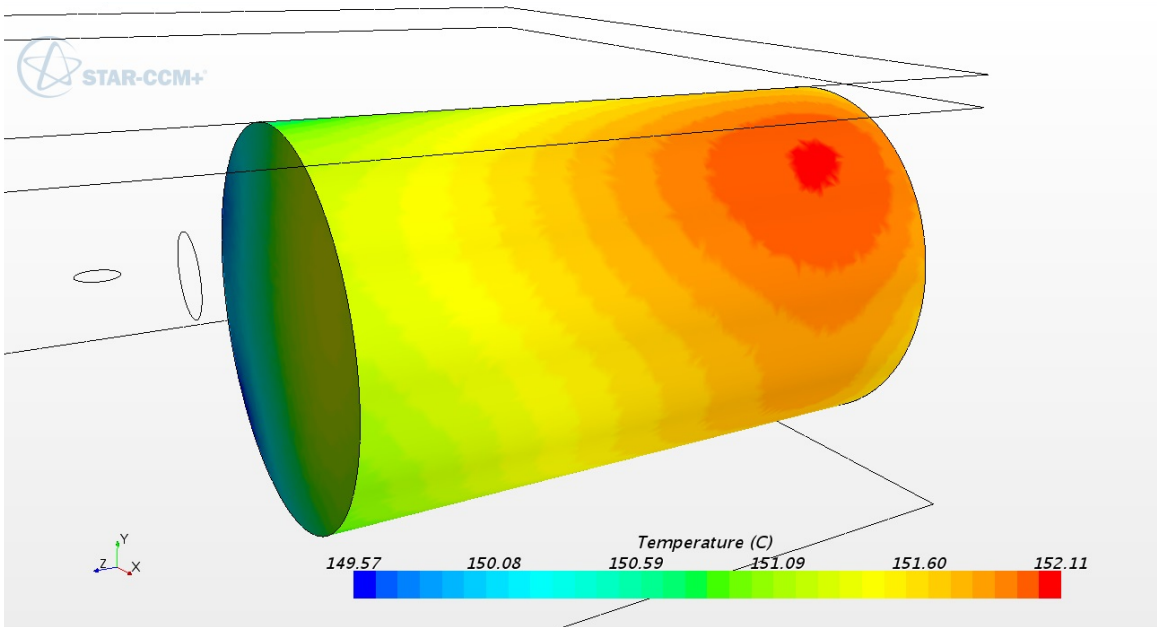

Figure 36: Motor temperatures distribution (case 2)

Another thermal phenomenon that we see is the hot spot in the motor surface. In an overall look temperature in motor surface still maintains nearly constant, only with a 2ºC difference for the same reasons as explained in the previous case. This time, we appreciate how the hot spot of the motor surface is slightly higher than in the previous case. This can be due to the influence of the insulation effect of the air region. Less heat if transmitted through the interface boundary between air and fluid. This means that fluid temperature increase near this interface and in combination with low velocities in this area show the expected results.

5.3 Case 3: Motor design improvement

5.3.1 Description of the simulation

As we still have in the multiphasic simulation too high temperatures compared to the desired ones, improvements in simulation design are needed. Motor region is where the biggest difference with reality to find is. This means that motor design improvements are necessary.

The first simulation was driven with a simple geometry model of the electric motor. It consisted in a simple cylindrical form with the biggest motor sizes referring to length and radius.

As exposed in chapter one, the electric motor is composed by more than one component (see references [2] and [12]). Each component has different thermal properties as we are studying components with different materials. The calculation for each part properties is exposed in Appendix B. Every component also generates their own heat losses (due to friction, resistance loss…). So in order to improve thermal results and achieve a more realistic model, motor was discretized in the basic parts that an induction motor has and can have a representative effect on the thermal dissipation and distribution (see references [7] and [14]):

- Rotor
- Stator
- Coils
- Shaft

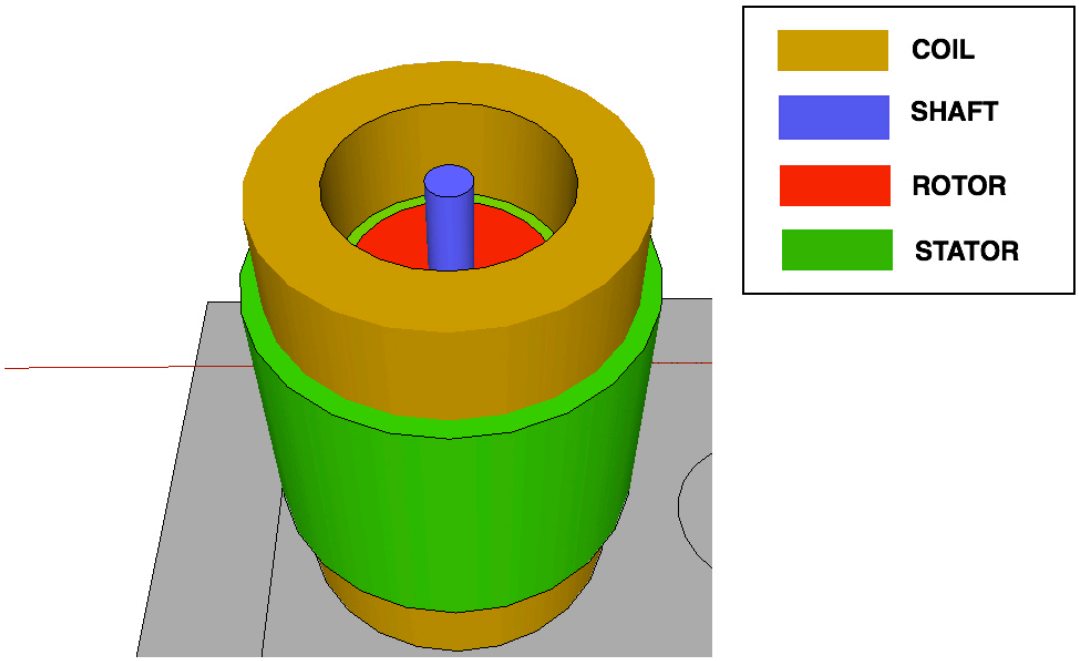

Figure 37: 3D motor parts view

5.3.2 Solution in STAR-CCM+

For this simulation in a CFD perspective, the main changes wherein the motor part. Each motor part was modelled with its own material properties and considered as an independent heat source part each one.

5.3.3 Result and discussion

Results in velocity field are not to be expected very different in this chapter compared to the previous one. Only in the surroundings areas of the motor, there is a difference induced by the new motor geometry, but, in any case, affecting in a special way stability from the general model.

This is a very good cut to appreciate the velocity coupling between the air and hydraulic region (see 4.4.1). As we can observe in the Figure 38, velocities in both sides of the boundary share the same velocity field. This has a direct effect in the evolution of the air flux in the air region, causing new air velocities.

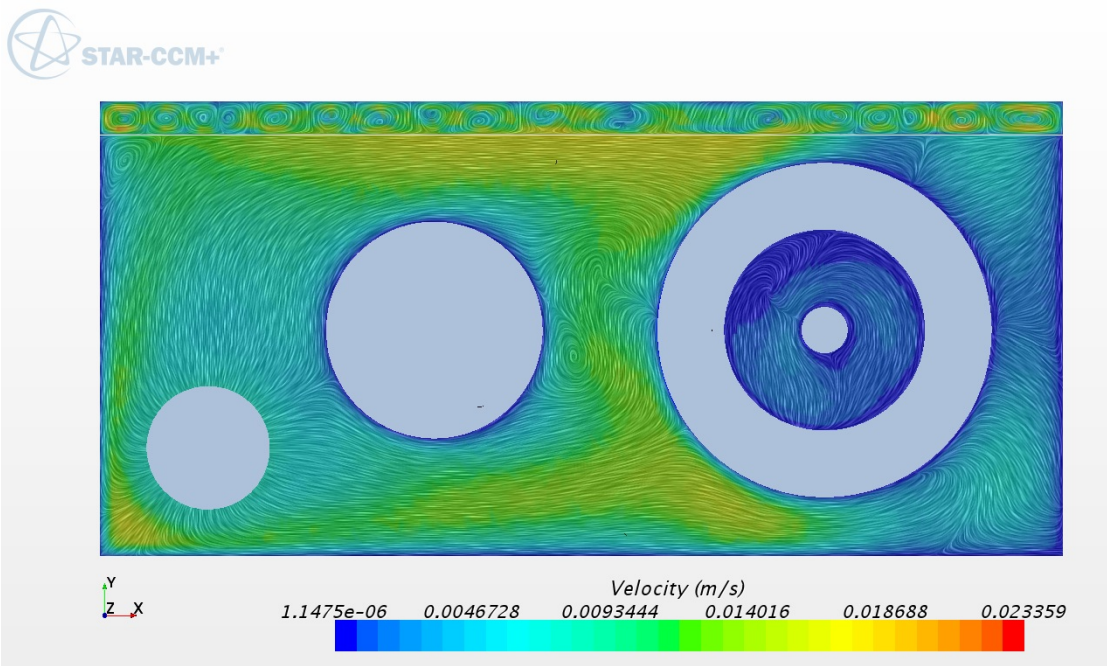

Figure 38: Projection of velocity vector onto the intersection plane - Vertical middle section flow cut (case 3)

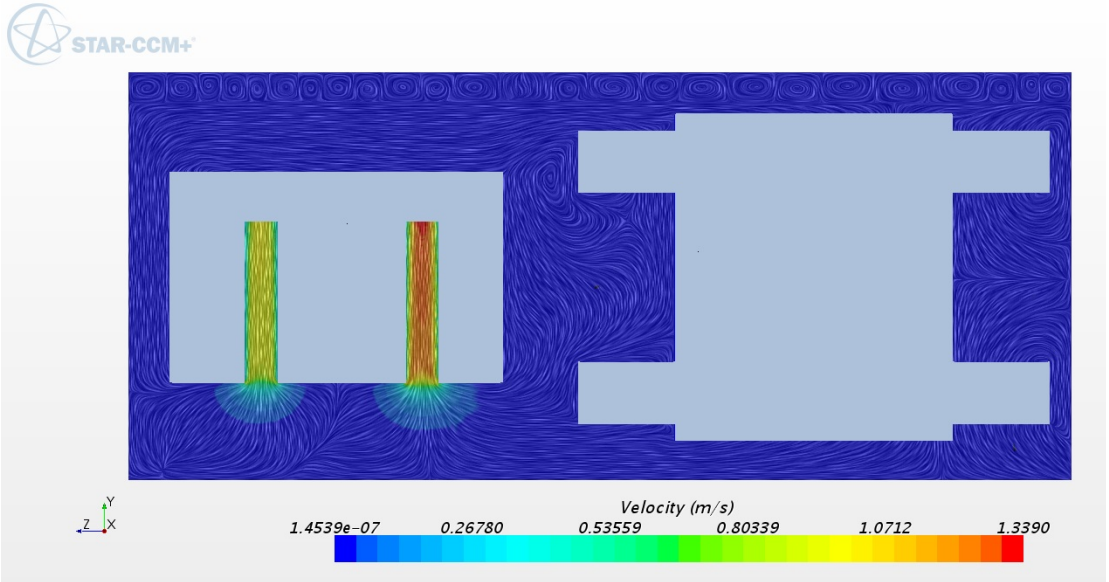

Figure 39: Projection of velocity vector onto the intersection plane - Vertical flow cut outlets-motor (case 3)

There is to see in Figure 39, that due to the effect to of coupling between fluid and air region, in the middle section of the boundary where the imported velocities are higher, the Bénard cells suffer a bigger distortions due to a moving lower surface.

In the regions kept between the coils, stator and rotor velocities are low driven by the complex geometry that does not make possible an easy flow inside it.

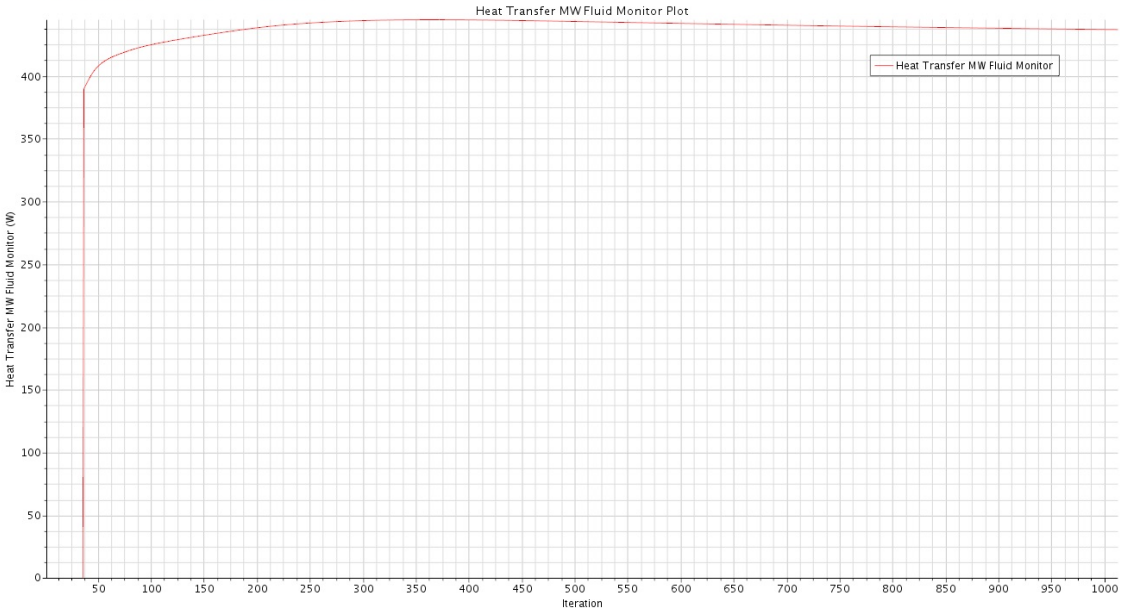

Figure 40: Heat transfer walls plot(case 3)

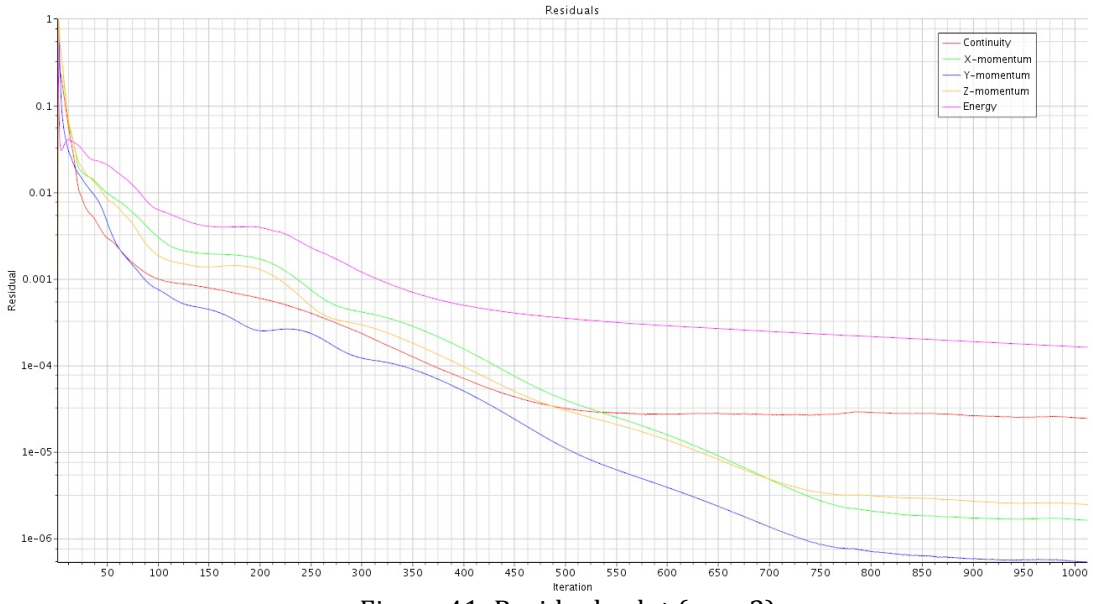

Figure 41: Residuals plot (case 3)

Heat transfer through walls and residuals gives a positive view of the simulation in terms of convergence.

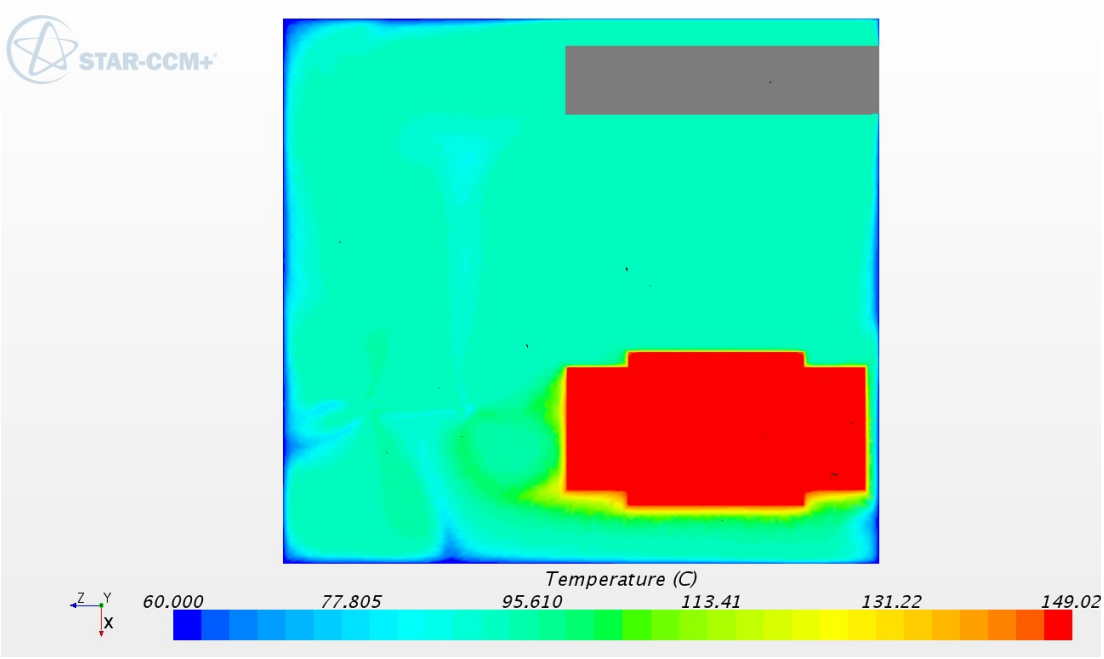

Figure 42: Horizontal cut temperatures (case 3)

We can see that in the walls near the inlet and motor region the temperature gradient is very small and if we look to further wall points we see an increased temperature gradient.

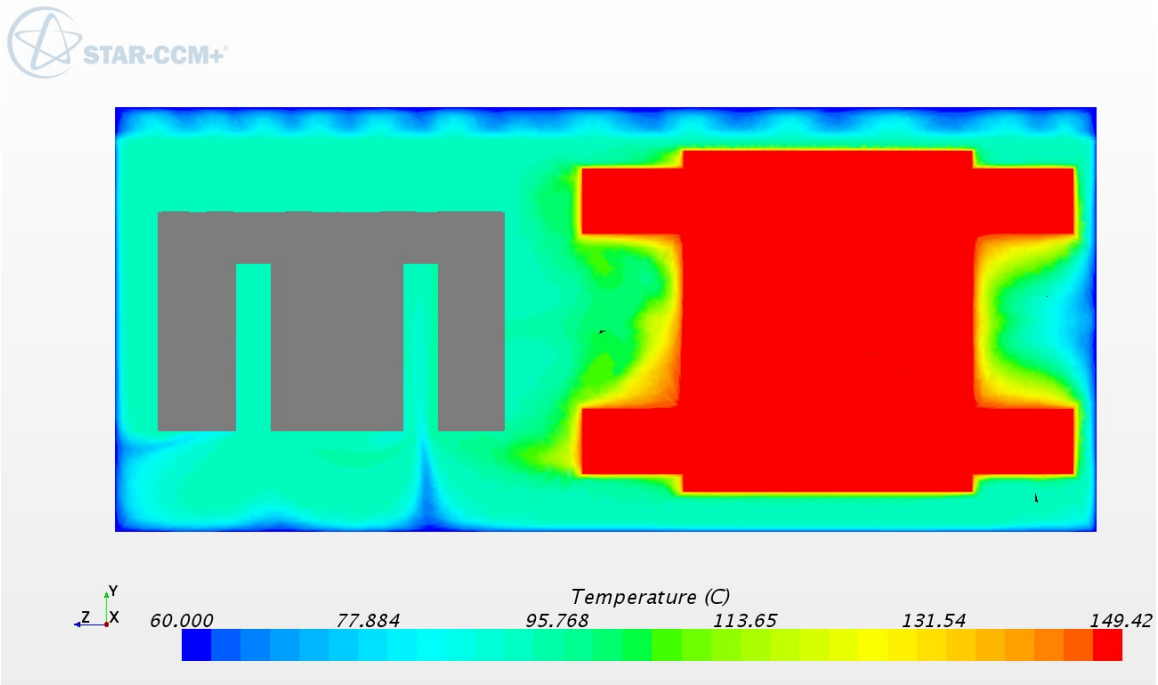

Figure 43: Vertical cut temperatures outlets-motor (case 3)

Due to motor geometry improvement we see a slight decrease of motor overall temperature. There is an improvement in heat transmissions with this new geometry allowing bigger heat transfer transition areas (especially in region comprehended between coil, rotor and stator).

5.4 Case 4: Simulation of gap flow influence

5.4.1 Description of the simulation

At this point, observing the results in case 1, 2 and 3 we arrive at a conclusion. Setting heat source as a homogeneous region condition leaves as a too high-temperature field in the motor area. This can only mean that we have another way of heat transfer inside the motor region to the fluid region.

Due to a differential pressure in both sides of the motor area, a pressure induced fluid flow appears. Through this flow between rotor and stator, part of the heat produced in the motor region is dissipated, inducing this way lower temperature values for the motor.

5.4.2 Solution in STAR-CCM+

A problem when starting the CFD simulation is the simulation of heat transfer in the gap area. We have now to simulate a motor gap of 0.5 mm and we have now also a cell size of 4 mm. In this gap area is recommendable to set at least 5-10 cells to get plausible results (we have fluid flow and heat transfer). So for that simulation a cell size of 0.1-0.05 mm would be needed. This means increasing the number of cells in the simulation in a notable way. This is an increase in simulation weight and, therefore, more time to achieve a convergent solution. Another fact of temperature reduction in the simulation was that inside the actuator, there were losses in other regions outside the motor, considering that our system is based in 430 W entering to the motor. So another three regions were identified: losses in the hydraulic pump, cylinder and throttle region. Throttle region is confined in a new actuator part. This new part consists in a region where the electronics of the actuator are. Inside this region, there is also a throttle mechanism that controls pressure in the hydraulic flow. In this region, there is only air (no hydraulic fluid). Between this electronic part and the old actuator design is a plate where heat is transmitted between both regions. Both actuator regions (the region from previous simulations) and electronics region are covered with a 7 mm aluminium thick layer where all the components are sheltered.

To avoid such a complex situation in the motor region, an alternative solution was presented. In order to achieve the most value of heat transfer through this gap, a simulated flow was implemented. Starting from the geometry from case 3, we appreciate that rotor and stator are directly in contact. An enclosed region over the rotor in each side, in the situation where in reality should be the gap, was modelled. Through this model, the needed mesh for a 0.5 mm gap was avoided.

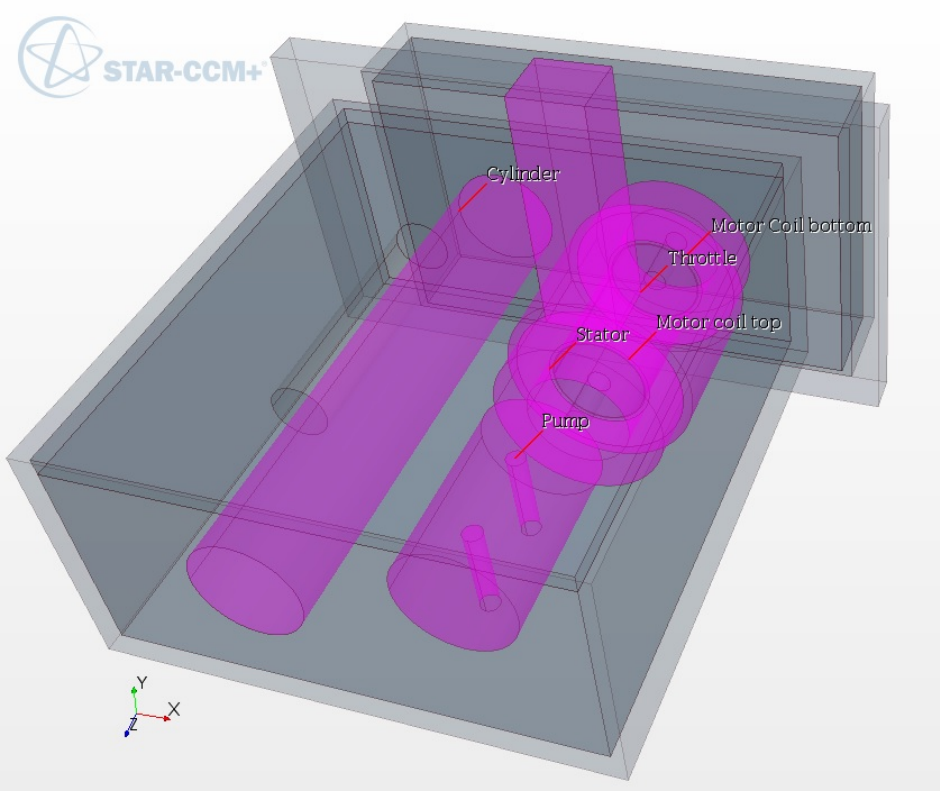

Figure 44: General view. Improved model

Two variables appear in this new simulation method to get a similar real simulation: heat transfer through the gap and fluid flow. As it is difficult to know this values and needs from experimental measures, a different situation where studied. First of all, the velocity of fluid flow inside the gap was simulated with different values: 0, 10, 30 and 50 mm/s fluid flow was simulated. This degree of velocities will also show how important fluid flow through the gap is for the motor heat transfer.

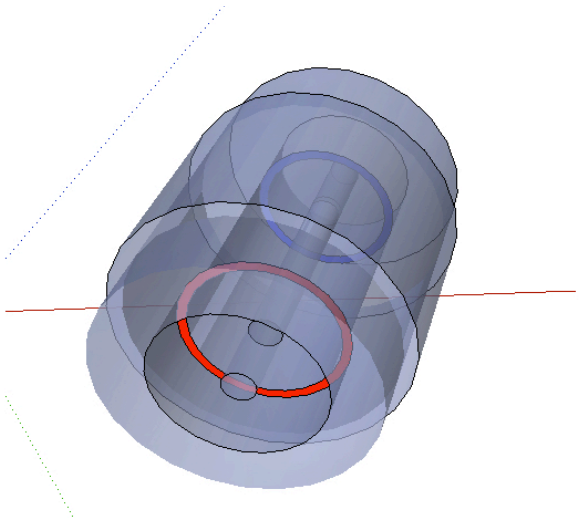

Figure 45: Gap flow regions. Inlet (red) outlet (blue)

Heat transfer profile inside this gap area is complex to calculate due to the fact that we have radial flow (induced by the rotor movement) and axial flow (induced by a difference of pressure in both sides of the gap region). So an assumption of maximal heat loss was established in order to achieve the biggest reduction in motor walls temperature. For that, the assumption was established that $T_{GAP\ OUTLET} = T_W$. Temperature from the fluid flowing out from the gap region achieves the maximal temperature that can get (the same temperature as the motor).

Regarding the new heat dissipation parts, heat source values were assigned to these parts according to the experimental values (in the pump and throttle region). The heat losses in the cylinder correspond to the heat that is assumed that can be lost in the pipes when hydraulic fluid recirculation from outlets (in the pump) to the inlet (filter). This hydraulic fluid comes out from the pump through two pipes to the cylinder, then to the throttle region and finally to the filter.

Another improvement was implemented in this case study in comparison to the previous ones. In order to get a more realistic temperature distribution in the external faces of the actuator (now the external faces of the tank), instead of a constant wall temperature, a convective model was implemented with the environment. An important role of the simulation is the implementation of a convection model. Convection or convective heat transfer is the transfer of heat from one place to another by the movement of fluids. This from is the combined process of conduction and advection. Movement of a fluid can be forced by convection by means other than buoyancy. For the exact calculation of the variables see Appendix C.

5.4.3 Result and discussion

0mm/s

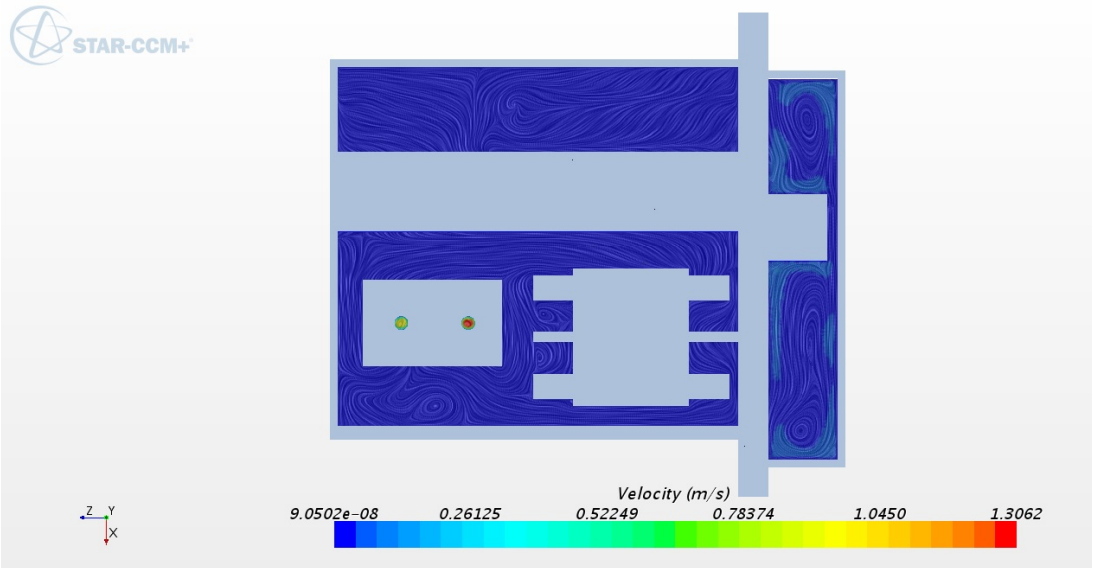

Figure 46: Projection of velocity vector onto the intersection plane - Horizontal middle section cut flow (0 mm/s)

We can already appreciate how the velocity field is distributed in all the regions. In the electronics part, we can see how there is an air movement induced by the heat source from the hydraulic fluid and motor region. This region also has a very slow velocity field, for that reason we do not suspect of a case with turbulence.

10 mm/s

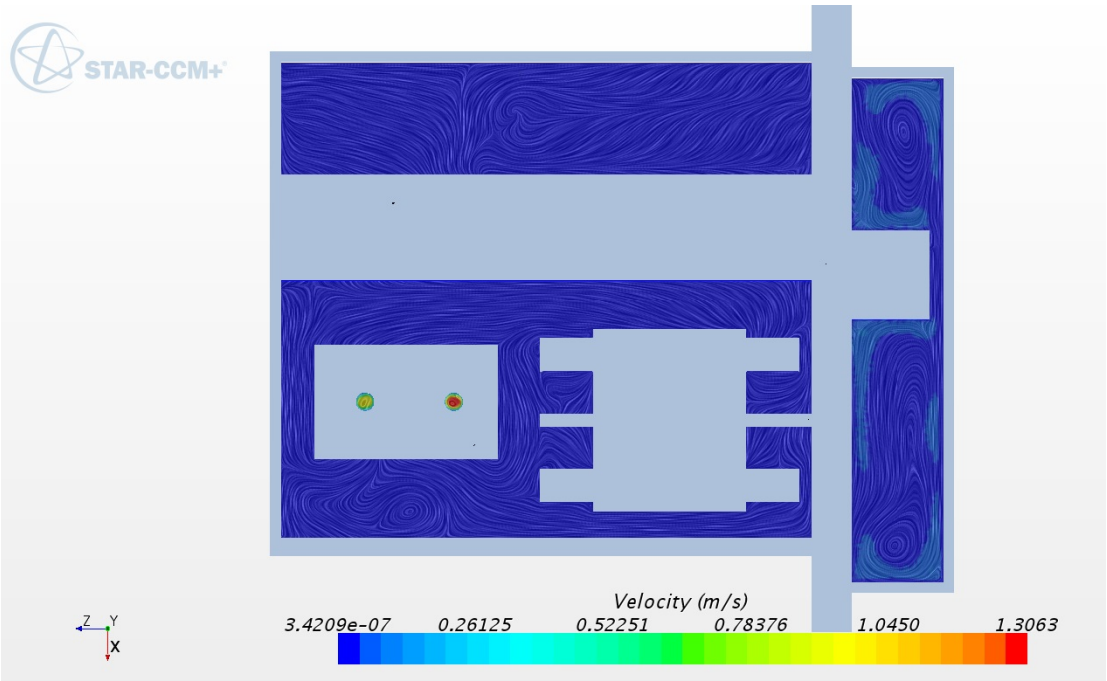

Figure 47: Projection of velocity vector onto the intersection plane - Horizontal middle section cut flow (10 mm/s)

30 mm/s

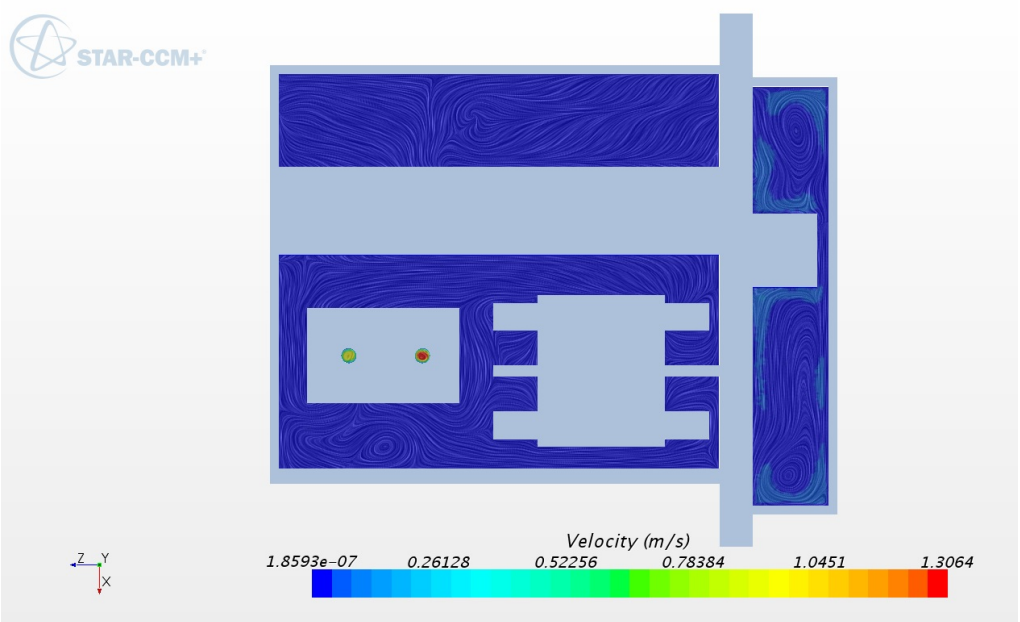

Figure 48: Projection of velocity vector onto the intersection plane - Horizontal middle section cut flow (30 mm/s)

As we do not have fluid flow through the gap, we do not see important flow characteristics in both regions of the gap that can affect the general stability of the simulation. In the following simulations where we increase gap flow velocity we still see the normal behaviour. In the electronics part, we see forced convection induced by throttle and plate heat that produces movement in the air region.

0 mmm/s

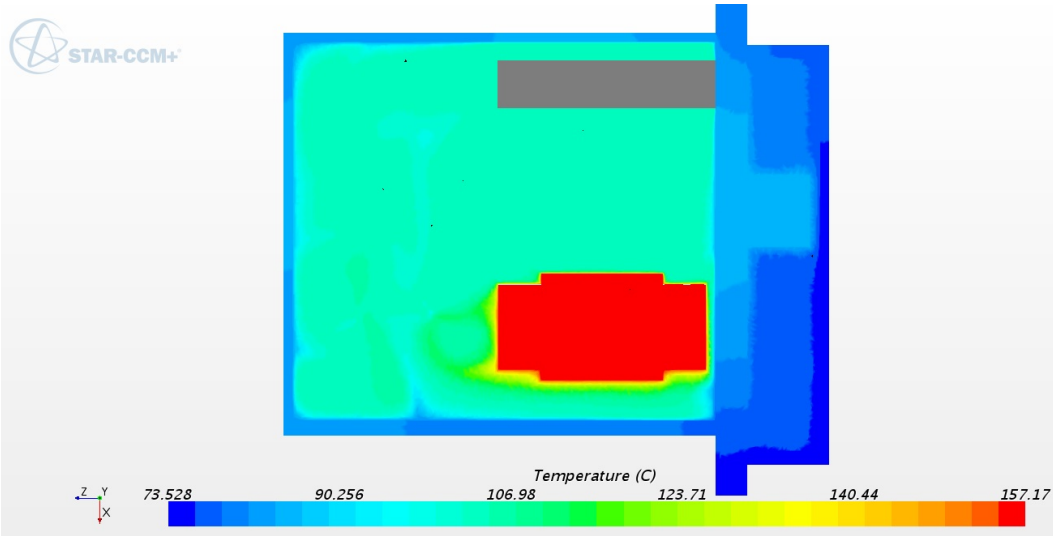

Figure 49: Horizontal cut temperatures (0mm/s)

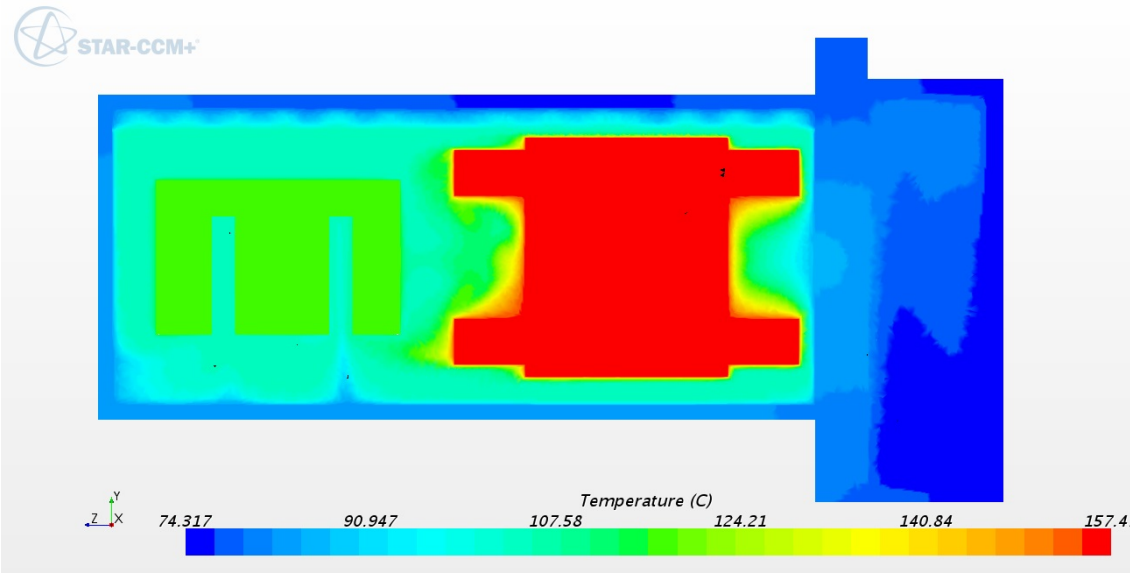

Figure 50: Vertical cut temperatures outlets-motor (0 mm/s)

10 mm/s

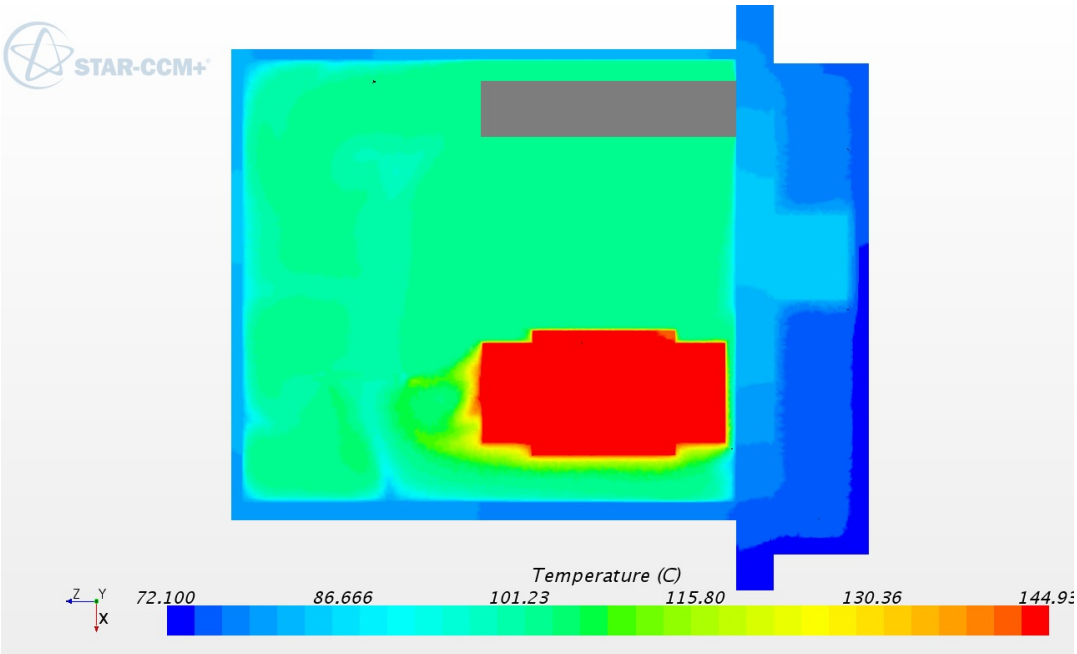

Figure 51: Horizontal cut temperatures (10 mm/s)

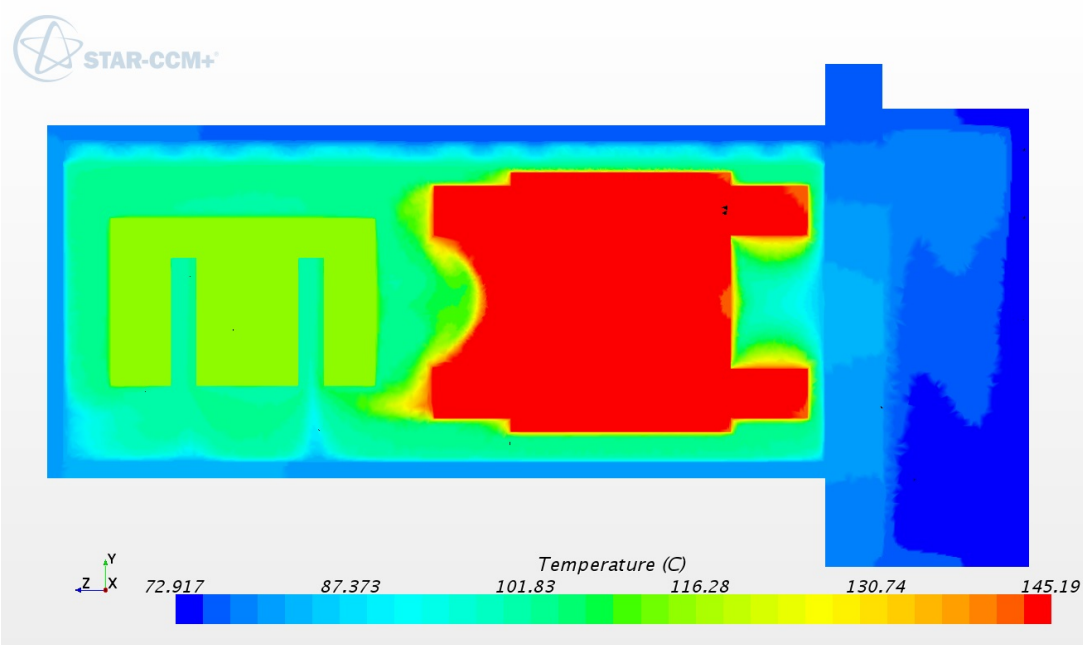

Figure 52: Vertical cut temperatures outlets-motor (10 mm/s)

30 mm/s

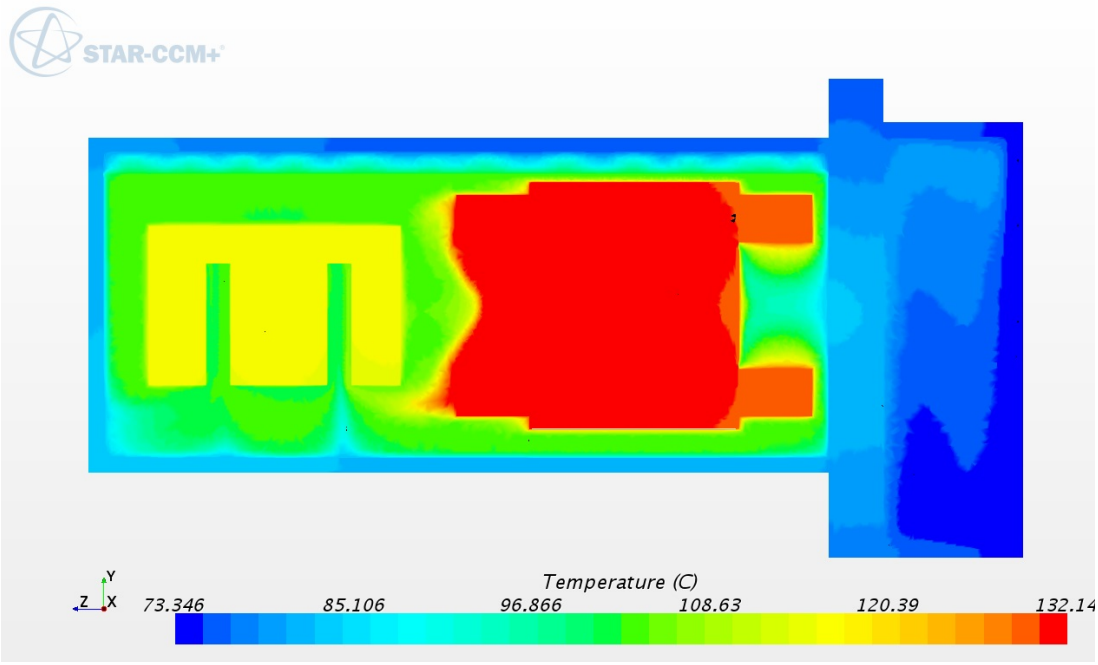

Figure 53: Vertical cut temperatures (30 mm/s)

50 mm/s

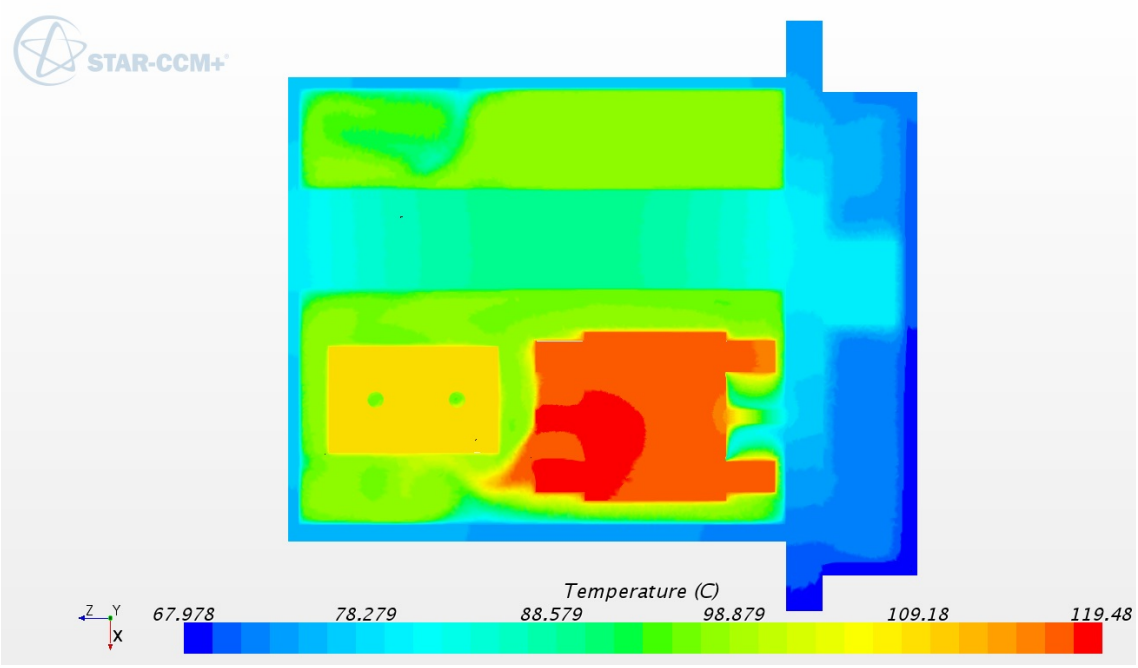

Figure 54: Horizontal cut temperatures (50 mm/s)

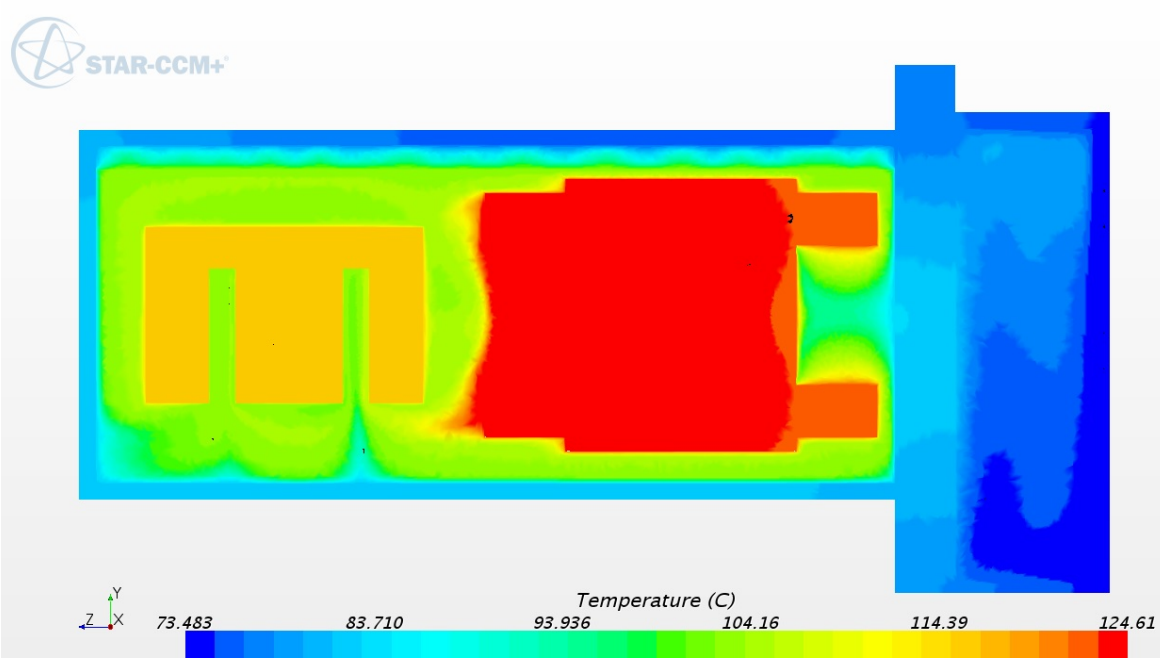

Figure 55: Vertical cut temperatures outlets-motor (50 mm/s)

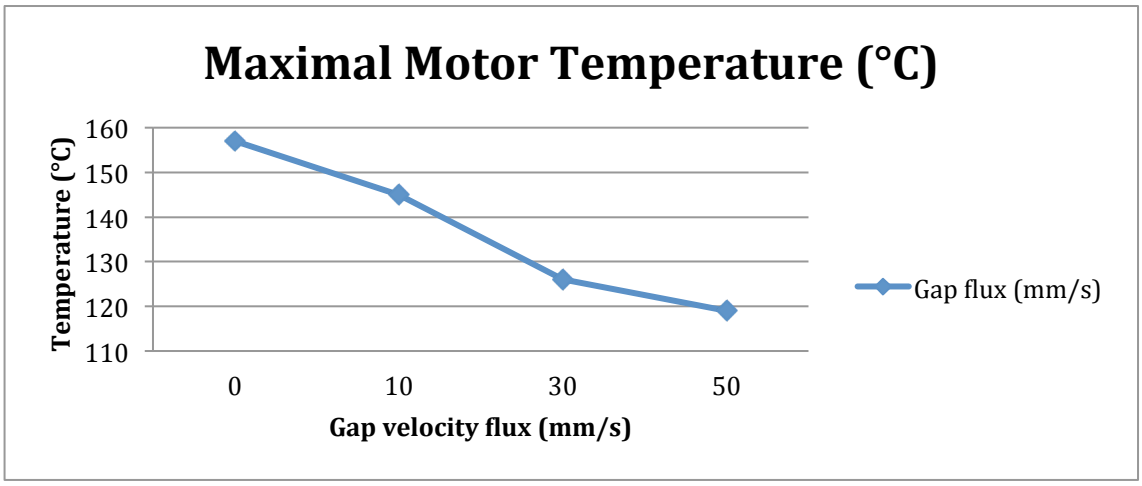

Figure 56: Maximal motor temperature graphic

As we can see, there is a significant maximal temperature reduction if we take in account the heat that can be dissipated through the gap. Total heat dissipated through the gap always followed the formula $\Delta U = \dot{m} C_p (T_{GAP\ OUTLET} - T_{GAP\ INLET})$. $T_{GAP\ INLET}$ corresponds to a parallel fluid section to the gap inlets (2 mm distance).

This shows how the heat transfer measure inside this gap region is critical to achieving the final temperature distribution in all the actuator, but especially in this motor region.

Another fact that we see is that fluid temperature flowing out the simulated gap presents a higher temperature value than the rest of the fluid region of the actuator. One of the possible problems with this simulated gap can be the way that the amount of heat is dissipated in the hydraulic fluid region. In a real gap, heat would not only be dissipated in one direction, because we have an open region in both motor sides, and for that temperature degree would not be so high as in this simulation.

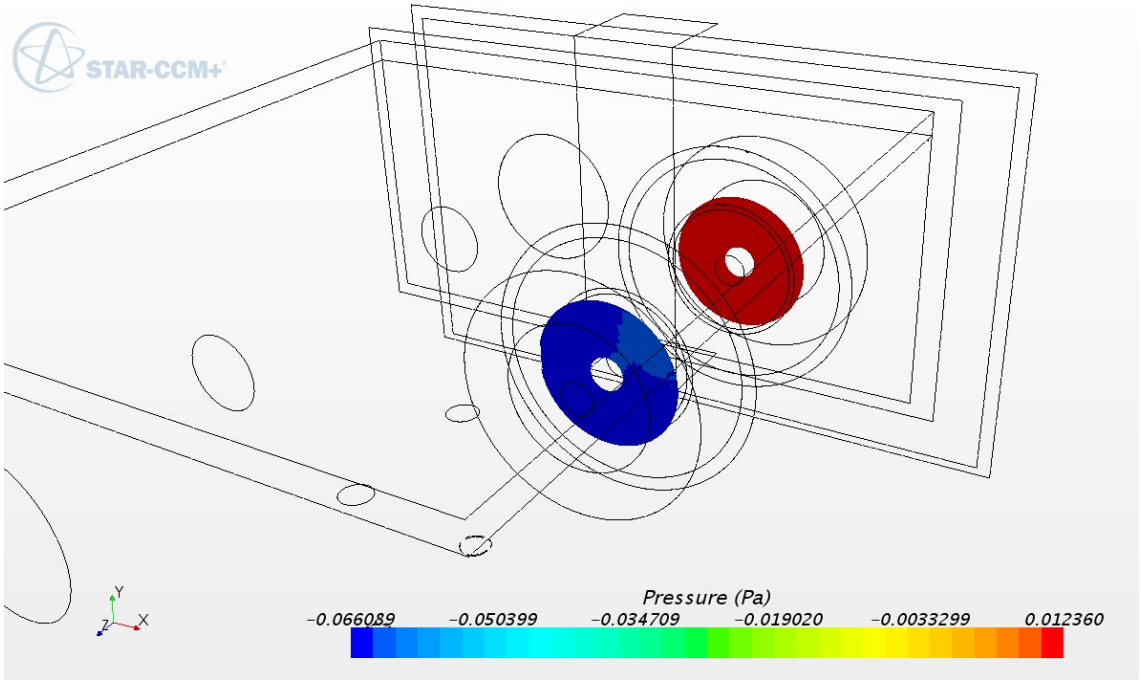

Figure 57: Differential pressure motor gap

If we set that fluid flow is induced by the pressure difference between both motor sides, this can be estimated by taking the pressure values from simulation 0 mm/s. Taking Poiseuille equation from axial flow we have:

$$v_z = \frac{1}{4\mu}\left(-\frac{\partial p}{\partial z}\right)\left[\frac{\ln\left(\frac{r}{r_1}\right)}{\ln\left(\frac{r_2}{r_1}\right)}(r_2^2 - r_1^2) - (r^2 - r_1^2)\right]$$

Replacing variable values in the formula, and taking the maximal velocity value, that would be in the middle of the velocity profile, to get the maximal heat loss through the gap, we arrive at a solution. This variables are r_1=0.0295m, r_2=0.03m and r=0.02975m. Knowing this, we arrive at a v_z value of 1.654E-4 m/s. This value demonstrates that there is a flux inside the motor region, but the value is not very high as expected in first predictions. This low value can be a result from different variables. Maybe one of the questions is the temperature that the hydraulic fluid flows inside this gap. Motor region is higher than the average hydraulic fluid. This means that we should take another dynamic viscosity value. If we have a fluid with higher temperature, viscosity has a lower value and for that fluid flows at a higher value through the gap.

All 4 simulations, in this case, presented a converged and stable solution. Controlling all the factors (residuals, heat transfer, temperatures,...), a converged solution has arrived in every simulation. More information about this point is to find in Appendix D.

5.5 Case 5: Simulation with rotational rotor

5.5.1 Description of the simulation

To try to avoid making gap heat transfer assumptions, a final simulation was carried on where two main modifications were carried out. First, the real gap was modelled. In this new simulation, there is a real gap between rotor and stator where the fluid is capable of flowing through. Second, this final simulation has a rotational rotor implemented with a velocity of 3000 rpm (as in the real case).

Trying to simulate this new situation means that all the problems exposed in case 4 (regarding the difficulty of a real gap in such a big model) where present and always trying to have them under control.

5.5.2 Solution in STAR-CCM+

Knowing that this decision would affect drastically the simulation weight and complexity, we went forward with the simulation. In order to make this possible, some modifications were made parting from the model from the last case.

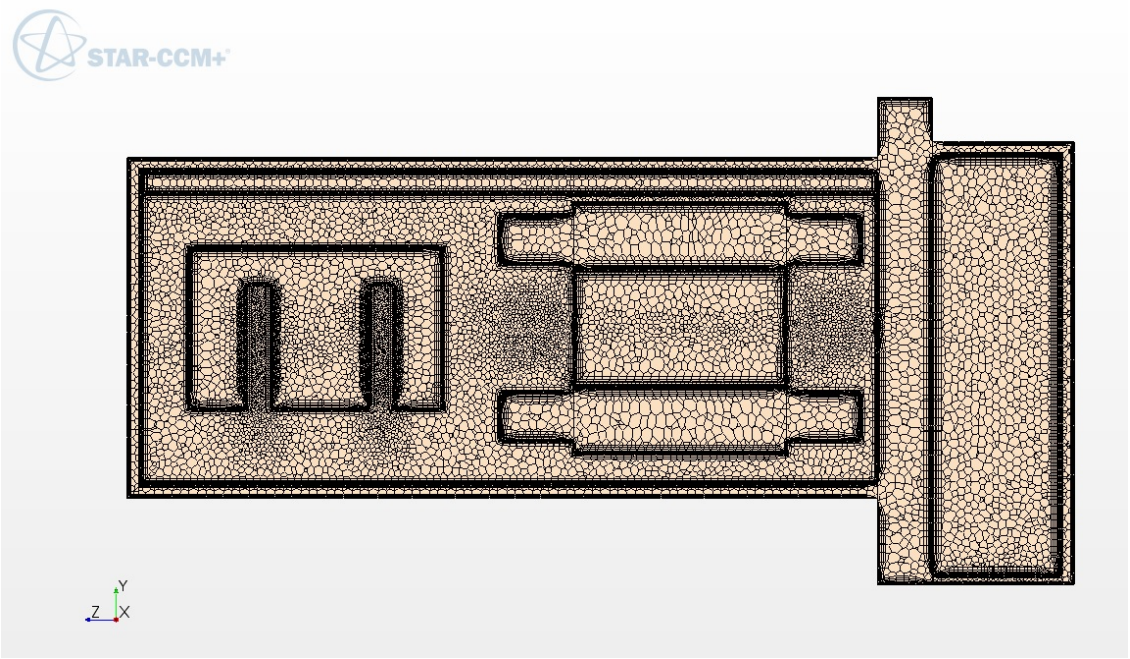

Figure 58: Vertical cut mesh (case 5)

Using the 3D-CAD tool from STAR-CCM+, a 0.7 mm was extruded (0.2 mm bigger than real value attempting to facilitate simulation). To achieve a mesh capable of

covering the big distances and the thin gap region, considerations were made with the initial hydraulic fluid mesh. Cell size minimum was reduced to 0.08 mm so that when the program tries to cell the gap, applies a smaller cell size. The growth rate was also changed to 2, o that when the program meshes inside the gap region when it tries to mesh the surrounding regions we have a fast growth, and this way a less number of cells. This growth was selected trying in all moment not to give a too much big value, so that information from one cell to the next one had coherence. Mesh in air region and solids was not modified.

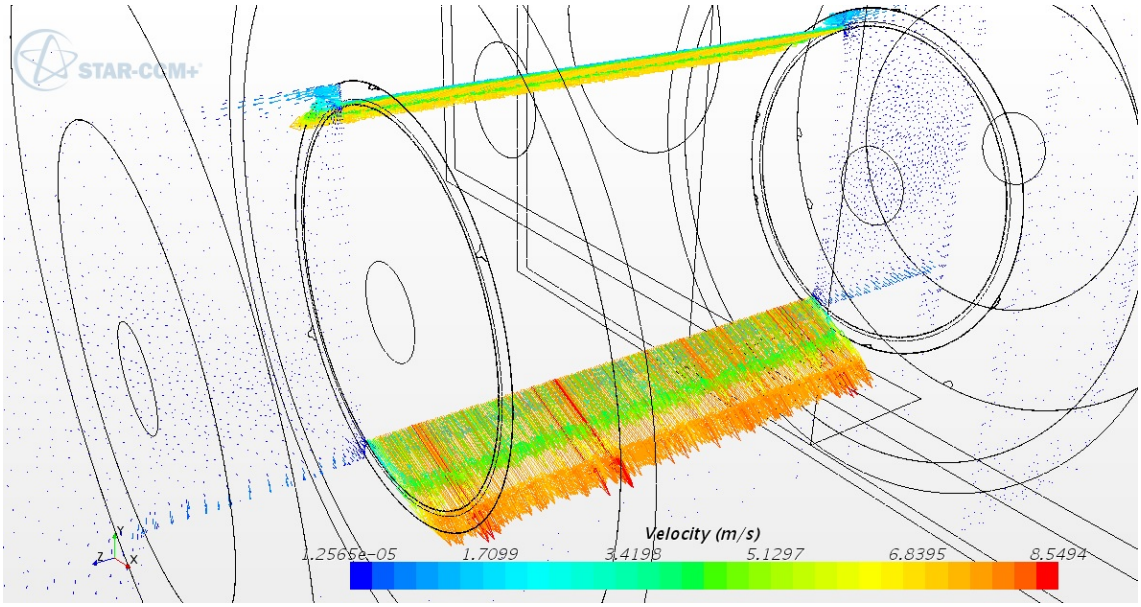

Figure 59: Velocity field motor gap

The rotor was also simulated with motion. Lateral rotor boundary was given a relative velocity of 3000 rpm on his axis. Rotation at the top and bottom of the rotor was neglected in order to reduce complexity in the simulation and achieve a more stable solution. For that reason if we look Figure 59 we can appreciate only important velocity values at the entrance and exit of the gap (besides of the velocity field inside the gap).

5.5.3 Result and discussion

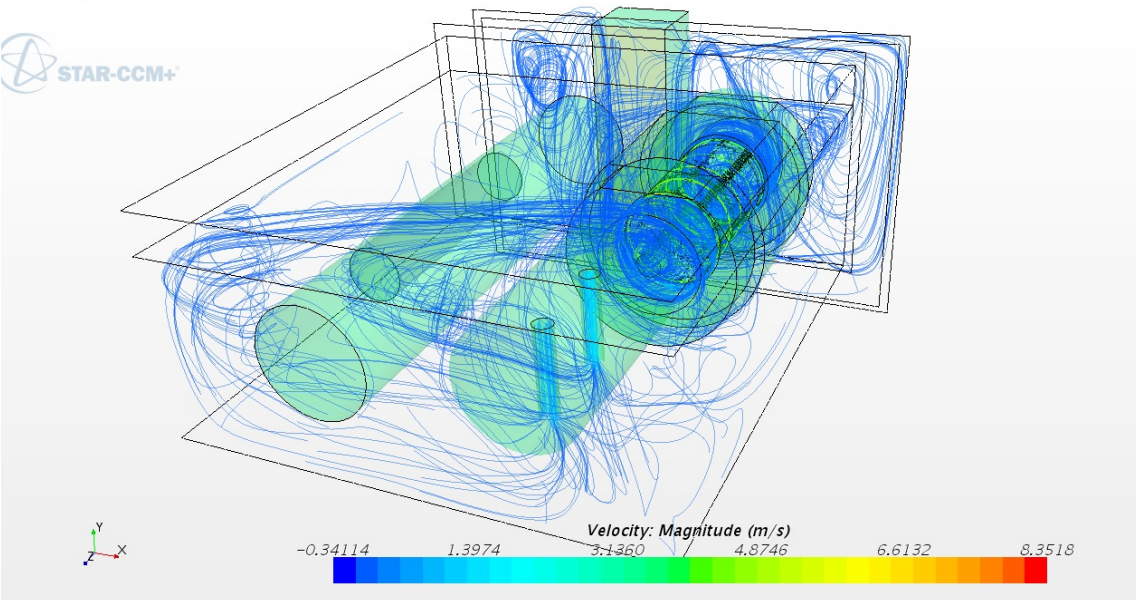

Figure 60: Streamlines actuator region

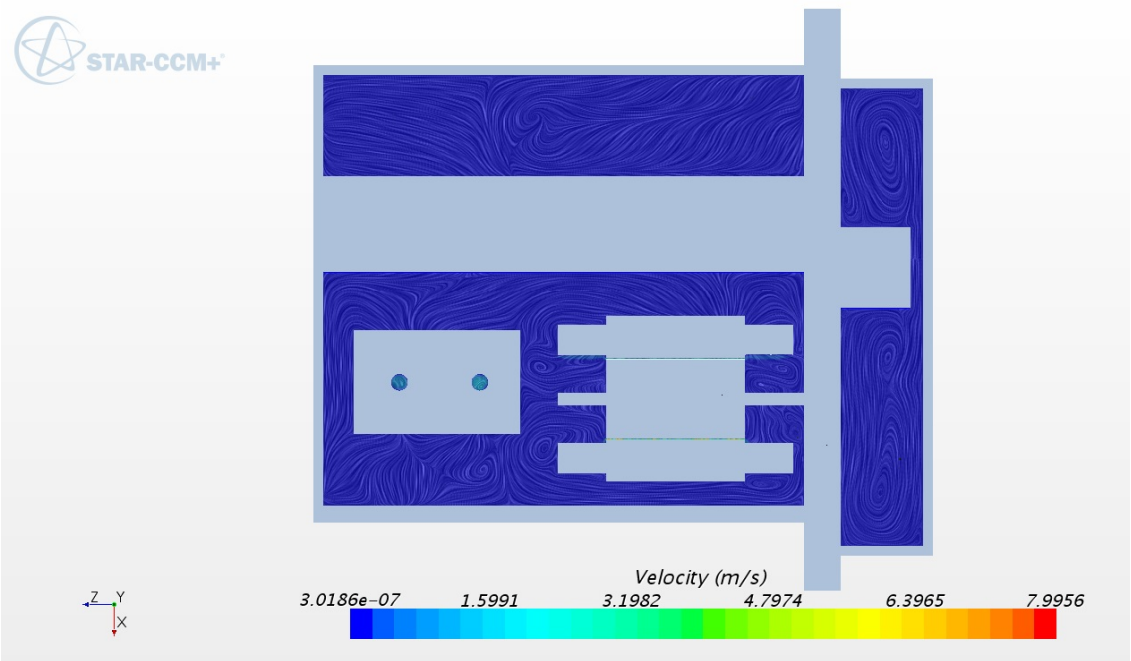

Figure 61: Projection of velocity vector onto the intersection plane - Horizontal cut middle section flow (case 5)

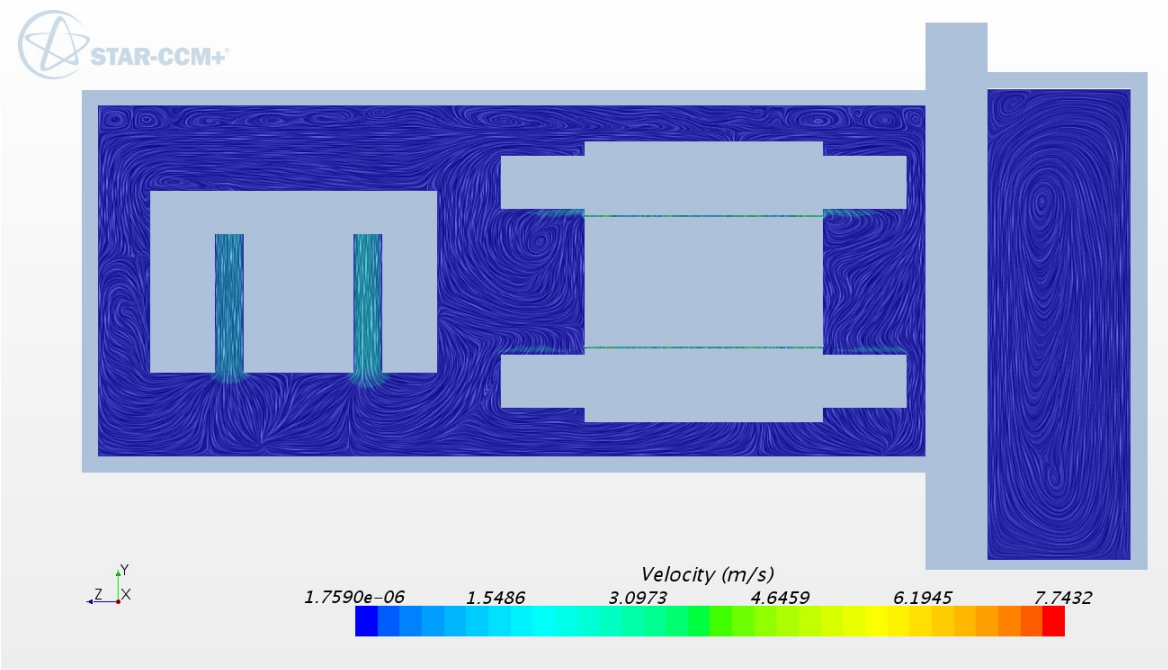

Figure 62: Projection of velocity vector onto the intersection plane - Vertical cut flow outlets-motor (case 5)

As we can see in a general overview of the simulation, we still see a very low-velocity field inside the actuator region. Due to the rotational rotor, a more agitated field is presented in both sides of the electric motor but always with low velocities. In Figure 60 we see how the rotational rotor induces a more agitated flow, even in the furthest corners of the actuator. This phenomenon can also be a variable that allows a better heat transfer with tank walls due to an improved velocity field near walls, rising convective effect.

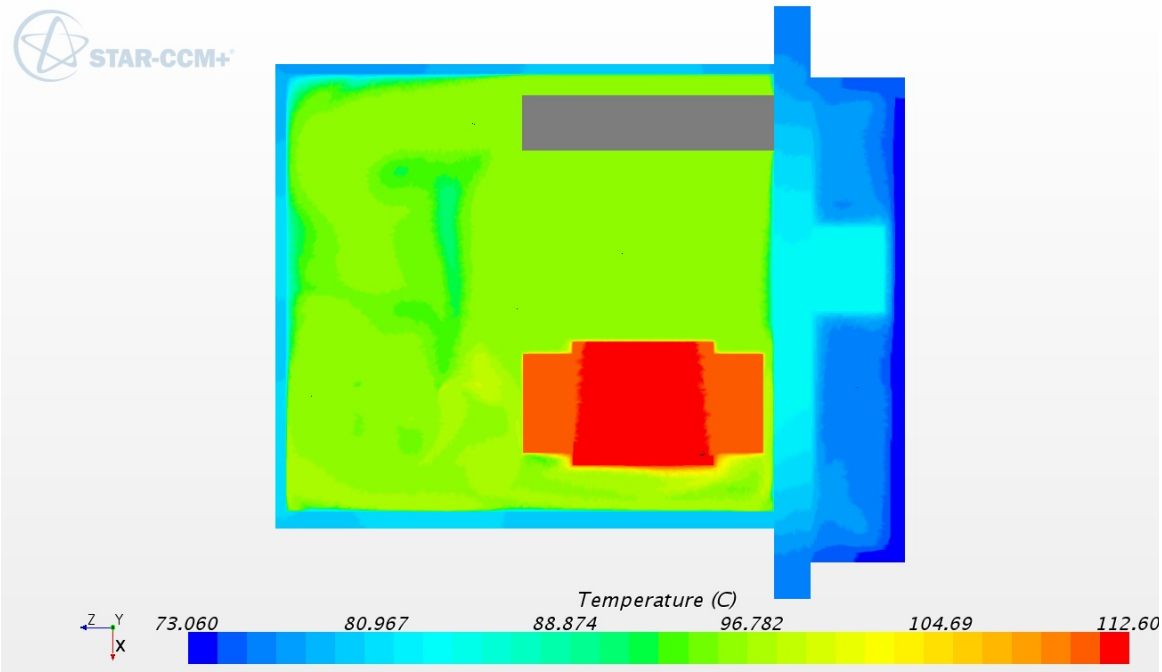

Figure 63: Horizontal cut temperatures (case 5)

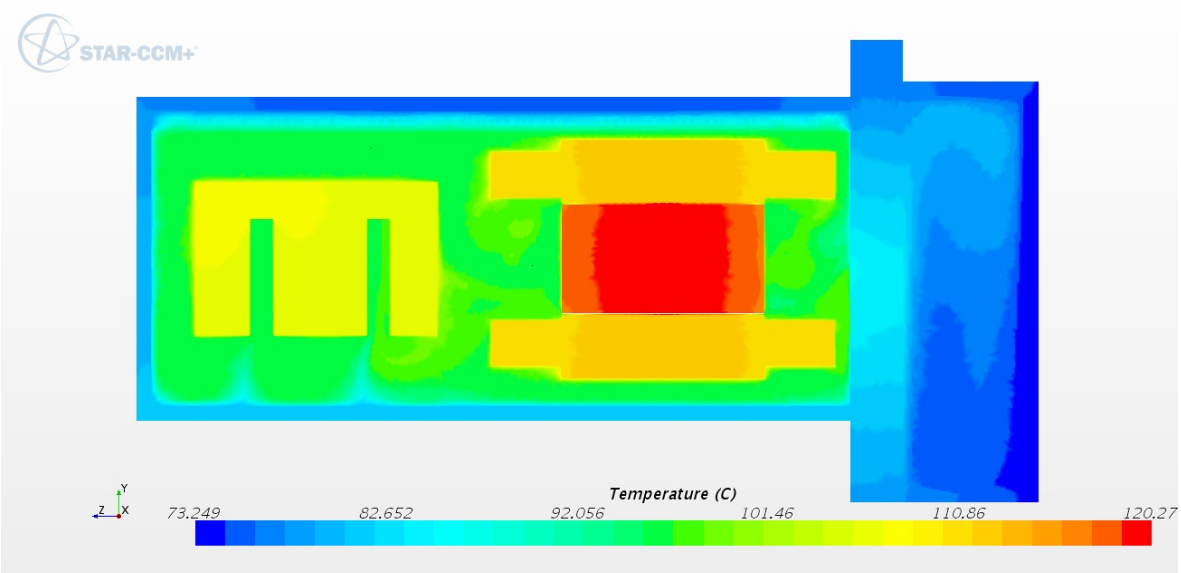

Figure 64: Vertical cut temperatures (case 5)

As a result of having a rotational rotor in the actuator, we see that heat transfer inside the motor region behaves differently and that there is a temperature difference between rotor and stator. Even though that the components still have the same good heat conduction faculties, rotor and stator do not achieve a common temperature. This is maybe induced by a bad heat transfer profile between both regions caused by a bad meshing in this thin gap or due to the effect of having an open channel between rotor and stator, heat is dissipated and there is no significant heat transfer between rotor and stator.

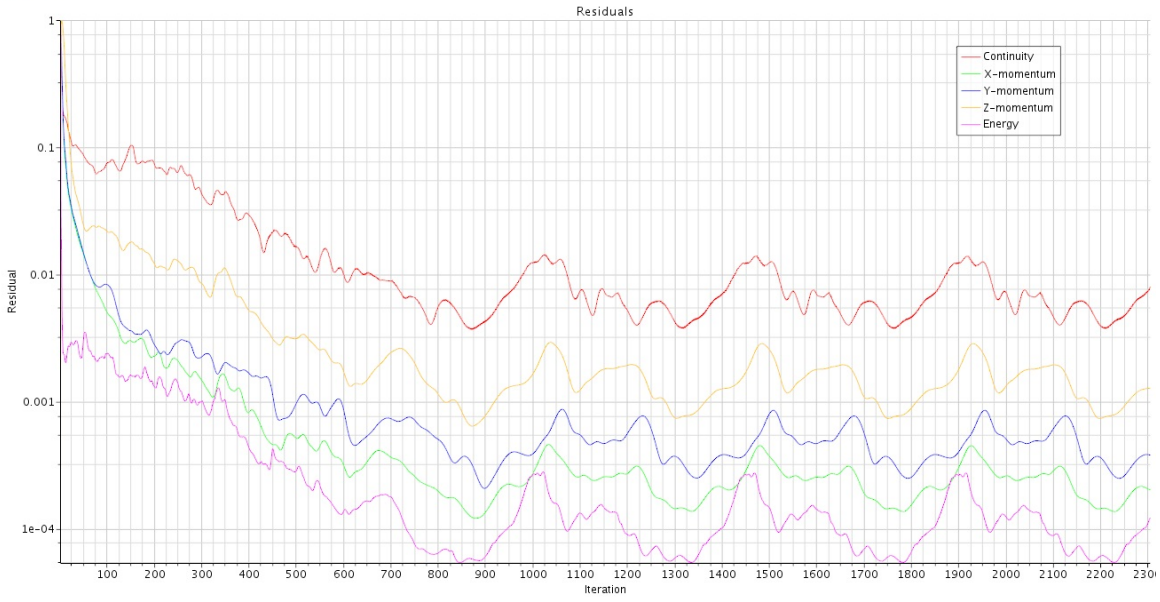

Figure 65: Residuals plot (case 5)

In the residuals (Figure 65), there is to notice that even though we see that variables tend to be low values (except continuity that stays around a 1e-02 value), these variables when converging are constantly oscillating, showing an unstable case. For that, values and results in this simulation are maybe inaccurate.

In order to resolve this situation, modifications in physics model can be suggested. One of the first thoughts that can come to mind is to change time model as we have now motion inside the simulation. That means that the model would have now an implicit unsteady model. For this time model, one of the main characteristics is the establishment of a time step with which the program solves the simulation. As we have done in this simulation, grid size was changed in some regions to a very low value. One of the most important things in the implicit unsteady model is to make sure the time step is chosen such that stability is conserved. A too high time step makes the solver jump cells, causing an unstable solution. Therefore, a decrease in cell size results in choosing a smaller time step. As the number of cells is increased, and the time step lowered the accuracy of the prediction increases. However, such an increase in accuracy also leads to an increase in computational time. Also, in this simulation with so many cells due to the actuator size, computational requisites increase bringing the question if not every computer can afford to solve it in a realistic amount of time.

6 Conclusions

This study investigated a CFD model, including both fluid dynamics and heat transfer in order to simulate the real conditions that the actuator suffers, where we have a hydraulic fluid flux and different heat sources inside our region. In the beginning of the project it was suggested a simplified model, both in geometry and physics, however, this complex model needed further improvements in this aspects to increase accuracy in results.

This model was a 3D multiphase model in STAR-CCM+, which we investigated as it has constant volume regions where we appreciate heat transfer between both regions. The aim was to find an appropriate model that gives us the most accurate results with a low discrepancy degree with real values. The hydraulic oil fills almost all the actuator region cooling especially the motor region. From the comparison between the models where we have the actuator full with hydraulic fluid and with air region, we see the influence of hydraulic fluid and air level on general temperature distribution. There is to appreciate the vital importance of hydraulic level to avoid temperatures in motor over the limit. As we vary hydraulic fluid level we see that motor temperatures increase or decrease due to the effect of the insulation of the air region.

Another studied fact is the comparison between a model with constant motor wall temperature and as a heat source. Possible reasons for this discrepancy were detected and evaluated, as it can be an improved heat transfer coefficient due to the effect of the gap. Different gap fluxes were simulated demonstrating an appreciable increase in heat transfer. For that reason to achieve a proper simulation that gives us real values, this variable has to be established accurately.

Critical temperatures zones on the electric motor were also detected. After modelling with CFD, zones around the motor with low velocities field and high temperatures were detected. These zones run the risk to achieve critical temperatures. Possible solutions to reduce hot spots in the motor surface region could be to increase fluid movement causing increased heat transfer in that part. In the simulation with rotational rotor, there is to appreciate how fluid flux is increased in the entire actuator region inducing a performed actuator.

An important fact was to achieve a high accuracy CFD model compared with real values. Through the implementation of new ideas in the studied CFD model, more accurate values were achieved. Although we have better values in the last simulation, these values still vary from the real values a 20% approximately. Knowing that for this simulation motor temperatures are critical in the

optimization process of the actuator and only 10^{o}C difference in motor temperatures are critical, it can be said that a deeper investigation in the motor region could be implemented in a further work.

Another physical event studied was the influence of convection in heat development. Notorious effect of heat transfers coefficient and exterior temperature in the development of the interior temperature distribution was seen. It was studied a model with constant wall temperatures and with a heat transfer value, gaining a more realistic model. Different temperatures development in the external wall region was observed.

Values with which was compared all the time this model were not very different and heat development was always as expected but an improvement in the motor region modelling is needed if more precise values are wanted. Due to the complex geometry and physics, the program requested high computer resources. Already in the last studied case, computer demand was already causing an unstable solution. To implement another possible improvement in the model meant to add complexity in the model and for that another and with better resources computer is needed.

7 Recommendations for further work

Additional geometry improvements must be simulated in order to discover of this variable is the reason for the discrepancy. Special attention is needed in the gap region of the motor that has been causing lots of problems in this simulation.

Since we have a modified geometry model maybe continua need also to be modified. It appears that if a rotational model is implemented a change in the time model is needed.

In this study the electro- magnetism is neglected, only the resulting heat losses are considered as a constant heat flux along the motor parts outer wall, and also as a constant surface temperature heat source. Further investigations of the magnetic field and the position of the poles should be carried out.

It would be also preferable that more experiments are conducted so more values are available to compare with.

Another important heat transfer model that can also be studied is the radiation model to evaluate how big can be the effect of this phenomenon in the temperature and heat evolution inside our system.

APPENDIX A

Properties of the Hydraulic Oil, Air and Solids

Each one of the materials modelled in this thesis had their own properties. For the hydraulic oil constant values were chosen and can be seen in the table.

Oil properties	Values
Density	870 Kg/m^3
Dynamic viscosity	0.0054 Pa-s
Specific heat	1850 J/Kg-K
Thermal conductivity	0.15 W/m-K
Prandtl number	66.6

Table 2: Oil properties

For the hydraulic fluid a constant dynamic viscosity was chosen due to the fact that as can be seen in the graphic, the viscosity value tends to a constant when we get higher temperatures. For that reason, constant properties can be considered suitable for the simulation.

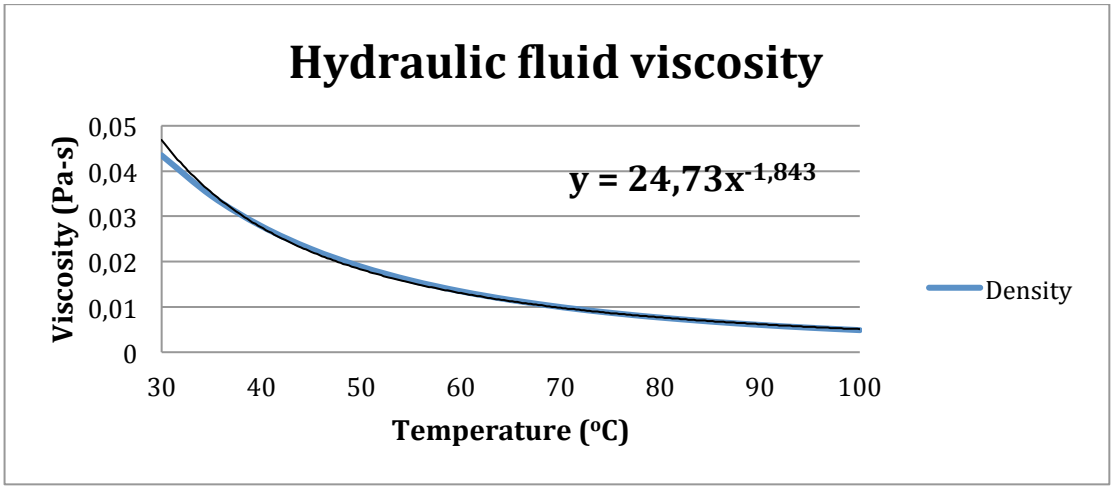

Figure 66: Hydraulic fluid graphic viscosity-temperature

For the air, the default values from STAR-CCM+ were chosen.

Air properties	Values
Molecular weight	28.9664 Kg/Kmol
Dynamic viscosity	1.85508E-5 Pa-s
Specific heat	1003.62 J/Kg-K
Thermal conductivity	0.0260305 W/m-K

Table 3: Air properties

For the materials, following properties were chosen:

Aluminium	Values
Density	2702 Kg/m^3
Specific heat	903 J/Kg-K
Thermal conductivity	237 W/m-K

Table 4: Aluminium properties

Steel	Values
Density	7832 Kg/m^3
Specific heat	434 J/Kg-K
Thermal conductivity	63.9 W/m-K

Table 5: Steel properties

Copper	Values
Density	8940 Kg/m^3
Specific heat	386 J/Kg-K
Thermal conductivity	398 W/m-K

Table 6: Copper properties

Each one of the different motor parts was independently modelled and their physical properties calculated.

- The stator was modelled with 24 copper gaps with a geometry of 3x12x100 mm. The rest of the stator is considered of magnetic steel. Du to this reasons we have that:

$$V = \pi * r^2 * h \tag{40}$$

$$V_{TOTAL} = \pi * 54^2 * 100 - \pi * 32.5^2 * 100 = 584.257{,}69\ mm^3$$
$$V_{Cu} = 24 * (12 * 3 * 100) = 86.400\ mm^3$$
$$V_{St} = V_{TOTAL} - V_{Cu} = 497.857{,}69\ mm^3$$

This volume distribution of material gives us a percentile for each of:

$$V_{Cu} \rightarrow 14{,}8\ \%$$
$$V_{St} \rightarrow 85{,}2\ \%$$

Knowing the volumetric distribution the next step is the modelling of thermal conductivity considering these values with a linear approximation:

$$\lambda_{Stator} = \lambda_{Cu} * 0.852 + \lambda_{St} * 0.148 = 60 * 0.852 + 400 * 0.148 = 110.32 \frac{W}{m * K}$$

- The rotor cage was modelled considering two structural factors: The closing rings and the aluminium bars in the axial direction.

The closing rings have a thick of 1 cm in the axial direction. The aluminium bars represent 1/18 of the rest of the volume from the rotor so the steel part will represent 17/18.

$$V_{TOTAL} = \pi * 32.5^2 * 100 = 331.830{,}72\ mm^3$$
$$V_{Al\ ring} = (\pi * 32.5^2 * 10) * 2 = 66.366{,}14\ mm^3$$
$$V_{St} = \frac{17}{18} * (\pi * 32.5^2 * 80) = 250.716{,}55\ mm^3$$
$$V_{Al} = \frac{1}{18} * (\pi * 32.5^2 * 80) = 14.748{,}03\ mm^3$$

This volume distribution of material gives us a percentile for each of:

$$V_{Al} \rightarrow 24{,}4\ \%$$
$$V_{St} \rightarrow 75{,}6\ \%$$

Knowing the volumetric distribution the next step is the modelling of thermal conductivity considering these values with a linear approximation:

$$\lambda_{Rotor} = \lambda_{Al} * 0.756 + \lambda_{St} * 0.244 = 60 * 0.756 + 237 * 0.244 = 103.18 \frac{W}{m * K}$$

As an overall view, the material properties of rotor and stator look like in the following tables:

Rotor	Values
Density	2702 Kg/m^3
Specific heat	548.44 J/Kg-K
Thermal conductivity	103.18 W/m-K

Table 7: Rotor properties

Stator	Values
Density	2702 Kg/m^3
Specific heat	426.896 J/Kg-K
Thermal conductivity	110.32 W/m-K

Table 8: Stator properties

APPENDIX B

Initial and boundary conditions

The following table gives an overview of the boundaries and their types chosen in a first instance for the simulation. We have to distinguish that lots of boundaries are double because we have on the one side the fluid boundary part and in the other side the solid boundary.

Region Type	**Boundary Name**	**Boundary Type**	**Value**	
Fluid	Inlet	Mass Flow Inlet	Mass flow	Temp.
			0.1566 Kg/s	Defined by user field function (energy balance)
Fluid	Outlet	Flow-Split Outlet	Mass flow	
			Outlet (near motor)	Outlet (far motor)
			0.0899 Kg/s	0.0667 Kg/s
Fluid	Motor fluid wall	Wall		
Fluid	Tank fluid wall	Wall	Temp.	
			333.15 K	
Fluid	Cylinder fluid wall	Wall		
Fluid	Filter top fluid wall	Wall		
Fluid	Pump fluid wall	Wall		
Solid	Motor wall	Wall	Heat source	
			430 W	
Solid	Cylinder lateral wall	Wall		
Solid	Cylinder top wall	Wall		
Solid	Filter lateral wall	Wall		
Solid	Filter top wall	Wall		
Solid	Pump wall	Wall		
Solid	Pump inf outlet	Wall		
Solid	Pump sup outlet	Wall		

Table 9: Initial boundary conditions

In the case were we have two different fluid regions we have to add the following boundaries:

Region Type	Boundary Name	Boundary Type	Specification
Fluid	Tank fluid wall	Wall	Temp.
			333.15 K
Fluid	Tank air wall	Wall	Temp.
			333.15 K
Fluid	Air contact	Wall	Slip
Fluid	Hydraulic fluid contact	Wall	Slip

Table 10: Boundary conditions due to multiphase simulation

Air contact and hydraulic fluid contact represents the layer where both fluids are in contact. This boundary is determined through a baffle and as a conducting interface.

When motor parts were added, different properties were settled for each region. Taken in account the part heat losses values, a heat source distribution were performed. The motor has a total power value of 300 W. Knowing this possible heat loss sources, a proper heat source model was established following this criterion (see references [7], [12] and [14]). For that reason at the end, the heat source distribution had the look:

Region Type	Region Name	Heat Type	Value
Solid	Motor shaft	Heat source	15 W
Solid	Motor coil bottom	Heat source	30 W
Solid	Motor coil top	Heat source	30 W
Solid	Rotor	Heat source	80 W
Solid	Stator	Heat source	125 W

Table 11: Heat source distribution

The remaining 150 W were included in the energy balance of the system through the ΔU (as +150 W) from the inlets and outlets. So in a general perspective, we still have 430 W that have to come out through the tank walls.

In the final design optimization new regions and for that boundaries were added to the model. The main new regions were: Plate, Tank, Tank circuit and Throttle.

An important role of the simulation is the implementation of a convection model. Convection or convective heat transfer is the transfer of heat from one place to another by the movement of fluids. This from is the combined process of

conduction and advection. Movement of a fluid can be forced by convection by means other than buoyancy.

Starting from the experimental data, it proceeds to extrapolate this values into ones that the STAR-CCM+ uses. From the experimental test two values are taken:

- $T_{amb} = 22^{º}C$
- $h = 6\ \frac{W}{K} * \frac{1}{A}$

These values correspond to the convection from the external surface of the tank with the environment.

Heat transfer coefficient still depends on an area variable. From the CFD modelling actuator, we have the sizes 340x311x160 mm for the tank.

$$A_{Tank} = 0{,}4198\ m^2$$

And the final heat transfer coefficient is

$$h = 14{,}2925\ \frac{W}{m^2 * K}$$

The tank was modelled with a T∞=22ºC and a constant heat transfer coefficient in all tank boundaries of h=14.384 W/m^2-K.

Region Type	**Boundary Name**	**Boundary Type**	**Value**	
Fluid	Plate fluid contact	Wall		
Solid	Plate fluid contact	Wall		
Fluid	Plate circuit air contact	Wall		
Solid	Plate circuit air contact	Wall		
Solid	Plate exterior	Wall	Convection	
			Heat transf. coefficient	T∞
			11.3 W/K-m^2	22º C
Fluid	Tank fluid contact	Wall		
Fluid	Tank fluid contact	Wall		
Solid	Tank exterior	Wall	Convection	
			Heat transf. coefficient	T∞
			11.3 W/K-m^2	22º C

Fluid	Tank electronics air contact	Wall		
Solid	Tank electronics air contact	Wall		
Solid	Tank electronics exterior	Wall	Convection	
			Heat transf. coefficient	T_∞
			11.3 W/K-m^2	22º C
Solid	Throttle plate contact	Wall		
Fluid	Throttle wall	Wall		
Solid	Throttle wall	Wall		
Solid	Shaft Plate contact	Wall		
Solid	Cylinder Tank contact	Wall		
Solid	Filter tank contact	Wall		

Table 12: Final boundary conditions

Physics continuum

Hydraulic Fluid:

Group Box	**Model**
Enabled Models	Three Dimensional Gradients
Time	Steady
Material	Fluid
Flow	Segregated Flow
Equation of State	Constant Density
Viscous Regime	Laminar
Optional Models	Segregated Fluid Temperature Gravity

Table 13: Hydraulic fluid physics model

Air:

Group Box	**Model**
Enabled Models	Three Dimensional Gradients
Time	Steady
Material	Gas

Flow	Segregated Flow
Equation of State	Constant Density
Viscous Regime	Laminar
Optional Models	Segregated Fluid Temperature Gravity

Table 14: Air physics model

Solids:

Group Box	**Model**
Space	Three Dimensional
Time	Steady
Material	Solid
Optional Models	Segregated Solid Energy Gradients
Equation of State	Constant Density

Table 15: Solids physics model

APPENDIX C

Stability factors Case 4

0 mm/s:

- **Heat transfer walls**

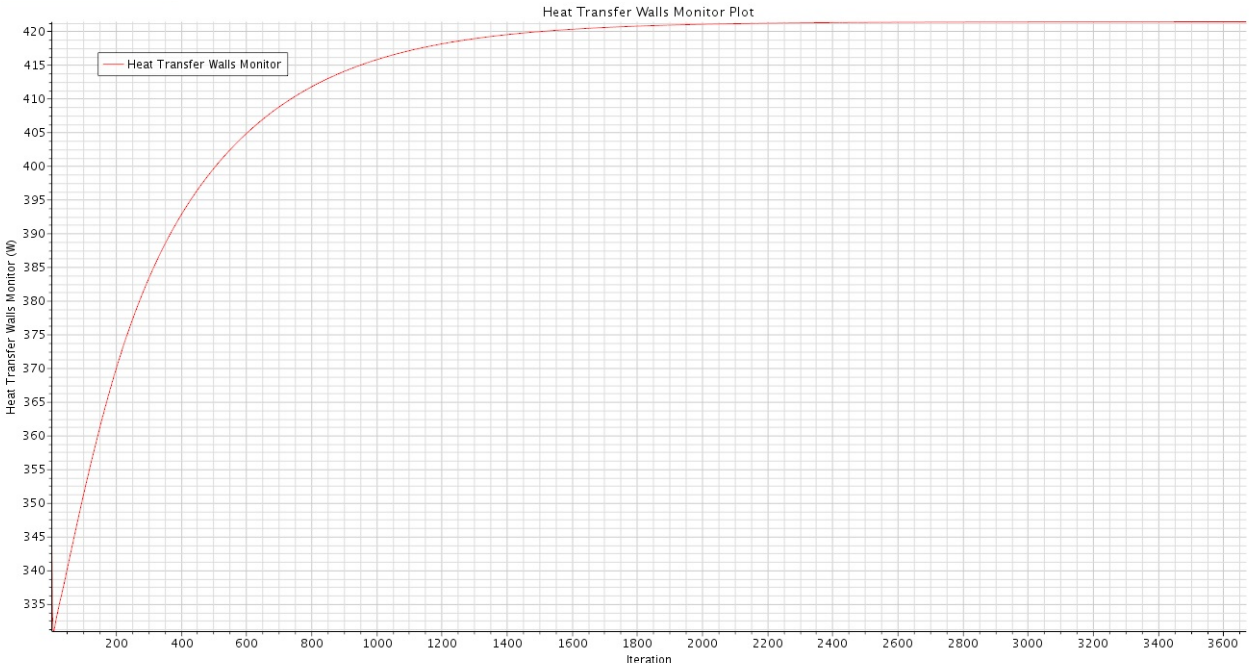

Figure 59: Heat transfer walls plot (0 mm/s)

- **Residuals**

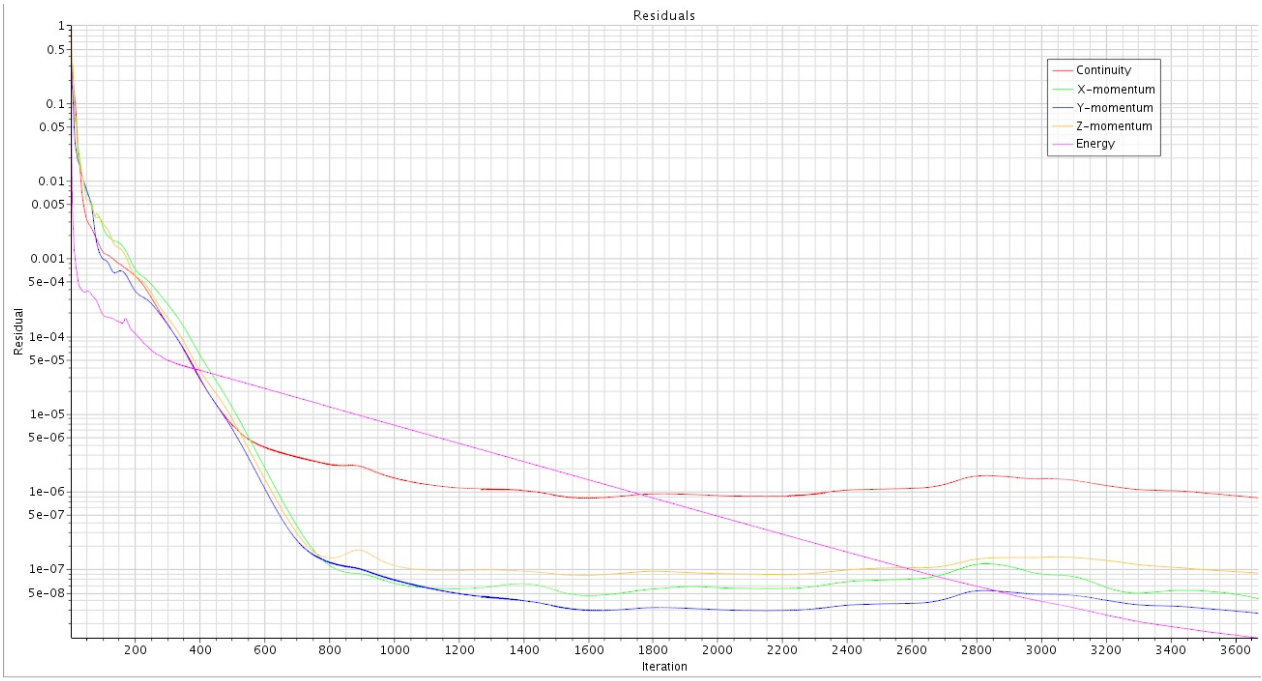

Figure 60: Residuals plot (0 mm/s)

10 mm/s:

- **Heat transfer walls**

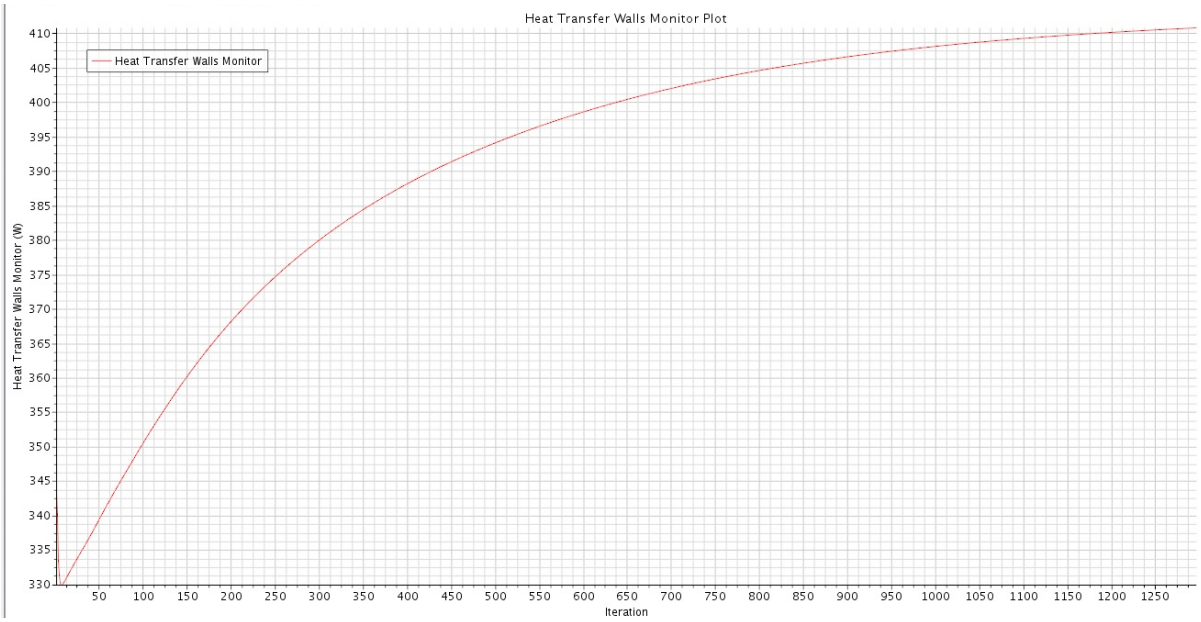

Figure 67: Heat trasnfer walls plot (10 mm/s)

- **Residuals**

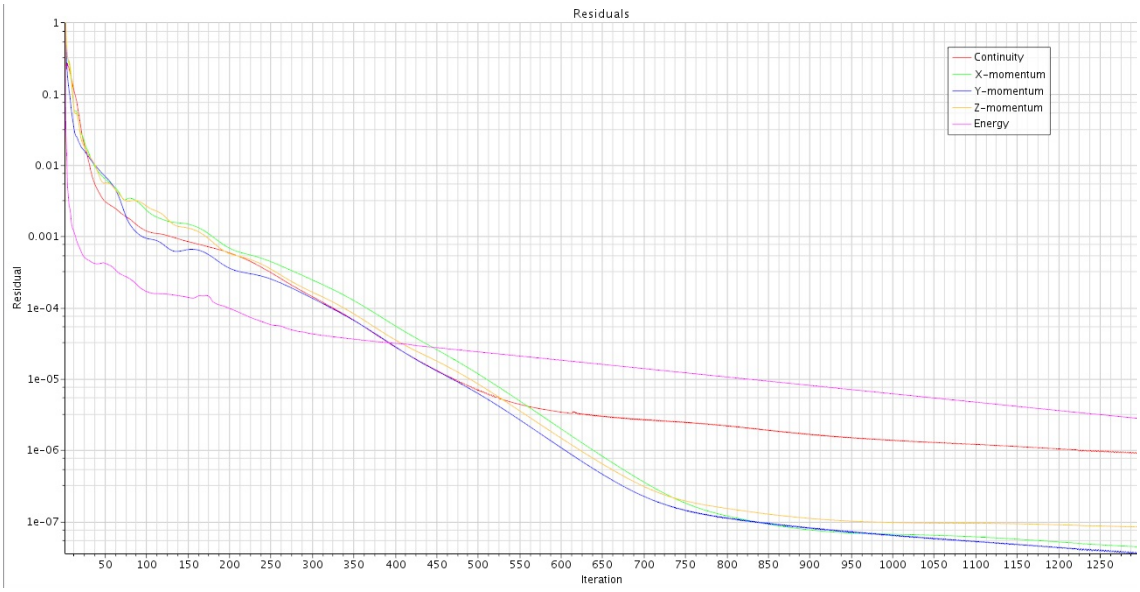

Figure 68: Residuals plot (10 mm/s)

30 mm/s:

- **Heat transfer walls**

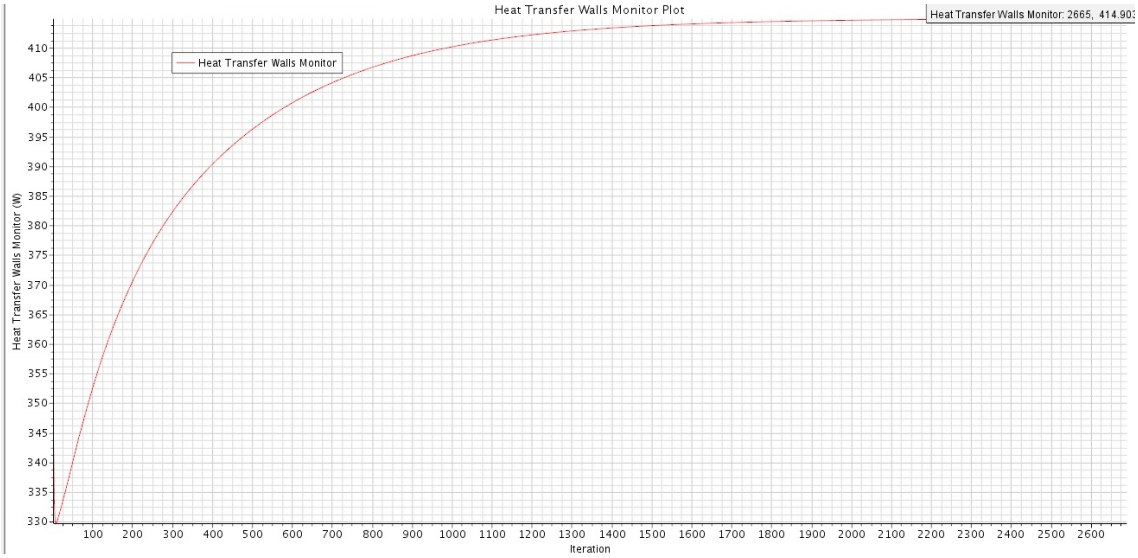

Figure 69: Heat transfer walls plot (30 mm/s)

- **Residuals**

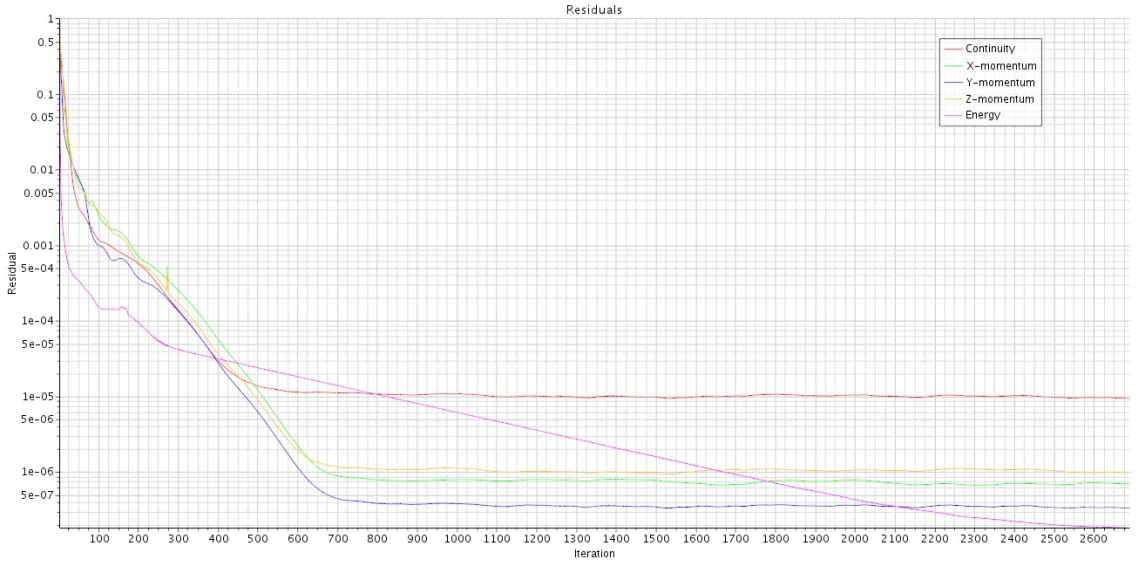

Figure 70: Residuals plot (30 mm/s)

50 mm/s:

- **Heat transfer walls**

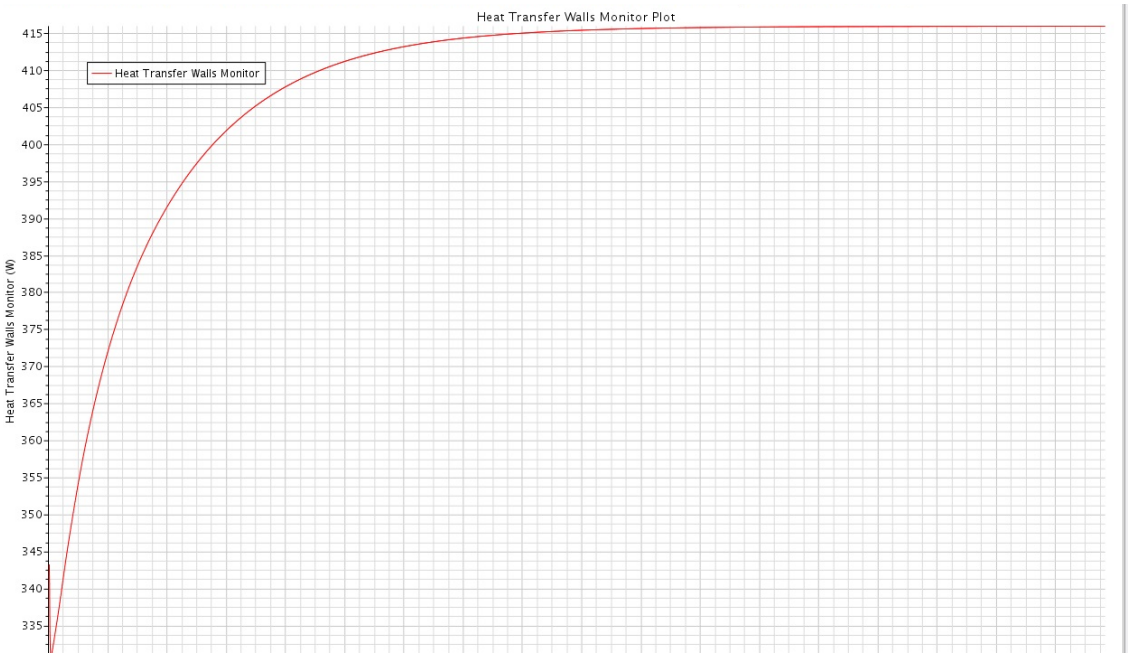

Figure 71: Heat transfer walls (50 mm/s)

- **Residuals**

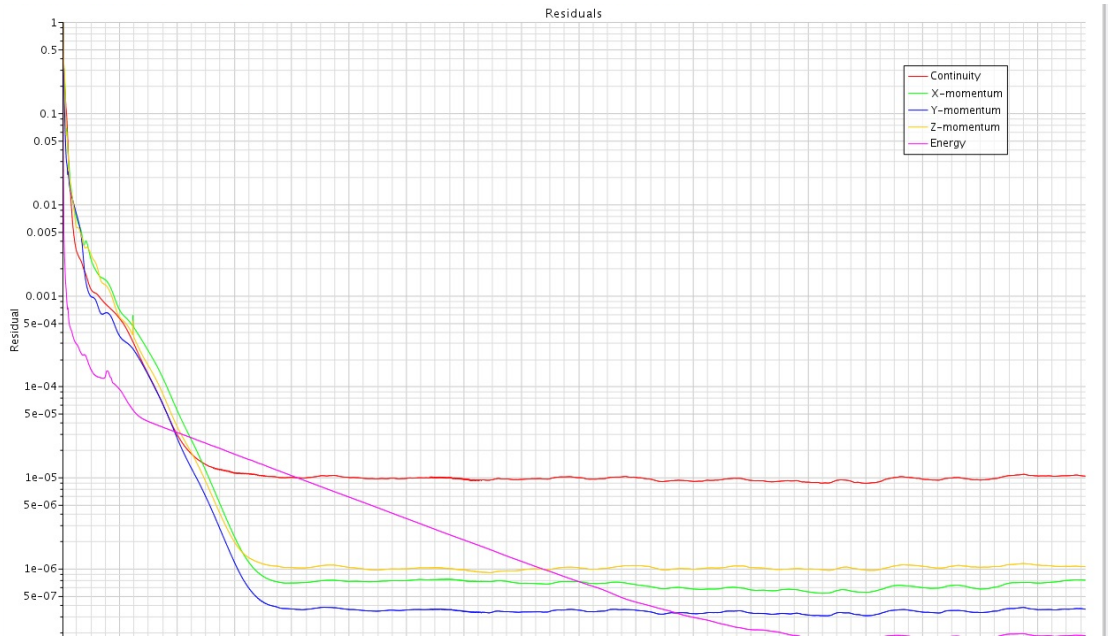

Figure 72: Residuals plot (50 mm/s)

Bibliography

[1] Bakker A. Multiphase Flows - Applied Computational Fluid Dynamics. Available on: www.bakker.org/dartmouth06/engs150/14-multi.pdf, 2014.

[2] Brian J. Chalmers. Electric motor handbook. Butterworths,1988.

[3] CD-adapco. User Guide - Star-CCM+. Available on: http://stevedocs.cd-adapco.com

[4] Hans Dieter Baehr & Karl Stephan. Heat and mass transfer. Springer, 2013.

[5] Hongmin Li. 2009. Cooling of a permanent magnet electric motor with a centrifugal impeller. International Journal of Heat and Mass Transfer, Volume 53, Issue 4, 2010.

[6] Nippon Steel & Sumitomo Metal. Develepement of Active Suspension with Electromechanical Actuators for Railway Vehicles. Available on: http://www.nssmc.com/en/tech/report/nssmc/pdf/105-09.pdf

[7] Paul Wide & Conrad U. Brunner. Energy-Efficiency Policy Opportunities for Electric Motor-Driven Systems. International Energy Agency. Available on: http://www.iea.org/publications/freepublications/publication/EE_for_ElectricSystems.pdf

[8] R. Teman. Navier Stokes Equations theory and numerical analysis. North-Holland Publishing Company, 1977.

[9] Ronghiou Zhou, Argyrios Zolotas & Roger Goodall. Integrated tilt with active lateral secondary suspension control for high speed railway vehicles. Available on: http://taw-co.ir/Portals/0/articles/1-s2.0-S0957415811001036-main.pdf

[10] Theodore L.Bergman, Adrienne S. Lavine, Frank P. Incorpora & David P. Dewitt. Fundamentals of heat and mass transfer. Wiley, 2011

[11] Versteeg H. & Malalasekera W. 2007. An Introduction to Computational Fluid Dynamics: The Finite Volume Method. Prentice Hall, 2007.

[12] Wei Tong. Mechanical design of electric motors. CRC Press, 2014.

[13] White F. 2003. Fluid Mechanics. McGraw-Hill Science, 2003.

[14] Kevin Bennion. Electric Motor Thermal Management. National Renewable Energy Laboratory. Available on: http://www1.eere.energy.gov/vehiclesandfuels/pdfs/merit_review_2011/adv_power_electronics/ape030_bennion_2011_o.pdf

[15] John F. Douglas, Janusz M. Gasiorek, John A. Swaffield, Lynne B. Jack. Fluid Mechanics. Pearson Education, 2005.